Government of Western Australia

Department of
Mines and Petroleum

REPORT
135

A MAGNETOTELLURIC TRAVERSE ACROSS THE EASTERN PART OF THE CAPRICORN OROGEN

by MC Dentith, SP Johnson, S Evans, ARA Aitken, A Joly, S Thiel, and IM Tyler

Centre for EXPLORATION TARGETING

ROYALTIES FOR REGIONS
EXPLORATION INCENTIVE SCHEME

Moombarriga Geoscience

Geological Survey of Western Australia

Government of **Western Australia**
Department of **Mines and Petroleum**

REPORT 135

A MAGNETOTELLURIC TRAVERSE ACROSS THE EASTERN PART OF THE CAPRICORN OROGEN

by
MC Dentith[1], SP Johnson, S Evans[2], ARA Aitken[1], A Joly[1], S Thiel[3], and IM Tyler

1 Centre for Exploration Targeting, The University of Western Australia, 35 Stirling Hwy, Crawley WA 6009
2 Moombarriga Geoscience, Box 1184, West Perth WA 6872
3 TRaX, Mawson Building, North Terrace Campus, The University of Adelaide, Adelaide SA 5005

Perth 2014

Geological Survey of Western Australia

REFERENCE
The recommended reference for this publication is:
Dentith, MC, Johnson, SP, Evans, S, Aitken, ARA, Joly, A, Thiel, S and Tyler, IM 2014, A magnetotelluric traverse across the eastern part of the Capricorn Orogen: Geological Survey of Western Australia, Report 135, 49p.

National Library of Australia Cataloguing-in-Publication entry:

Author:	Dentith, Mike, author.
Title:	A magnetotelluric traverse across the eastern part of the Capricorn Orogen / MC Dentith, SP Johnson, S Evans, A Aitken, A Joly, S Thiel, and IM Tyler.
ISBN:	9781741685558 (ebook)
Subjects:	Magnetotelluric prospecting--Western Australia--Gascoyne Region. Orogeny--Western Australia--Gascoyne Region. Geological surveys--Western Australia--Gascoyne
Other Authors/Contributors:	Johnson, S. P., author. Evans, S., author. Aitken, Alan, author. Joly, A, author. Thiel, Stephan, author. Tyler, I. M., author.
Dewey Decimal Classification:	622.15309941

ISSN 1834–2280

Grid references in this publication refer to the Geocentric Datum of Australia 1994 (GDA94). Locations mentioned in the text are referenced using Map Grid Australia (MGA) coordinates, Zones 50 and 51. All locations are quoted to at least the nearest 100 m.

Copy editor: K Hawkins
Cartography: M Prause, AK Symonds
Desktop publishing: RL Hitchings
Printed by Images on Paper, Perth, Western Australia

Published 2014 by Geological Survey of Western Australia
This Report is published in digital format (PDF) and is available online at <www.dmp.wa.gov.au/GSWApublications>.

Further details of geological publications and maps produced by the Geological Survey of Western Australia are available from:
Information Centre
Department of Mines and Petroleum | 100 Plain Street | EAST PERTH | WESTERN AUSTRALIA 6004
Telephone: +61 8 9222 3459 Facsimile: +61 8 9222 3444 **www.dmp.wa.gov.au/GSWApublications**

Cover photograph: Auger drilling for deployment of the z-component electrode during acquisition of the eastern Capricorn Orogen magnetotelluric traverses

Contents

Appendix

Figures

Tables

A magnetotelluric traverse across the eastern part of the Capricorn Orogen

by

MC Dentith[1], SP Johnson, S Evans[2], ARA Aitken[1], A Joly[1], S Thiel[3], and IM Tyler

Abstract

Two near-orthogonal magnetotelluric (MT) traverses were conducted through the eastern part of the Capricorn Orogen (totalling 350 km in length with 42 broadband MT recordings) in order to elucidate the crustal-scale architecture of this region.

Standard processing methods were used for MT data, including robust remote-reference algorithms based on the coherence-sorted cascade decimation method. Most data showed significant three-dimensional (3D) MT responses that could not be modelled using standard 2D modelling methods, and thus the data were reprocessed using a 3D inversion algorithm, which produced more geologically plausible results.

Distinct variations in mantle and crustal electrical conductivity are interpreted as being caused by juxtaposition of a series of discrete tectonic blocks separated by crustal-scale faults or shear zones. The major structures in the eastern Capricorn Orogen dip towards the centre of the orogen; by contrast, in the western part, major structures consistently dip towards the south. However, this survey shows the presence of an exotic conductive tectonic block, which separates the more resistive Yilgarn and Pilbara Cratons. This conductive tectonic block is similar to the Glenburgh Terrane in the western part of the orogen.

KEYWORDS: crustal evolution, crustal structure, geophysical interpretation, geophysical models, magnetotelluric surveys, resistivity, structural terranes

Introduction

The Capricorn Orogen of Western Australia is an approximately 1000 km-long, 500 km-wide region of variably deformed meta-igneous, metasedimentary, and low-grade sedimentary rocks located between the Pilbara and Yilgarn Cratons (Fig. 1a). The orogen records the two-stage Paleoproterozoic assembly of these two cratons, and an exotic Archean to Paleoproterozoic crustal fragment, the Glenburgh Terrane of the Gascoyne Province, to form the West Australian Craton (Johnson et al., 2011a). More than one billion years of subsequent intracratonic reworking is also recorded (Cawood and Tyler, 2004; Sheppard et al., 2010a,b; Johnson et al., 2011a,b). The orogen includes the deformed margins of the Pilbara and Yilgarn Cratons and associated deformed continental margin rocks of the Fortescue, Hamersley, Turee Creek, and lower Wyloo Groups in the Ophthalmia Fold Belt. Medium- to high-grade meta-igneous and metasedimentary rocks of the Glenburgh Terrane and Gascoyne Province form the core of the orogen. These rocks are overlain by several basins containing variably deformed low-grade metasedimentary rocks, including the upper Wyloo, Bresnahan, Mount Minnie, Padbury, Bryah, Yerrida, Earaheedy, Edmund, and Collier Basins (Figs 1–3; Cawood and Tyler, 2004; Sheppard et al., 2010a). Compared to other Australian Precambrian provinces, the Capricorn Orogen is unique in having distinctly different, opposing, continental fragments exposed along both its northern and southern margins, together with the exposure of upper- to mid-crustal rocks within the orogen itself.

During 2010, 581 km of deep seismic reflection, gravity, and magnetotelluric data were acquired through the western part of the Capricorn Orogen (Fig. 1; Johnson et al., 2011d, 2013). The survey provided an unprecedented view of the deep crustal architecture of the West Australian Craton (Fig. 4), supporting the view of Occhipinti et al. (2004) and Johnson et al. (2011a) that the craton was formed by the collision or accretion of three distinct tectonic blocks, the Pilbara Craton, the Glenburgh

1 Centre for Exploration Targeting, The University of Western Australia, 35 Stirling Hwy, Crawley WA 6009

2 Moombarriga Geoscience, Box 1184, West Perth WA 6872

3 TRaX, Mawson Building, North Terrace Campus, The University of Adelaide, Adelaide SA 5005

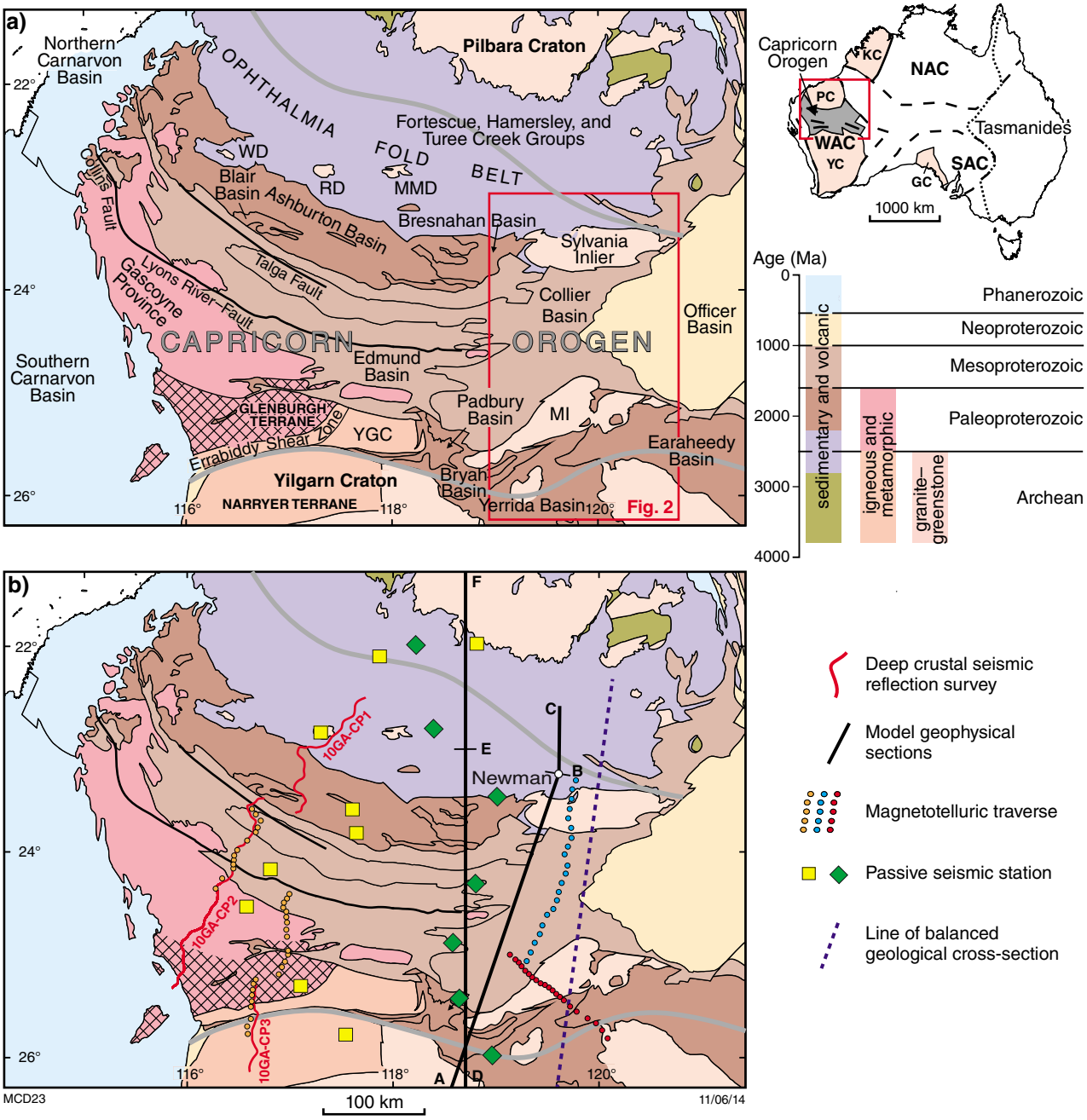

Figure 1. **a) Elements of the Capricorn Orogen and surrounding cratons and basins, modified from Martin and Thorne (2004). Thick grey lines delimit the northern and southern boundaries of the Capricorn Orogen: GC, Gawler Craton, KC, Kimberley Craton; MI, Marymia Inlier; MMD, Milli Milli Dome; NAC, North Australian Craton; PC, Pilbara Craton; RD, Rocklea Dome; SAC, South Australian Craton; WAC, West Australian Craton; WD, Wyloo Dome; YC, Yilgarn Craton; YGC, Yarlarweelor Gneiss Complex; b) map showing the location of previous geophysical studies in the Capricorn Orogen, including the seismic refraction studies of Drummond (1979) (A–B–C; Fig. 8a), model gravity section of Hackney (2004) (D–E–F; Fig. 8b); passive seismic stations of Reading and Kennett (2003) (green diamonds) and Reading et al. (2012) (yellow squares); and magnetotelluric (MT) studies of Selway (2007) (orange circles). Geophysical studies of Heinson et al. (2011) are coincident with the reflection seismic survey (10GA–CP1, 2, 3) of Johnson et al. (2011d, 2013) (solid red lines). Also shown are the locations of the balanced geological cross-section shown in figure 27b of Cawood and Tyler (2004) (dashed purple line). The location of the present MT survey is shown in red circles (Traverse 1) and blue circles (Traverse 2).**

Terrane, and the Narryer Terrane of the Yilgarn Craton, during two, separate, and distinct Proterozoic orogenic events. These events were the 2215–2145 Ma Ophthalmian and 2005–1950 Ma Glenburgh Orogenies. The survey identified the location and orientation of the suture zones and many major crustal-scale faults that transect the entire crustal profile from the surface to the upper mantle. From a mineral exploration view, these structures are critical for deposit-forming mineral systems because they facilitate the transport of metal-bearing fluids from the uppermost mantle to the upper crust (Begg et al., 2010; Hronsky et al., 2012; Johnson et al., 2013).

The eastern part of the Capricorn Orogen contains several major mineral deposits such as the world-class Plutonic gold deposit, and has had a recent history of major mineral discovery including the DeGrussa Cu–Au deposit at Doolgunna (Fig. 2). Due to extensive regolith cover in the region, the surface geology and crustal architecture in this part of the Capricorn Orogen are not particularly well constrained and thus it has been difficult to project the major structures identified in the Capricorn Orogen seismic survey eastward into this area. So, in 2011, a Royalties for Regions, Exploration Incentive Scheme (EIS)-funded magnetotelluric (MT) traverse was conducted through the eastern part of the orogen in order to view the electrical conductivity of the crust and attempt to identify the location and orientation of major crustal structures that could constrain the crustal-scale architecture of this part of the orogen. The survey consisted of two traverses totalling 350 km in length with 42 broadband MT recordings, one trending roughly northwest–southeast (Traverse 1) and an adjoining northeast–southwest traverse (Traverse 2) (Figs 1 and 2). Traverse 1 tracks along the northern, fault-dissected margin of the Yilgarn Craton, passing close to the Thaduna, DeGrussa, and Plutonic deposits (Fig. 2), in order to better constrain the basinal and structural architecture that may have assisted base metal and gold mineralization. Traverse 2 was designed to determine the larger crustal-scale structure of the region by locating the Yilgarn and Pilbara Craton margins and whether Proterozoic rocks of the Glenburgh Terrane are present between the two cratons (Figs 1 and 2).

Magnetotelluric method

The magnetotelluric method is a deep-penetrating, passive (natural-source), frequency-domain electromagnetic method that allows variations in electrical conductivity to be mapped in the crust and upper mantle. A comprehensive description of the method is provided by Chave and Jones (2012) and Simpson and Bahr (2005). Briefly, natural fluctuating magnetic fields, due to the interaction of the geomagnetic field and the solar wind, and at higher frequencies, lightning strikes, induce telluric (electric) currents in the Earth. These variations span a broad range of frequencies or periods. Both terms 'frequency' and 'period' describe MT data: frequency (*f*) in Hertz (Hz) is the reciprocal of period (P) in seconds (s).

Because magnetic fields vary at a range of frequencies, electrical conductivity variations at depth can be determined. The penetration, that is, attenuation with distance, of an electromagnetic field into a medium depends on the medium's electrical conductivity and the frequency of the variations in the electromagnetic field. Although lower frequencies penetrate more deeply, greater subsurface conductivity reduces penetration for a given frequency. After recording, the electric and magnetic fields can be mathematically separated into components with different frequencies, and therefore electrical properties at different depths can be estimated. For this reason, during the description of the processing and interpretation of the MT data, the period can be thought of as a proxy depth parameter. However, because the conductivity of the Earth varies from location to location, the conversion factor from period to depth also varies. The maximum period (depth) of interest dictates the length of the time interval over which the variations in the electric and magnetic fields must be recorded. Penetration to mantle depths requires recording for some tens of hours.

Regional geology

The geology of the eastern Capricorn Orogen is relatively poorly exposed, because the region is draped by an extensive cover of mostly colluvial and alluvial regolith deposits that may be up to 100 m thick in paleochannels (Occhipinti et al., 1998a; Pirajno and Occhipinti, 1998). Despite this cover, the sporadic outcrop consists mostly of low-grade siliciclastic and carbonate (meta)sedimentary rocks that have been grouped into numerous basins of Proterozoic age, including the Yerrida, Bryah, Padbury, Earaheedy, Edmund, and Collier Basins (Pirajno et al., 1998, 2004; Martin and Thorne, 2004; Martin et al., 2008; Figs 1–3). Along the margins of the orogen, these (meta) sedimentary rocks unconformably, or structurally, overlie basement inliers of Archean granite–greenstones, the Marymia and Sylvania Inliers of the Yilgarn and Pilbara Cratons, respectively (Fig. 2). However, in the central part of the orogen these rocks may overlie unexposed high-grade metamorphic rocks and gneisses of the Glenburgh Terrane (Figs 1 and 2). A more detailed description of the geology of the area crossed by the MT survey is provided below.

Archean cratons

Yilgarn Craton

The Yilgarn Craton is an extensive region of Archean continental crust dominated by granite–greenstone terranes. On the basis of recent geological mapping and a re-evaluation of geological data at all scales (Cassidy et al., 2006), this craton has been divided into several distinct tectonic entities, the Narryer, Youanmi, and South West Terranes, and the Eastern Goldfields Superterrane. The Narryer and South West Terranes are dominated by granite and granitic gneiss with only minor supracrustal (greenstone) inliers, whereas the Youanmi Terrane and the Eastern Goldfields Superterrane contain substantial greenstone belts separated by granite and granitic

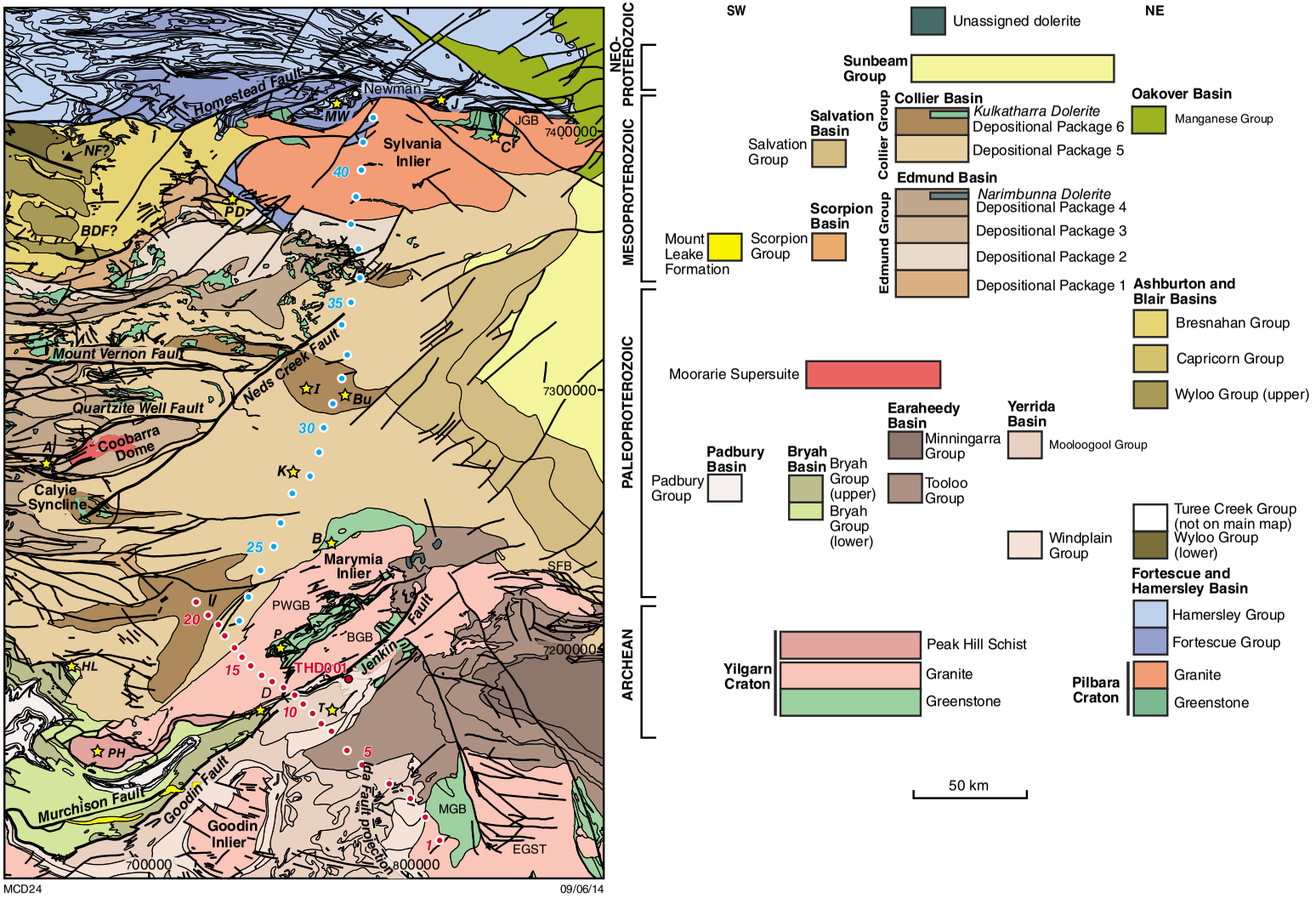

Figure 2. **Geological map and stratigraphic section of the eastern Capricorn Orogen. The location of individual MT broadband stations are in red (Traverse 1) and blue (Traverse 2) circles. Significant gold, base metal and iron ore deposits are shown by yellow stars. Deposits: A, Abra; B, Beyondie; Bu, Butcherbird; C, Coobina; D, DeGrussa/Doolgunna; HL, Horseshoe Lights; I, Ilgarari; IF, projection of the Ida Fault from the south; J, Jimblebar; K, Kumarina; MW, Mount Whaleback; P, Plutonic; PD, Prairie Downs; PH, Peak Hill; T, Thaduna. Other abbreviations: BDF, Bearing Downs Fault; BGB, Baumgarten greenstone belt; EGST, Eastern Goldfields Superterrane; JGB, Jimblebar greenstone belt; MGB, Merrie greenstone belt; NF, Nanjilgardy Fault; PWGB, Plutonic Well greenstone belt; SFB, Stanley Fold Belt; THD001, co-funded EIS diamond drillhole.**

gneiss. The Narryer Terrane contains the oldest rocks in Australia, the c. 3730 Ma Manfred Complex, and the oldest detrital zircons on Earth, at c. 4400 Ma (Froude et al., 1983; Compston and Pidgeon, 1986; Wilde et al., 2001). Supracrustal rocks in the Youanmi Terrane are as old as c. 3080 Ma (Yeates et al., 1996; Wang et al., 1998; Rasmussen et al., 2010b; Van Kranendonk et al., 2013); however, greenstone successions across the Yilgarn Craton are dominated by rocks that formed after c. 2820 Ma (Ivanic et al., 2010). The Eastern Goldfields Superterrane is separated from the Youanmi Terrane by the Ida Fault, which is interpreted as a major crustal structure that extends to the base of the crust (Drummond et al., 2000). Although it has a similar history to the Youanmi Terrane after c. 2820 Ma, the Eastern Goldfields Superterrane is characterized by a much younger history of supracrustal deposition and mafic magmatism to c. 2660 Ma. All of the northern Yilgarn Craton (super)terranes were intruded by high-Ca tonalite–trondhjemite–granodiorite (TTG) rocks between c. 2690 and 2660 Ma, and low-Ca granites between c. 2660 and 2620 Ma (Cassidy et al., 2006; Champion and Cassidy, 2007; Wyche et al., 2013).

The southern end of Traverse 1 covers granitic rocks belonging to the Kalgoorlie Terrane of the Eastern Goldfields Superterrane and passes directly to the south of the Merrie greenstone belt (Fig. 2). A basement inlier, the Goodin Inlier, about 65 km to the west of the MT line, consists of granitic rocks that are assigned to the Youanmi Terrane, implying that the Ida Fault may pass close to the line of the survey.

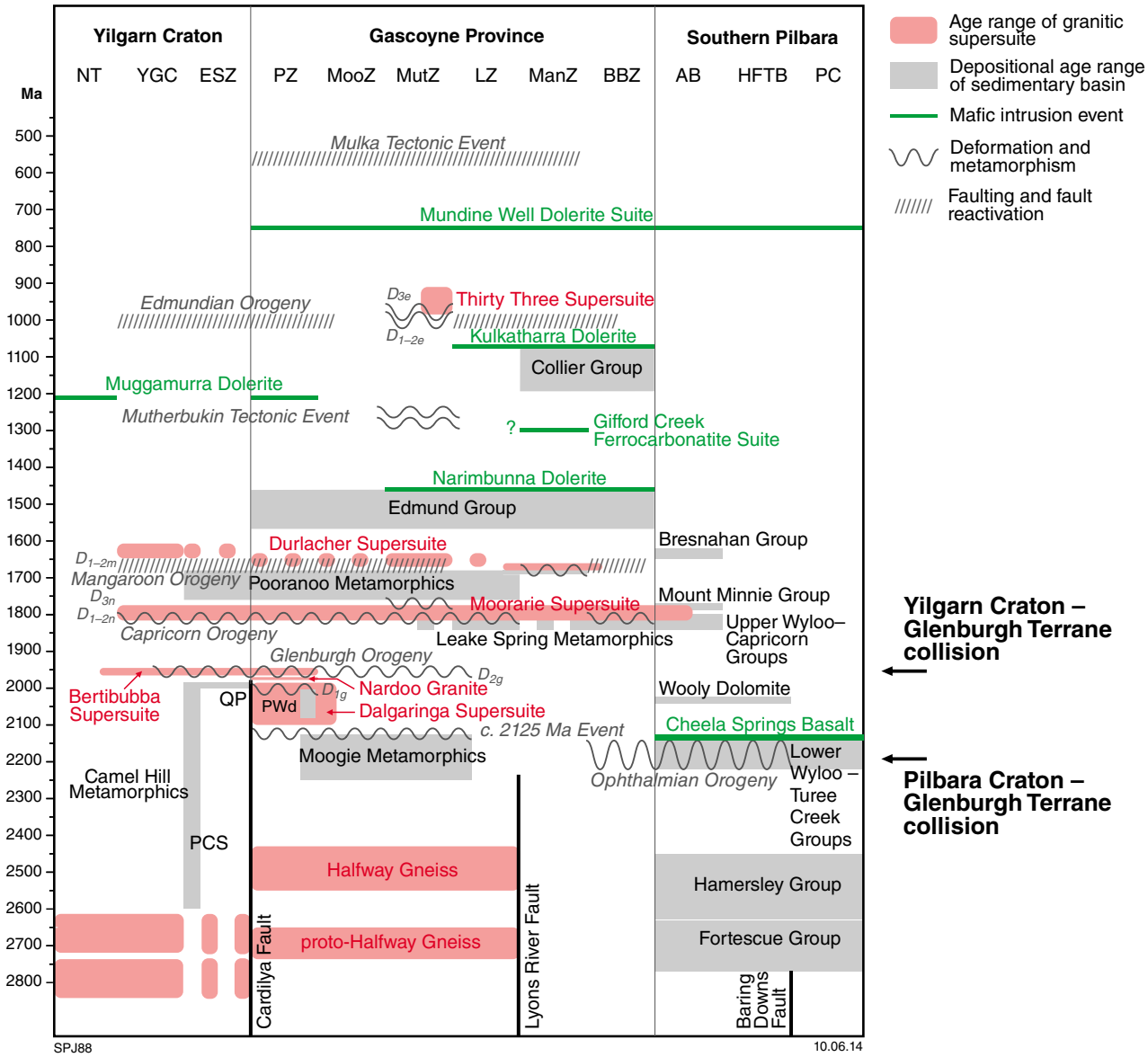

Figure 3. **Time–space plot for the Capricorn Orogen. AB, Ashburton Basin; BBZ, Boora Boora Zone; ByhB, Bryah Basin; EarB, Earaheedy Basin; ESZ, Errabiddy Shear Zone; HFTB, Hamersley, Fortescue, and Turee Creek Basins; LZ, Limejuice Zone; ManZ, Mangaroon Zone; MooZ, Mooloo Zone; MutZ, Mutherbukin Zone; NT, Narryer Terrane; PadB, Padbury Basin; PC, Pilbara Craton; PCS, Petter calc-silicate; PWd, Paradise Well diatexite; PZ, Paradise Zone; QP, Quartpot pelite; YerB, Yerrida Basin; YGC, Yarlarweelor Gneiss Complex**

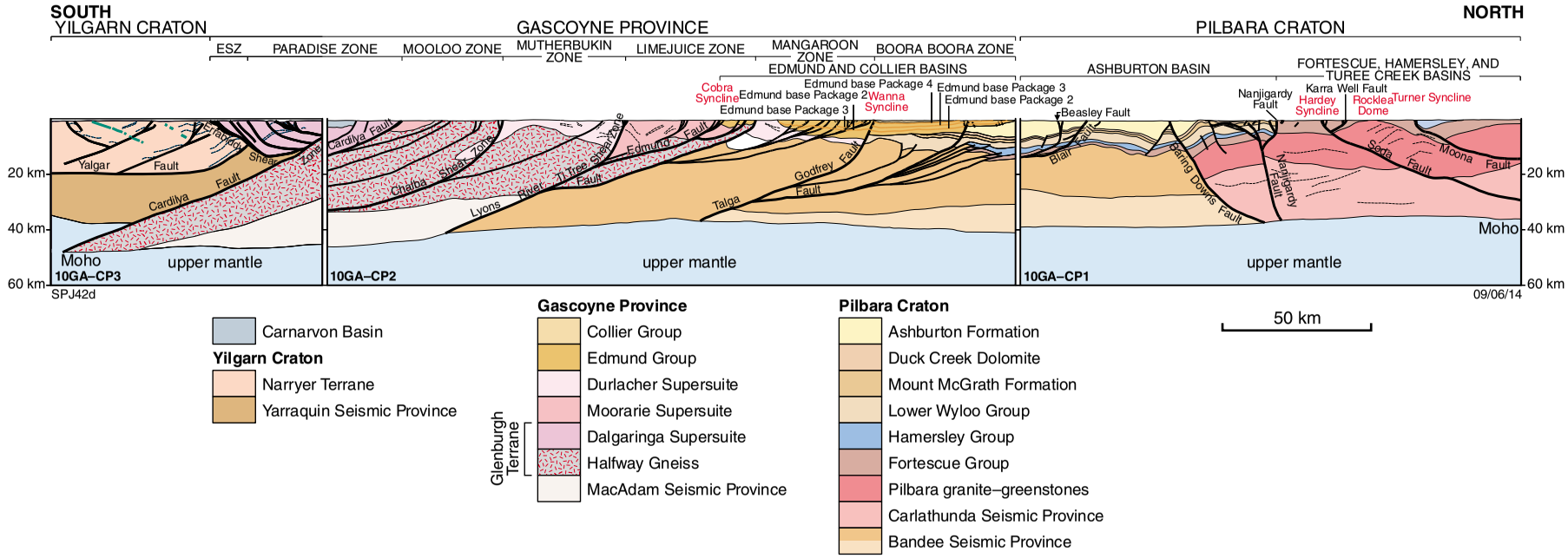

Figure 4. Cross-section of the deep crustal reflection seismic transect across the western part of the Capricorn Orogen (Johnson et al., 2011d, 2013), combining seismic lines 10GA–CP1, 2, and 3, and showing key faults, terranes, zones, basins, and seismic provinces

Marymia Inlier

The Marymia Inlier is an approximately 150 km-long, 40 km-wide, northeast-trending, fault-bounded block of Archean granite–greenstones, adjacent to the younger basins of the Padbury, Bryah, Yerrida, Earaheedy, Edmund, and Collier Basins (Fig. 2). The inlier contains two named greenstone successions, the Plutonic Well and Baumgarten greenstone belts, both of which trend northeast–southwest, almost orthogonal to the regional trends of the Youanmi Terrane and Eastern Goldfields Superterrane greenstones to the south (Figs 1 and 2). The Plutonic Well greenstone belt is interpreted by Bagas (1999a,b) as a complex composite synclinorium. The northwestern and southeastern edges of the belt consist of metamorphosed and foliated assemblages of ultramafic rocks (including komatiite and pyroxenite with interlayered pelite), tholeiitic basalt, banded iron-formation, chert, felsic tuff, arkose, and pelite. On the northern margin of the inlier is a third, unnamed, area of greenstone (Fig. 2). Here, two distinct linear magnetic anomalies are associated with exposures of iron formation (Emergent Resources, 2014). The geometry of the anomalies suggests a plunging fold or structural repetition.

The origin of the Marymia Inlier is controversial and has been interpreted as a stable Archean remnant rifted and separated from the northern margin of the Yilgarn Craton during the Capricorn Orogeny (Pirajno et al., 2004), a rotated and separated portion of the Yilgarn Craton (Occhipinti et al., 1998c; Krapež and Martin, 1999), and a remnant, essentially in situ, portion of Archean basement (Gee, 1979). Stratigraphic comparisons of the greenstone successions have been made with those in the Youanmi Terrane (Bagas, 1999a); however, more recent geochronological, petrographic, and stratigraphic analyses in the southwestern part of the Plutonic Well greenstone belt (Vickery 2004; Gazley, 2011; Gazley et al., 2011) favour a correlation with those in the Eastern Goldfields Superterrane.

On its southern side, the inlier is separated from the Proterozoic basins by the Jenkin Fault, which also dissects the Baumgarten greenstone belt (Fig. 2). The Paleoproterozoic basins presumably once had unconformable relationships with the granite–greenstones, although most contacts are now tectonic in character. The Jenkin Fault is interpreted as a steeply north-dipping thrust with now-inverted granite–greenstones thrust southward over the Proterozoic basins (Bagas, 1999a,b; Cawood and Tyler, 2004; Vickery, 2004). This fault appears to have been subsequently reactivated into a strike-slip zone, highlighting the complex Proterozoic deformational history of this region. The northern margin of the Marymia Inlier is unconformably overlain by sedimentary rocks of the Mesoproterozoic Collier Group, obscuring any older faults.

Traverse 1 passes through granitic rocks of the Marymia Inlier directly southwest of the Plutonic Well greenstone belt (Fig. 2).

Pilbara Craton and associated basins

Within the northern Capricorn Orogen, Pilbara Craton granite–greenstone basement rocks are exposed in the Wyloo, Rocklea, and Milli Milli Domes, and in the Sylvania Inlier in the northeastern part of the orogen (Fig. 1). These rocks are unconformably overlain by low-grade metasedimentary and metavolcanic rocks of the Fortescue, Hamersley, Turee Creek, and Wyloo Groups (Fig. 5). Little is known about the age, composition, and tectonic affinity of these basement domes except that the rocks pre-date the deposition of the c. 2775 Ma Fortescue Group (Trendall et al., 2004). If the granite–greenstones formed in a similar timeframe to those in the northern Pilbara Craton then they probably formed between c. 3800 and 2830 Ma (Van Kranendonk et al., 2007; Hickman and Van Kranendonk, 2008).

The overlying metasedimentary and metavolcanic rocks of the 2775–2630 Ma Fortescue and 2630–2450 Ma Hamersley Groups formed during a protracted period of continental rifting and passive margin formation (Blake, 1993; Thorne and Trendall, 2001). The Fortescue Group is up to 6 km thick and is dominated by thick mafic and ultramafic successions and abundant siliciclastic sedimentary rocks (Fig. 5). The approximately 3 km-thick Hamersley Group conformably overlies the Fortescue Group, and was deposited in a passive margin setting (Morris and Horwitz, 1983; Blake and Barley, 1992; Thorne and Trendall, 2001). Rocks of the Hamersley Group reflect this largely deeper marine distal setting, and are dominated by banded iron-formation, shale, chert, and fine-grained carbonate (Fig. 5). Deposition of the Turee Creek and lower Wyloo Groups took place during the early foreland-basin stage of the 2215–2145 Ma Ophthalmian Orogeny, when the Pilbara Craton collided with the Glenburgh Terrane to the south (Blake and Barley, 1992; Martin et al., 2000; Martin and Morris, 2010; Johnson et al., 2011a). The Turee Creek and lower Wyloo Groups have a maximum thickness of about 4 km and about 3 km, respectively (Fig. 5). Both groups are dominated by coarse-grained siliciclastic sedimentary rocks, although the upper part of the lower Wyloo Group contains up to 2 km of fine-grained mafic rock of the c. 2210 Ma Cheela Springs Basalt (Martin et al., 1998; Müller et al., 2005; Martin and Morris, 2010).

Although rocks of the Fortescue, Hamersley, and lower Wyloo Groups are not exposed along Traverse 2, these rocks outcrop on the southwestern margin of the Sylvania Inlier and may extend eastward beneath the cover of the younger Edmund and Collier Groups into the line of the survey (Cawood and Tyler, 2004).

Sylvania Inlier

The Sylvania Inlier is an approximately 130 km-long, 50 km-wide, east–west-trending block of Archean granite and greenstone (Fig. 2). The inlier is dominated by granitic rocks, although there are also discontinuous greenstone

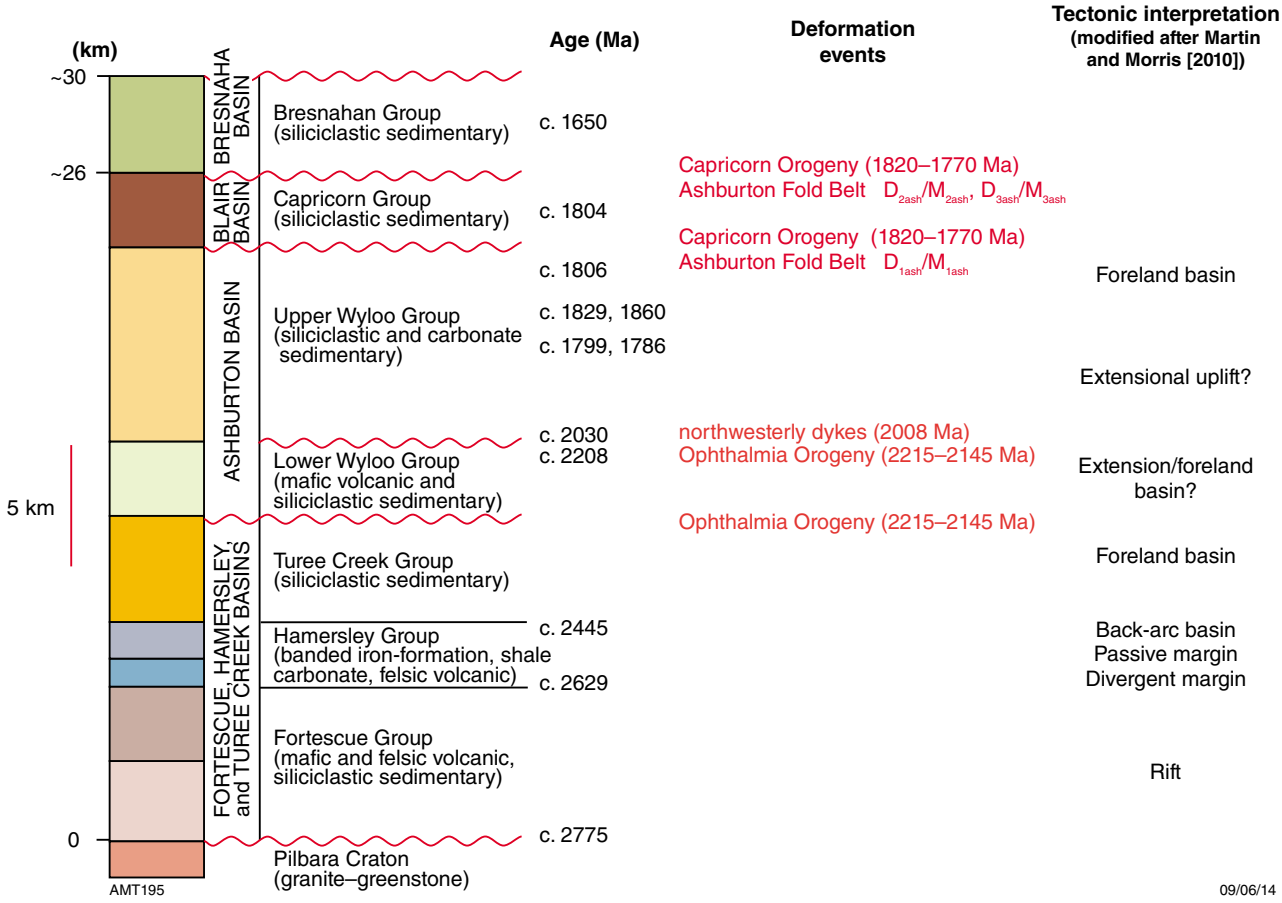

Figure 5. Generalized stratigraphy and deformation history of the northern Capricorn Orogen; tectonic interpretation after Martin and Morris (2010)

belts, the largest of which is the Jimblebar greenstone belt in the northeastern part of the inlier (Tyler, 1991; Fig. 2). The age, chemistry, and tectonic setting of the granite–greenstones are unknown; however, the granite and greenstone units must be older than c. 2775 Ma, the age of unconformably overlying metasedimentary rocks of the Fortescue Group (Fig. 3). Based on the structural and metamorphic history, Tyler (1991) and Tyler and Thorne (1990) divided the Sylvania Inlier into two zones, a relatively undeformed western zone comprising about 30% of the inlier, and a much larger, more-deformed eastern zone.

In the eastern part, sedimentary rocks of the lowermost c. 2775 Ma Fortescue Group unconformably overlie the northern margin of the inlier, whereas farther west, the two units are in fault contact. Fortescue Group rocks are also present along the southwestern margin where they are in fault contact with granitic rocks. Most of the southern margin is unconformably overlain by, and locally in fault contact with, sedimentary rocks of the Mesoproterozoic Edmund and Collier Groups. The pre-Mesoproterozoic architecture has been interpreted to have resulted from northward-direct thrusting during the Ophthalmian Orogeny (Tyler and Thorne, 1990); thus, the major faults are interpreted to dip moderately southward.

Traverse 2 passes through granitic rocks in the central part of the inlier, and towards the northern end of the line, into a normal-fault-bounded outlier containing rocks of the Fortescue Group (Fig. 2). The northern contact of the granite-dominated inlier with the sedimentary rocks of the Fortescue and Hamersley Groups was not reached in this survey.

Gascoyne Province and Glenburgh Terrane

The Gascoyne Province is exposed in the western part of the Capricorn Orogen (Fig. 1). The province is composed of Archean to Proterozoic medium- to high-grade meta-igneous and metasedimentary rocks that record both the formation of the West Australian Craton, and more than one billion years of intracratonic reworking (Johnson et al., 2010, 2011a; Sheppard et al., 2010a). The oldest exposed rocks, the Glenburgh Terrane, are in the southern part of the province, and consist of 2555–2430 Ma heterogeneous granitic gneisses (Johnson et al., 2011c), the Halfway Gneiss, which are overlain by an unknown thickness of siliciclastic metasedimentary rocks, the Moogie Metamorphics, which were deposited some time between c. 2240 and 2125 Ma, perhaps in a foreland-basin

setting (Johnson et al., 2010, 2011a). Along the southern margin of this terrane, the gneisses and metasedimentary rocks are intruded by an extensive c. 2000 Ma granite batholith, the Dalgaringa Supersuite, which is interpreted to have formed in a continental margin arc, leading up to the final suturing of the West Australian Craton (Sheppard et al., 2004; Johnson et al., 2011a). The isotopic evolution of all these rocks implies that the Glenburgh Terrane is exotic to both the Pilbara and Yilgarn Cratons and is an exotic microcontinent within the Capricorn Orogen (Johnson et al., 2011c).

Following the final assembly of the West Australian Craton during the 2005–1950 Ma Glenburgh Orogeny, the province was structurally, metamorphically, and magmatically reworked during numerous intraplate orogenic events. During the 1820–1770 Ma Capricorn Orogeny, the province was reworked at low to moderate metamorphic grades and was accompanied by the intrusion of voluminous granite stocks and batholiths of the 1820–1775 Ma Moorarie Supersuite across the entire province, including the northern margin of the Yilgarn Craton, and the Ashburton Basin to the north (Sheppard et al., 2010a,b). Granitic rocks of the Moorarie Supersuite are also recognized in the Coobarra Dome (formerly the 'Western Inlier' of Brakel et al., 1978; Fig. 2) where they are unconformably overlain by sedimentary rocks of the Edmund Group. These rocks form the easternmost-known extent of the Gascoyne Province; however, it is not known whether these granitic rocks were intruded into basement rocks of the Glenburgh Terrane, the southern margin of the Pilbara Craton (the Bandee Seismic Province; Fig. 4), or the northern margin of the Yilgarn Craton.

During the 1680–1620 Ma Mangaroon Orogeny, sedimentation and magmatism took place across the entire province (Sheppard et al., 2005, 2010a). Precursor siliciclastic sedimentary rocks of the Pooranoo Metamorphics were laid down in fluvial to shallow-marine conditions some time between c. 1740 and 1680 Ma (Sheppard et al., 2005, 2010a) and were deformed, metamorphosed, and intruded by voluminous granitic rocks of the 1680–1620 Ma Durlacher Supersuite during the early parts of the Mangaroon Orogeny at 1680–1677 Ma (Sheppard et al., 2005). Intrusion of granites across the remainder of the province, including the northern margin of the Yilgarn Craton, took place between c. 1665 and 1620 Ma (Sheppard et al., 2010a).

Localized intrusion of leucocratic tourmaline-bearing granites and pegmatites of the Thirty Three Supersuite (Sheppard et al., 2010a) took place in the central part of the province during the 1030–955 Ma Edmundian Orogeny.

Although neither of the MT traverses directly crosses outcropping geology of the Gascoyne Province or Glenburgh Terrane, that magmatic and metasedimentary rocks may be present at depth beneath the Proterozoic (meta)sedimentary rocks. Because the structural evolution of the eastern Capricorn Orogen is also poorly understood, many of the structures and events that have affected the Gascoyne Province may have also affected the rocks in this part of the orogen.

Proterozoic sedimentary basins

Yerrida Basin

Rocks of the Yerrida Basin unconformably overlie the granite–greenstones of the Yilgarn Craton (Fig. 2) and have a stratigraphic thickness of more than 3 km (Fig. 6; Pirajno et al., 2004). The basin has been divided into two disconformable groups, the Windplain Group and the overlying Mooloogool Group; the deposition of these groups is separated by a hiatus of about 330 Ma (Pirajno et al., 2004). The Windplain Group comprises a basal succession, the Juderina Formation, of siliciclastic rocks containing stromatolitic carbonates of the Bubble Well Member, and a thick upper succession of graphitic and pyritic shales known as the Johnson Cairn Formation. The sediments were deposited in a continental sag basin, ranging from coastal and shallow-marine environments, grading to intertidal and supratidal sabkha lagoons (Gee and Grey, 1994; Pirajno et al., 1998; Pirajno and Occhipinti, 2000). Paleocurrent analysis, combined with the ages of detrital zircons from within the Juderina Formation, indicate that most detritus was derived from the Yilgarn Craton, and although the date of deposition is poorly constrained, a Pb–Pb date for stromatolitic carbonates in the Bubble Well Member suggest deposition close to c. 2170 Ma (Woodhead and Hergt, 1997; Figs 3 and 6). These data imply that the Windplain Group was deposited on the continental margin of the Yilgarn Craton before assembly of the West Australian Craton.

The lower part of the disconformably overlying Mooloogool Group, the Killara, Doolgunna, and Thaduna Formations, is composed of conglomerates and turbidite-facies rocks (Fig. 6), and extensive mafic intrusive and extrusive units that have chemistries consistent with a continental flood basalt origin (Pirajno et al., 1997, 2004). These mafic units have peperitic margins with finely laminated siltstone and sulfidic shales of the overlying Maraloou Formation, indicating that the mafic rocks were intruded into the succession although the sediments were unlithified. Hydrothermal or metamorphic monazites within the peperitic margins have been dated, using U–Th–Pb sensitive high-resolution ion microprobe (SHRIMP), at c. 1840 Ma (Rasmussen and Fletcher, 2002). These data indicate that mafic magmatism and the deposition of the Mooloogool Group occurred at this time, some 330 Ma after deposition of the Windplain Group (Figs 3 and 6).

The southern part of Traverse 1 crosses the Windplain and Mooloogool Groups, both of which contain significant thicknesses of black, pyritic, and graphitic shales (Johnson Cairn Formation of the Windplain Group, and the Maraloou Formation of the Mooloogool Group), lithotypes that are highly conductive. High conductivity reduces the penetration of MT data and it is likely that where these units are present, responses from deeper features will be hard to recognize.

Bryah Basin

Sedimentary and igneous rocks of the Bryah Basin have been deformed and metamorphosed within the greenschist

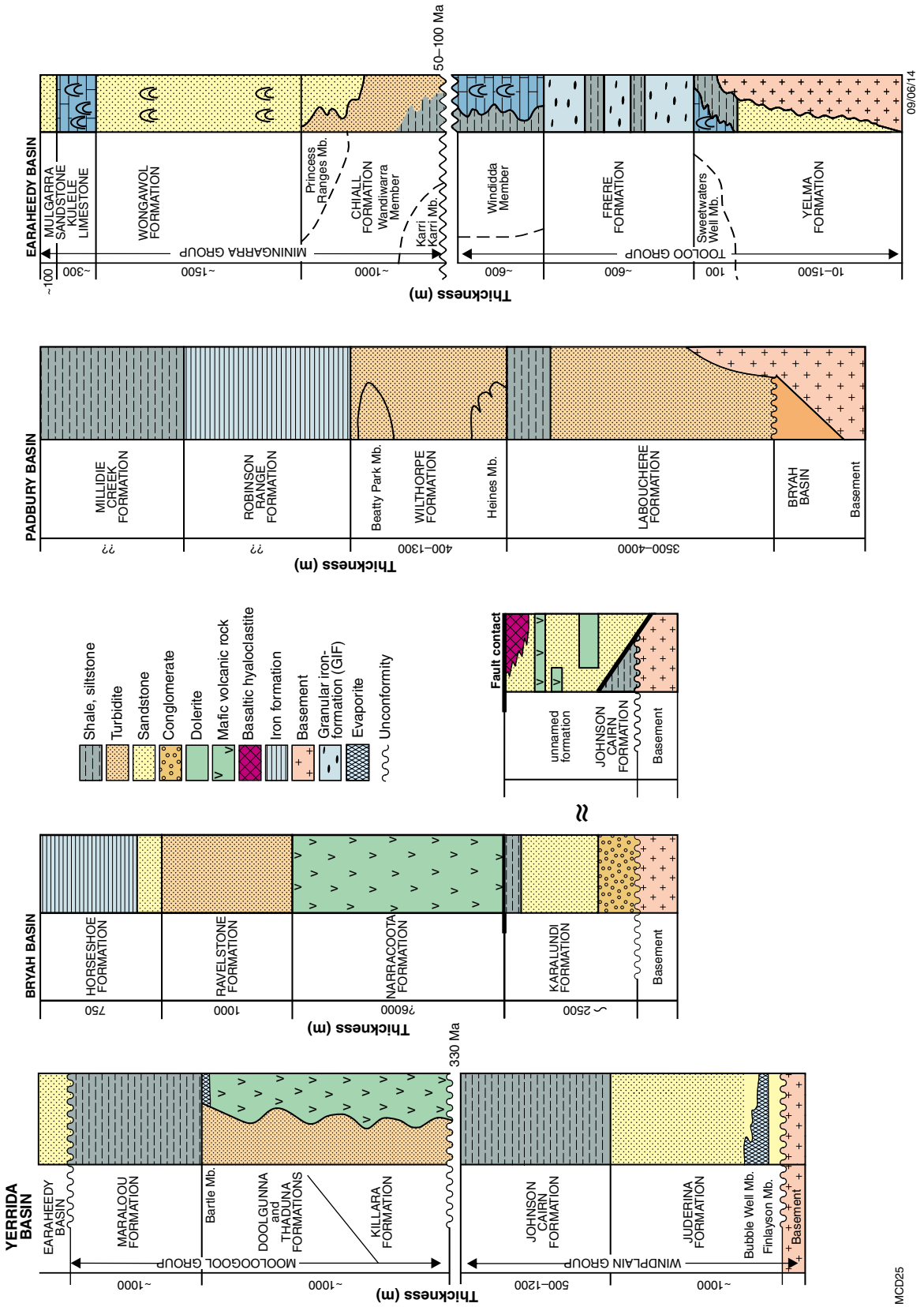

Figure 6. Stratigraphy of the Proterozoic basins in the eastern Capricorn Orogen; modified from Pirajno et al. (2004)

facies, and are everywhere in tectonic contact with older lithotectonic units including granite–greenstones of the Yilgarn Craton and sedimentary rocks of the Yerrida Basin (Fig. 2; Pirajno et al., 2004). The entire succession is about 9 km thick, although it is divided into an approximately 3 km-thick upper succession of siliciclastic metasedimentary rocks, the Ravelstone and Horseshoe Formations, and a lower approximately 6 km succession of mafic to ultramafic intrusive and volcaniclastic rocks of the Narracoota Formation, and siliciclastic rocks of the Karalundi Formation (Fig. 6; Pirajno and Occhipinti, 1998). Some of the stratigraphic thickness may be due to structural repetition during deformation.

The Narracoota Formation is composed of peridotitic and high-Mg basalt, mafic volcaniclastic rocks including pillow-structured metabasalts, mafic intrusive rocks, and mafic to ultramafic schists (Pirajno and Occhipinti, 1998). The mafic rocks have whole-rock, major, trace, and rare earth element compositions similar to those in oceanic plateaus (Pirajno et al., 1998; Pirajno and Occhipinti, 2000; Pirajno et al., 2004), and are interpreted to have formed in an intra-oceanic setting between the Yilgarn Craton and Glenburgh Terrane, prior to their collision and suturing during the 2005–1950 Ma Glenburgh Orogeny (Occhipinti et al., 1997; Pirajno et al., 1998; Pirajno and Occhipinti, 2000; Pirajno et al., 2004). The Narracoota Formation is disconformably overlain by turbiditic siliciclastic rocks of the Ravelstone Formation (Fig. 6), interpreted as a rift-fill succession deposited on top of the Narracoota Formation following its accretion to the northwestern margin of the Yilgarn Craton (Pirajno et al., 2004). The Horseshoe Formation is conformable with the underlying Ravelstone Formation, and consists of predominantly fine-grained siliciclastic and chemical rocks, including interbedded siltstone and shale, wacke, and iron formation. The formation is interpreted as the post-rift-fill deposits of a sediment-starved basin (Pirajno et al., 2004).

A discrete, currently unnamed package of siliciclastic and mafic intrusive rocks (Fig. 6), which probably formed in a narrow rift setting along the northern margin of the Yilgarn Craton, is present along the southern margin of the Marymia Inlier (Occhipinti et al., 1997; Pirajno et al., 1998, 2004; Pirajno and Occhipinti, 2000). The whole-rock, major, trace and rare earth element chemistry of the mafic intrusive rocks, the Killara Formation, is distinct from the chemistry of the Narracoota Formation, and implies intrusion into an extended continental margin. Importantly, this succession hosts extensive copper–gold volcanic-hosted massive sulfide mineralization, including the DeGrussa deposit (Fig. 2). Although there are no precise time constraints for deposition of the sedimentary succession, or the intrusion of the mafic rocks, the package is considered a time equivalent of the Narracoota Formation.

Although neither of the MT traverses transects metasedimentary or meta-igneous rocks of the Bryah Basin, outcrops are present along strike of the major fault structures, particularly the Jenkin Fault (Fig. 2). Thus, tectonically dismembered parts of the basin may exist at depth along these structures. Furthermore, it is not known whether rocks of the Bryah Basin are present north of the Marymia Inlier, beneath the sedimentary rocks of the Edmund and Collier Basins.

Padbury Basin

The Padbury Basin contains more than 6 km of siliciclastic sedimentary rocks (Fig. 6) including turbidites, siltstones, fine-grained sandstones, and an extensive iron formation (Gee, 1990; Windh, 1992; Martin, 1994, 1998). The lowermost part of the basin, the Labouchere and Wilthorpe Formations, is an upward-coarsening, foreland-basin succession of deep-water turbidites (Martin, 1994, 1998) derived mainly from the Yilgarn Craton, and the reworking of underlying metasedimentary and metamafic volcanic rocks of the Bryah Basin. The ironstones and shales of the overlying Robinson Range and Millidie Creek Formations, respectively, represent a change from deep- to shallow-water conditions in a lacustrine or marine platform environment (Martin, 1994).

Rocks of the Padbury Basin are not exposed at the surface along the line of the two MT traverses. It is not known whether these rocks extend beneath the Edmund and Collier Basins on the northern side of the Marymia Inlier, and so may potentially be imaged at depth along the northern and southern parts of Traverses 1 and 2, respectively (Fig. 2).

Earaheedy Basin

Shallow-marine clastic and chemical sedimentary rocks of the Earaheedy Basin are up to about 5 km thick (Fig. 6). They unconformably overlie the granite–greenstones of the Yilgarn Craton and Marymia Inlier, and the (meta) sedimentary rocks of the Yerrida and Bryah Basins (Fig. 2; Pirajno et al., 2004, 2009). The basin currently defines an asymmetric east-plunging regional syncline with a vertical to locally overturned northern limb known as the Stanley Fold Belt (Fig. 2). The Earaheedy Basin is divided into a lower shallow-marine succession, the Tooloo Group, of sandstone and siltstone, granular iron-formation, and carbonate rocks of the Yelma and Frere Formations, and a low-energy shallow-marine succession, the Minningarra Group, of turbiditic sandstones and lesser carbonates of the Chiall and Wongawol Formations, Kulele Limestone, and Mulgarra Sandstone (Figs 3 and 6). Recent dating of felsic volcanic horizons within the Tooloo Group (Rasmussen et al., 2012) implies the presence of a significant disconformity with the overlying Minningarra Group (Halilovic et al., 2004), and suggests that the Tooloo Group may have been deposited in a similar timeframe to the (meta)sedimentary rocks within the Padbury and Bryah Basins (Fig. 3).

The southern and central parts of Traverse 1 cross interbedded sandstones and siltstones of the Yelma Formation of the Tooloo Group (Fig. 2).

Edmund and Collier Basins

The Edmund and Collier Basins consist of 4–10 km of fine-grained siliciclastic and carbonate sedimentary rocks that were deposited under fluviatile to deep-marine conditions (Martin and Thorne, 2004). The groups have been divided into six depositional packages, each separated by an unconformity or basal marine-flooding surface (Fig. 7). Rocks of the Edmund Basin are exposed mainly in the western part of the Capricorn Orogen, where the sediments unconformably overlie granites of the 1680–1620 Ma Durlacher Supersuite of the Gascoyne Province (Sheppard et al., 2010a). These sediments were deposited sometime between c. 1620 Ma and 1465 Ma. Sedimentary rocks within the Collier Basin were deposited across both the Gascoyne Province and locally deformed sedimentary rocks of the Edmund Basin sometime between c. 1200 Ma and 1070 Ma. The Collier Basin is relatively restricted in the west, although it widens significantly in the eastern part of the orogen to a maximum width of about 200 km (Fig. 1).

The main depositional and structural elements of the Edmund Basin were controlled principally by major crustal structures in the underlying Gascoyne Province basement, including the Talga, Godfrey, Lyons River, Edmund, and Minga Bar Faults (Cutten et al., 2011; Johnson et al., 2013) (Fig. 1). Extensional movements on these faults formed several half-grabens, into which the sediments were deposited (Cutten et al., 2011; Johnson et al., 2013). Paleocurrent analyses combined with the U–Pb date (Martin et al., 2008) and Lu–Hf composition of detrital zircons (GSWA, 2011, unpublished data) indicate that detritus was sourced from the northern part of the orogen, including the Ashburton Basin. The uppermost depositional package of the group, Depositional Package 4 (Fig. 7), locally contains felsic volcaniclastic rocks, the deposition of which have been dated at c. 1465 Ma (Wingate et al., 2010), thus providing a minimum depositional date for the group. These felsic volcaniclastic rocks were erupted at the same time as the intrusion of voluminous mafic sills and dykes of the Narimbunna Dolerite, dated to between

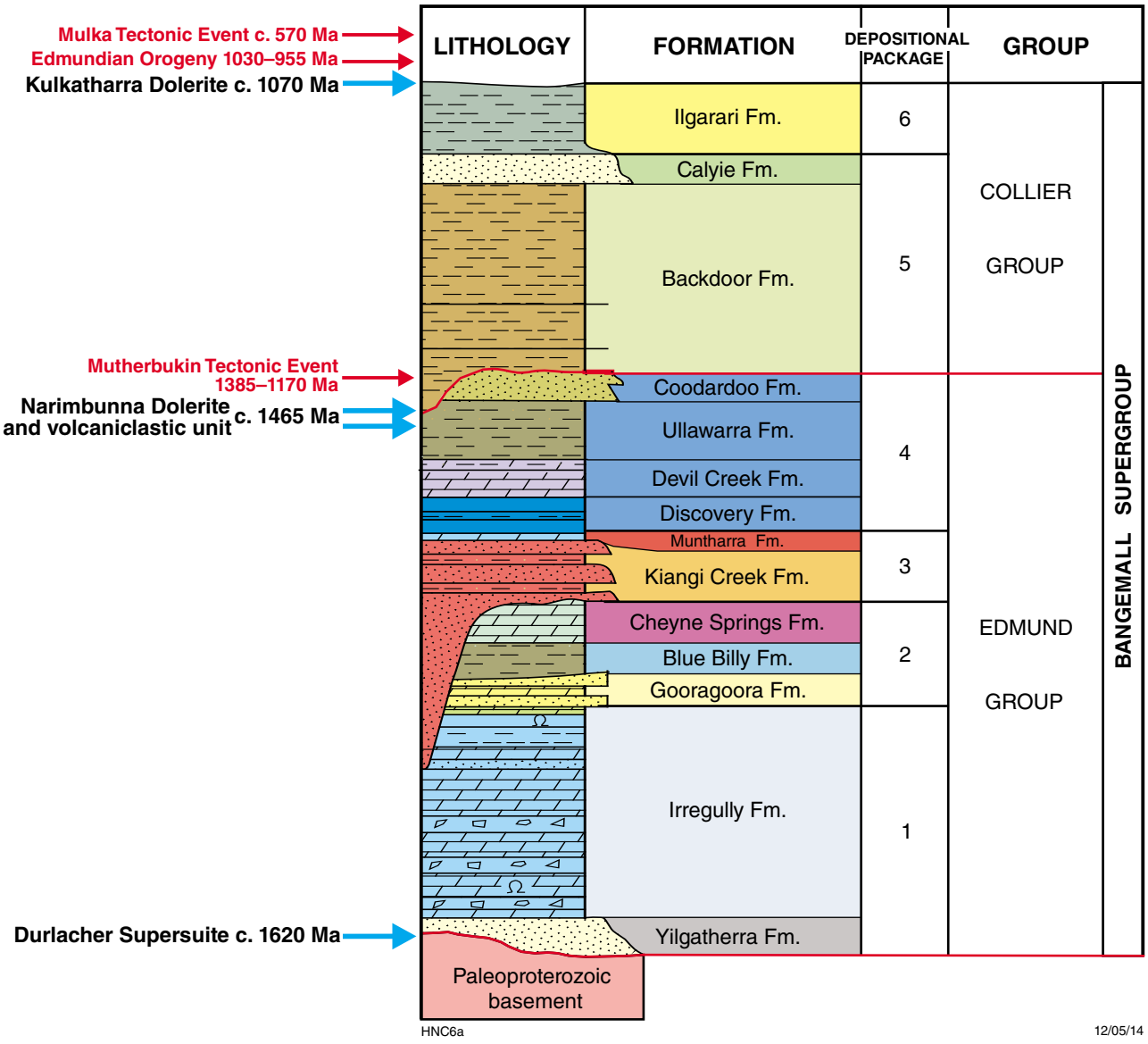

Figure 7. Stratigraphy of the Mesoproterozoic Edmund and Collier Basins; after Martin and Thorne (2004)

c. 1515 and 1465 Ma (Wingate 2002; Wingate et al., 2012), which were emplaced throughout the Edmund Basin (Fig. 2; Morris and Pirajno, 2005). Transpressional reactivation on these major basement faults during the 1385–1170 Ma Mutherbukin Tectonic Event and the 1030–955 Ma Edmundian Orogeny were responsible for folding and faulting in the basin (Martin and Thorne, 2004; Johnson et al., 2013).

Deposition of the Collier Group took place after the 1385–1170 Ma Mutherbukin Tectonic Event, and appears to have been less influenced by significant fault movements (Cutten et al., 2011), although little is known about the architecture of the basin in the east of the orogen where outcrop is more extensive. Paleocurrent analyses combined with the U–Pb date (Martin et al., 2008) and Lu–Hf composition (GSWA, 2011, unpublished data) of detrital zircons imply that detritus was sourced predominantly by the erosion of the underlying Edmund Basin (Martin et al., 2008), possibly because of basin inversion during the Mutherbukin Tectonic Event. Both the Collier and Edmund Basins have been intruded by voluminous mafic sills of the c. 1070 Ma Kulkatharra Dolerite (Figs 2 and 7), which form part of the more regionally extensive Warakurna Supersuite (Morris and Pirajno, 2005). The local presence of peperitic textures in sedimentary rocks of the lowermost Collier Group (Muhling and Brakel, 1985; Martin, 2003; Martin et al., 2008), the Backdoor Formation (Fig. 7), implies that the mafic sills were emplaced into unlithified sediments; thus, deposition of the Collier Basin may have been initiated close to c. 1070 Ma. Transpressional folding and faulting, and basin inversion, took place during the 1030–955 Ma Edmundian Orogeny (Martin and Thorne, 2004).

The northern end of Traverse 1 and most of Traverse 2 transect extensive outcropping sedimentary rocks of the Collier Basin, and presumably sedimentary rocks of the Edmund Basin at depth.

Tectonic evolution of the eastern Capricorn Orogen

Intracratonic reworking during the 1820–1770 Ma Capricorn Orogeny appears to have been the dominant reworking event in the eastern part of the orogen (Occhipinti et al., 1998b,c). The effects of the Capricorn Orogeny include intense structural reworking and intrusion of voluminous syntectonic granitic rocks along the northern Yilgarn Craton margin in the Yarlarweelor Gneiss Complex (Occhipinti et al., 1998b), reactivation of pre-existing faults including intense folding, thrusting, and imbrication of older sedimentary basins with basement rocks, and extensive hydrothermal fluid flow resulting in significant gold and base metal mineralization, for example, at the Plutonic gold deposit (Vielreicher et al., 2002; Gazley, 2011) and the Magellan Pb–Zn deposit (Muhling et al., 2012). The intense structural and magmatic reworking in this region, however, has made it difficult to identify any primary structures associated with the assembly of the West Australian Craton during the 2215–2145 Ma Ophthalmian Orogeny and the 2005–1950 Ma Glenburgh Orogeny. In the west these older events appear to have controlled the style and orientation of most subsequent intracratonic reworking events (Johnson et al., 2011d, 2013).

The 1680–1620 Ma Mangaroon Orogeny encompasses complex deformation, metamorphism, magmatism, and sedimentation. Although structures and metamorphic assemblages associated with this event are mostly constrained to the Mangaroon Zone in the northern part of the Gascoyne Province (Sheppard et al., 2005, 2010a), sedimentation and magmatism took place across a wider part of the orogen. In the eastern part, activity centred on the intrusion of c. 1620 Ma granitic rocks, the Discretion Granite of the Durlacher Supersuite, along the northern margin of the Yilgarn Craton (Sheppard et al., 2010a), fault reactivation and deformation within the Stanley Fold Belt as recorded by c. 1650 Ma $^{40}Ar/^{39}Ar$ mica dates (Pirajno et al., 2009), and the formation of intense shear zones along the southern margin of the Sylvania Inlier (Sheppard et al., 2006). Movement on these shear zones appears to have been synchronous with the deposition of the Bresnahan Group to the west of the Sylvania Inlier (Fig. 1; Sheppard et al., 2006).

The 1385–1170 Ma Mutherbukin Tectonic Event is a recently recognized, and currently poorly defined, event (Rasmussen et al., 2010a; Sheppard et al., 2010a; Johnson et al., 2011b). The effects of deformation and low- to medium-grade metamorphism are primarily recognized within the Mutherbukin Zone of the Gascoyne Province, although sedimentary rocks of the Edmund Group appear to have been affected throughout the orogen (Johnson et al., 2011b). In the eastern part of the orogen, this event is expressed mainly by extensive sinistral, strike-slip faulting and folding of sedimentary rocks of the Edmund Group, although there could have been extensive reactivation of faults between older rock packages. Recent geochronological investigations suggest that the Abra polymetallic Pb–Ag–Cu–Au deposit may have formed, or the primary ore may have undergone secondary upgrading, during this event (Rasmussen et al., 2010a; Cutten et al., 2011).

The 1030–955 Ma Edmundian Orogeny is best known for widespread folding and low-grade metamorphism of the Edmund and Collier Groups (Martin and Thorne, 2004), and for reworking a southeast-striking corridor within the Gascoyne Province (Sheppard et al., 2007). However, much of the intense folding and faulting shown by the Edmund Group sedimentary rocks have now been reassigned to the Mutherbukin Tectonic Event (GSWA, 2014, unpublished data). In the eastern and central parts of the orogen, the Collier Group is only weakly deformed, forming broad, open folds such as those of the Coobarra Dome and Calyie Syncline (Fig. 2), suggesting that the effects of the Edmundian Orogeny are relatively restricted. However, the Collier Group is host to several major copper and base metal deposits, including Kumarina, Ilgarari, and Butcherbird (Fig. 2), suggesting significant syntectonic or post-tectonic hydrothermal fluid flow and mineralization.

Following the Edmundian Orogeny, the Capricorn Orogen was subject to punctuated fault reactivation. Several $^{40}Ar/^{39}Ar$ mica dates of 960–820 Ma have been obtained from various rock units from the Errabiddy Shear Zone and southern Gascoyne Province (Occhipinti, 2007). These dates document low temperature (<325°C) fault and shear zone reactivation, presumably during extensive uplift and unroofing of the southern part of the orogen (Occhipinti, 2007). In the west, fault reactivation took place mostly during the c. 570 Ma Mulka Tectonic Event with the generation of anastomosing, dextral strike-slip shear zones and faults (Sheppard et al., 2010a).

Previous geophysical studies

Prior to the recent deep crustal seismic reflection and MT surveys in the western part of the Capricorn Orogen (Selway, 2007; Selway et al., 2009; Johnson et al., 2011d), numerous geophysical studies were conducted in order to gain information on the subsurface structures in the eastern and central parts of the Capricorn Orogen.

Passive seismic and gravity constraints

The earliest geophysical study of the eastern Capricorn Orogen is the wide-angle refraction seismic work described by Drummond (1979, 1981) and Drummond and Shelley (1981). This work involved modelling travel times of seismic waves created by mining operations and one specifically prepared blast. Of most relevance are data recorded along a traverse from Newman to Meekatharra (section A–B–C in Fig. 1b), which roughly coincides with MT Traverse 2 presented here. The basis of the method is the creation of a model cross-section including variations in seismic velocity, where the model is adjusted iteratively until the calculated travel times match the observations, a form of 'forward' modelling. Studies of this type have far less resolution than those of a typical seismic reflection survey; however, the depth and velocity information is more reliable. With station spacings of around 20 km and shots spaced by hundreds of kilometres, the resolution of the survey is low by the standards of more recent work. Further, due to the availability of seismic sources (blasting at mine sites) at either end of the section, the middle parts of the section are relatively poorly constrained.

Based on the refraction data, Drummond (1979) presented three possible (although fundamentally similar) crustal velocity models for the region (Fig. 8a). Drummond (1979) did not model the sedimentary basins, and the basement was divided into a continuous upper crustal layer with a velocity of 6.0 – 6.2 km/s and a lower crustal layer with velocities of around 6.5 km/s. The work identified two regions with vertical velocity gradients and a zone of high seismic velocity (6.9 – 7.0 km/s) in the south. The structure of the lower crust and the Mohorovičić discontinuity (Moho) is poorly constrained, with wedge-shaped features and displaced (faulted or monoclinal-folded) blocks possible. The mantle has a velocity of around 8.3 km/s, may be slightly higher under the Yilgarn Craton, and is deeper, around 50 km to the south, than around 30 km near Newman.

Reading and Kennett (2003) describe a teleseismic receiver function study where recorders formed a north–south transect across the Capricorn Orogen at about longitude 119°E (green diamonds in Fig. 1b). The study suffered from equipment problems and a lack of earthquakes during the recording window. The results confirmed that the crust is thicker beneath the Yilgarn Craton than the Pilbara Craton (40 vs 30 km) and the Moho is a 'sharp' feature in both places. In the Capricorn Orogen there is almost no response from the Moho, indicating a low contrast in seismic velocity and that the base of the crust coincides with a broad velocity gradient. These results are consistent with those of Drummond (1979), which shows significant lateral and vertical changes in velocity in the lower crust. The available seismic data are of insufficient resolution to map lateral changes in structure in the upper crust, and the lower crust has a complex, albeit unresolved, velocity structure consistent with the complex tectonic and intrusive and metamorphic history of the Capricorn Orogen (Sheppard et al., 2010a; Johnson et al., 2013). Reading et al. (2012) describe additional receiver function work across the western part of the orogen (yellow squares in Fig. 1b). Although there are few stations, the data suggest significant differences in crustal structure between the two cratons and the central part of the orogen, between the craton edges and their centres, and within various parts of the orogen. These differences appear as variations in Moho depth and the nature of the Moho (velocity contrast, sharp vs transitional), and as intracrustal layering. Away from their margins, the cratons appear homogenous; however, layering is present beneath the Proterozoic sedimentary basins and along the craton margins, presumably due to tectonism. The depth to the Moho is about 30 km for the Pilbara Craton and 40 km for the Yilgarn Craton, and it reaches a maximum of about 45 km below the Gascoyne Province. These data suggest the presence of different crustal 'blocks' in the basement to the Capricorn Orogen.

Drummond and Shelley (1981) used the models from Drummond (1979) as a basis for modelling the deep-seated gravity anomalies in the orogen. Isostatic equilibrium is achieved at subcrustal depths. Of particular interest is a high-density (3.03 g/cm^3) feature in the lower crust and adjacent lateral change in density in the mantle at the northern margin of the Yilgarn Craton. Drummond (1981) interpreted these features in terms of a zone of garnet granulite beneath the Yilgarn Craton, possibly an equivalent of the MacAdam Seismic Province identified from seismic reflection data in the western part of the orogen (Fig. 4; Johnson et al., 2011a, 2013; Aitken et al., 2014). The zone of vertical velocity gradients below the Capricorn Orogen is also of high density (3.08 g/cm^3), and this is interpreted as a crustal root of dense rocks. Both features are suggested as the result of Proterozoic underplating. Hackney (2004) modelled a north–south gravity profile across the orogen (section D–E in Fig. 1b) concentrating on the state of isostatic equilibrium. The density model presented (Fig. 8b) also includes an area of thickened crust, a major gravity low, at the southern end of the profile, directly north of the Marymia Inlier (Fig. 8b). This root is interpreted as Pilbara Craton crust that underlies the northern margin of the Yilgarn Craton (Hackney, 2004). A similar feature exists in the

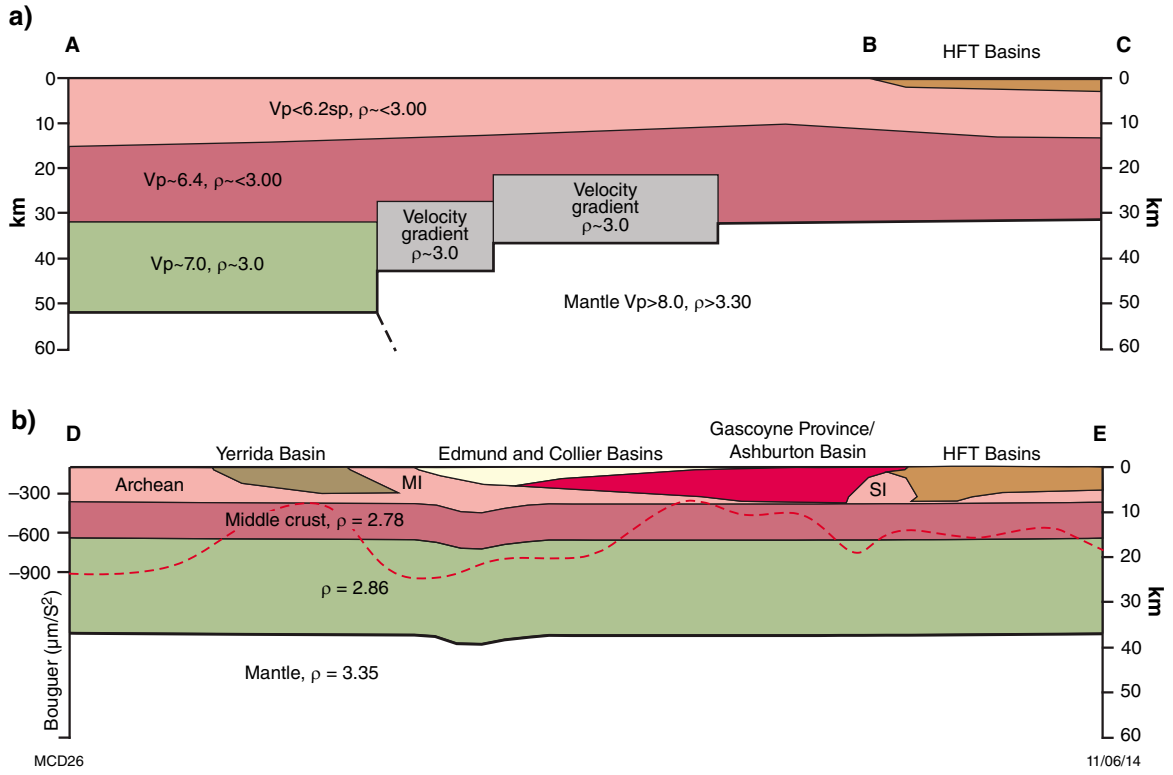

Figure 8. Geophysically derived cross-sections across the Capricorn Orogen: a) seismic velocity; after Drummond (1979). Location of survey shown by section A–B–C in Figure 1b; b) Bouguer anomaly (red broken line); after Hackney (2004). Note only section D–E is shown from model cross-section (D–E–F in Fig. 1). HFT, Hamersley, Fortescue, and Turee Creek; MI, Marymia Inlier; SI, Sylvania Inlier

western part of the orogen where the Glenburgh Terrane and underlying MacAdam Seismic Province have been underthrust beneath the northern Yilgarn Craton during the Glenburgh Orogeny (Fig. 4; Johnson et al., 2011a, 2013).

Previous magnetotelluric surveys

The combined seismic reflection and MT survey in the western Capricorn Orogen (Figs 4 and 9) provide valuable clues about the causes of variations (or not) in electrical conductivity (Heinson et al., 2011; Johnson et al., 2011a; Thorne et al., 2011; red lines 10GA–CP1, 2, 3 in Fig. 1b). The MT data are an extension of a smaller survey described by Selway (2007) and Selway et al. (2009) (orange circles in Fig. 1b). Unfortunately, this smaller survey experienced difficulties during data acquisition and interpretation because most of the data could not be modelled in 2D (Fig. 10). However, the results of this smaller survey (Selway 2007; Selway et al. 2009) imply that both the Pilbara and Yilgarn Cratons are highly resistive and that the Glenburgh Terrane and Gascoyne Province, which lie between the two cratons, form a region of high conductivity (Fig. 10). At the southern end of the survey, highly conductive material is interpreted to underlie the northern margin of the Yilgarn Craton, with the contact roughly coincident with the Errabiddy Shear Zone (Selway 2007; Selway et al. 2009). At the northern end of the survey, the contact between the conductive ?Gascoyne Province with the resistive Pilbara Craton is steep (Fig. 10) and roughly coincident with the Talga Fault (Selway 2007; Selway et al. 2009). Variations in conductivity in the central part of the survey were not imaged due to data acquisition difficulties.

The larger survey, described by Heinson et al. (2011), comprised 40 long-period (station spacing 15 km) measurements and 116 broadband measurements (station spacing 5 km) (Fig. 9). As with the earlier data from Selway et al. (2009), responses were mainly from a 3D conductivity distribution. Responses from that part of the survey north of the Lyons River Fault showed a resistive layer (10^3 Ωm) to about 2 km depth underlain by an unexpectedly conductive layer (10 Ωm) (Fig. 9). The higher conductivity is tentatively interpreted as caused by the presence of magnetite, presumably associated with iron formations of the Hamersley Group. The electrical structure below about 10 km depth cannot be reliably derived in this area. South of the Lyons River Fault, the crust is much more resistive (~10^4 Ωm), as expected in cratonic crust. The boundary between the two regions, the Lyons River Fault, dips southward and correlates closely with the seismically inferred northern margin of the Glenburgh Terrane (Figs 4 and 9). In the south, the higher resistivity allows recognition of thin zones of higher conductivity, which correlate with known major

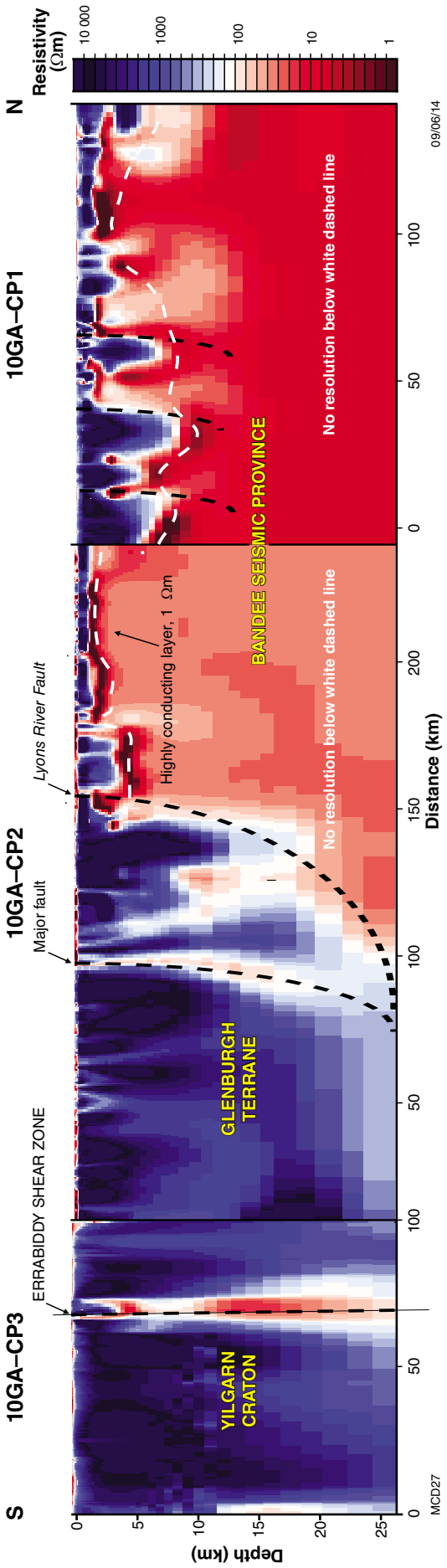

Figure 9. Results of the magnetotelluric (MT) survey across the western part of the Capricorn Orogen, coincident with the reflection seismic survey (location as 10GA–CP1, 2, and 3 in Fig. 1b); after Heinson et al. (2011)

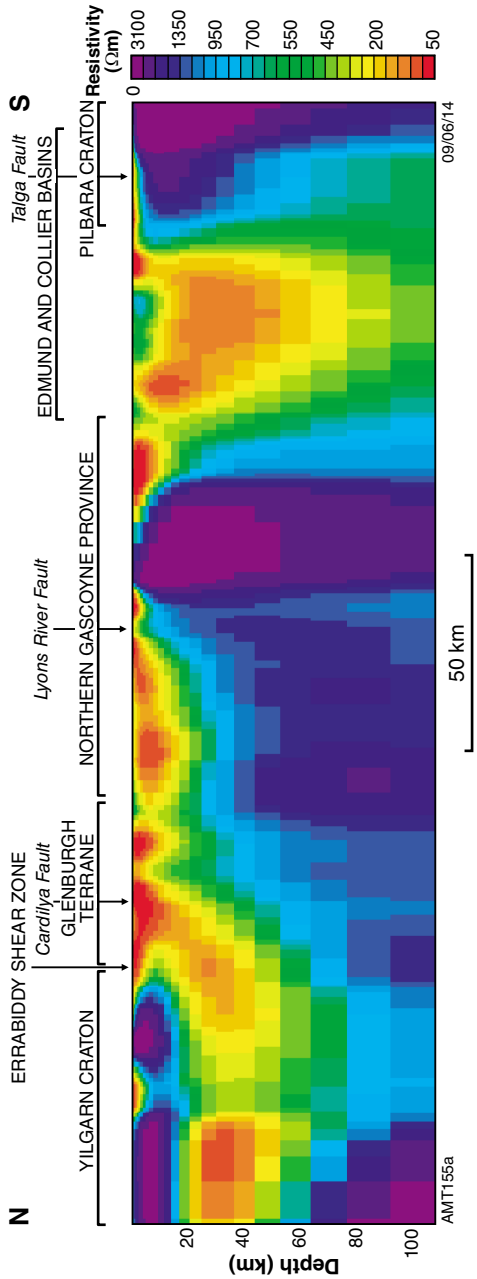

Figure 10. Results of the magnetotelluric (MT) survey across part of the western Capricorn Orogen (Selway, 2007); location shown as orange circles in Figure 1b

faults. The best example of this is the Errabiddy Shear Zone, which is a 10 km-wide zone of low resistivity that extends down to at least 25 km. In general, the dip of these conductive features is much steeper than was derived from the seismic reflection data and their positions are poorly matched (Figs 4 and 9), probably due to the resolving limitations of the MT method, and also modelling the data in 2D.

Both previous MT surveys (Selway 2007 and Selway et al. 2009; Heinson et al., 2011) have produced different and contradictory results, with sections of each model reproducing different parts of the interpreted seismic reflection data (Fig. 4). For example, the survey by Heinson et al. (2011) highlights the position and orientation of the contact between the Glenburgh Terrane and the Bandee Seismic Province along the Lyons River Fault (Fig. 9), whereas the survey by Selway (2007) and Selway et al. (2009) reproduce the contact between the Glenburgh Terrane and the Yilgarn Craton along the Cardilya Fault and Errabiddy Shear Zone in exquisite detail (Fig. 10).

Implications of previous geophysical studies

Despite the numerous geophysical surveys in the eastern part of the Capricorn Orogen, the deep crustal structure is still poorly known. In the west, where the architecture is better constrained, most of the major crustal structures are shown to dip moderately to the south, and the Pilbara and Yilgarn Cratons are separated by the Glenburgh Terrane (Johnson et al., 2011a, 2013; Fig. 4). However, based on passive seismic and gravity data modelling, this may not be the case farther east. Furthermore, the previous geological and geophysical studies have some important implications for the interpretation of the MT data presented here:

- Several sedimentary basins in the eastern part of the orogen may contain strata that are highly conductive. These units may greatly reduce the depth penetration of the MT data. The Johnson Cairn and Maraloou Formations of the Yerrida Basin are likely conductive, as are the Blue Billy and Discovery Formations (Figs 6 and 7) of the Edmund Basin, and the Ilgarari Formation of the Collier Basin.

- The interpretation of the seismic reflection data includes three 'seismic provinces' (Johnson et al., 2011a, 2013). These provinces are defined by differences in reflection character and are apparently distinct from geological entities that outcrop. This interpretation, along with the inferred presence of the Glenburgh Terrane and Hamersley Group (Fig. 4) in the middle crust, suggest lateral changes in middle to lower crustal conductivity, as is seen, for example, in the southern Yilgarn Craton (Dentith et al., 2013).

- The western Capricorn MT data (Heinson et al., 2011) show there is a marked conductivity contrast between the Yilgarn Craton – Glenburgh Terrane (resistive) and the Pilbara Craton (conductive), suggesting this feature may be mappable in the eastern part of the Capricorn Orogen.

- The contradictory interpretation of the MT and seismic reflection data compared to the earlier MT survey of Selway (2007) and Selway et al. (2009), and the restricted conclusions that can be drawn from the extended MT dataset coincident with the seismic reflection profile, serves as a warning of the difficulty of interpreting MT in isolation in a complex 3D conductivity environment.

Magnetotelluric survey

Data acquisition

The MT survey across the eastern Capricorn Orogen was conducted to provide information on the deep crustal architecture of this part of the orogen. The data were collected in a single campaign in May 2011 by personnel from Moombarriga Geoscience, the Centre for Exploration Targeting at The University of Western Australia, and the Geological Survey of Western Australia. The survey used 42 broadband receiver stations, each of which recorded data for between 22 and 51 hours, with an average station recording time of 42.6 hours. Coordinates and recording times for all stations are given in Table 1.

Figure 11 illustrates the equipment layout at each MT station. Two (horizontal) components of the electric field and three components of the magnetic field variation were measured at each site. Data were recorded using Phoenix Ltd MTU-5A data recorders with MTC-50 magnetic induction coils. The coils are very sensitive to noise and this is reduced by burying them, a non-trivial task for a vertical coil approximately 2 m long. Electric dipoles and horizontal coils were installed in magnetic north–south and east–west azimuths, and the electric dipoles at all sites were approximately 100 m long. The electric field was measured using non-polarizing ($Pb/PbCl_2$ solution) electrodes. These consist of a container with a porous base filled with an electrolyte solution, which provides electrical contact with the ground.

Traverse 1 (Fig. 2) mainly follows an unsealed road, crossing the Great Northern Highway a few kilometres south of the Plutonic mine. The stations were a few hundred metres from the road to reduce responses associated with infrastructure and traffic. Traverse 2 (Fig. 2) follows the Great Northern Highway, and again stations were located away from the road to reduce acoustic noise.

Although the survey sites were all relatively flat, they had several potential sources of cultural electromagnetic noise. The main source of data noise is caused by vehicles travelling on the Great Northern Highway. Other potential sources are the Goldfields gas pipeline (which runs subparallel to much of the survey), the Plutonic mine and associated power lines, and electric fences near the Great Northern Highway.

Table 1. Locations and recording times of magnetotelluric (MT) stations

Site	*Latitude*	*Longitude*	*Elevation (m)*	*Deployment time (GMT)*	*Extraction time (GMT)*	*Duration (hours)*
Traverse 1						
MRY001A	–25°56'35.76"	+120°06'44.16"	563	5 May 2011 5:25	7 May 2011 0:22	43
MRY001B	–25°56'35.76"	+120°06'44.16"	565	7 May 2011 2:00	9 May 2011 0:18	46
MRY002A	–25°51'41.64"	+120°03'26.10"	559	5 May 2011 8:00	7 May 2011 2:08	42
MRY003A	–25°47'53.70"	+119°59'50.04"	569	5 May 2011 9:10	7 May 2011 2:38	41
MRY004A	–25°44'57.54"	+119°55'01.98"	577	6 May 2011 4:00	8 May 2011 1:35	46
MRY005A	–25°41'06.06"	+119°48'27.36"	543	6 May 2011 6:50	8 May 2011 2:19	43
MRY006A	–25°37'58.56"	+119°44'52.08"	544	7 May 2011 5:30	8 May 2011 23:42	42
MRY006A	–25°37'58.50"	+119°44'52.08"	541	9 May 2011 9:00	10 May 2011 23:56	39
MRY007A	–25°34'35.10"	+119°41'09.54"	560	7 May 2011 7:30	9 May 2011 1:06	42
MRY008A	–25°32'32.76"	+119°38'54.96"	570	8 May 2011 6:00	10 May 2011 0:53	43
MRY009A	–25°30'40.38"	+119°36'43.14"	578	8 May 2011 7:20	10 May 2011 1:20	42
MRY010A	–25°28'48.48"	+119°34'38.70"	585	9 May 2011 3:50	10 May 2011 21:27	42
MRY011A	–25°27'01.50"	+119°32'33.24"	604	9 May 2011 5:00	11 May 2011 1:04	44
MRY012A	–25°25'32.16"	+119°30'07.86"	604	10 May 2011 3:30	12 May 2011 3:29	48
MRY013A	–25°24'21.06"	+119°27'24.30"	586	10 May 2011 4:30	12 May 2011 4:05	48
MRY014A	–25°22'46.50"	+119°24'55.08"	565	11 May 2011 3:00	12 May 2011 22:35	44
MRY015A	–25°20'56.64"	+119°22'26.16"	553	11 May 2011 4:30	13 May 2011 2:09	46
MRY016A	–25°19'06.90"	+119°20'30.42"	546	11 May 2011 6:00	13 May 2011 1:26	43
MRY017A	–25°17'11.46"	+119°18'32.46"	541	12 May 2011 7:00	14 May 2011 0:27	41
MRY018A	–25°14'28.56"	+119°16'23.46"	532	12 May 2011 8:30	14 May 2011 1:17	41
MRY019A	–25°12'27.84"	+119°14'36.96"	525	13 May 2011 6:00	15 May 2011 0:57	43
MRY020A	–25°10'37.38"	+119°12'43.56"	516	13 May 2011 7:30	15 May 2011 1:16	42
MRY021A	–25°07'54.84"	+119°09'45.00"	517	13 May 2011 9:00	15 May 2011 0:34	40
Traverse 2						
MRY022A	–25°11'42.78"	+119°19'30.72"	542	14 May 2011 3:00	16 May 2011 0:25	45
MRY023A	–25°06'29.76"	+119°21'42.18"	541	14 May 2011 4:20	16 May 2011 0:54	45
MRY024A	–25°00'57.00"	+119°24'16.56"	550	15 May 2011 4:00	17 May 2011 0:03	44
MRY025A	–24°55'56.70"	+119°27'06.78"	559	15 May 2011 5:00	17 May 2011 1:02	44
MRY026A	–24°50'44.04"	+119°28'33.30"	571	15 May 2011 6:30	17 May 2011 1:34	43
MRY027A	–24°44'33.60"	+119°31'32.58"	638	16 May 2011 4:00	18 May 2011 0:38	45
MRY028A	–24°41'06.78"	+119°35'05.52"	620	17 May 2011 3:00	19 May 2011 0:32	46
MRY029A	–24°36'07.56"	+119°37'04.80"	650	16 May 2011 7:00	18 May 2011 1:48	43
MRY030A	–24°31'05.52"	+119°38'07.56"	638	17 May 2011 5:30	19 May 2011 1:30	44
MRY031A	–24°25'56.94"	+119°40'02.70"	611	17 May 2011 7:30	19 May 2011 2:09	43
MRY032A	–24°20'30.36"	+119°42'05.22"	626	18 May 2011 3:30	20 May 2011 1:25	46
MRY033A	–24°15'40.32"	+119°43'09.78"	619	18 May 2011 4:30	20 May 2011 1:54	45
MRY034A	–24°09'11.82"	+119°41'31.56"	602	21 May 2011 2:00	23 May 2011 5:13	51
MRY035A	–24°04'36.84"	+119°43'30.18"	589	19 May 2011 6:00	21 May 2011 0:53	43
MRY036A	–23°59'24.60"	+119°45'37.74"	627	19 May 2011 6:50	21 May 2011 1:43	43
MRY037A	–23°53'34.44"	+119°45'23.10"	619	20 May 2011 4:00	21 May 2011 23:26	43
MRY037B	–23°53'34.44"	+119°45'23.10"	623	23 May 2011 5:00	24 May 2011 3:04	22
MRY038A	–23°48'07.26"	+119°43'28.20"	623	20 May 2011 5:00	21 May 2011 15:32	35
MRY038B	–23°48'07.26"	+119°43'28.20"	625	23 May 2011 4:15	24 May 2011 2:40	22
MRY039A	–23°42'46.14"	+119°44'28.20"	610	22 May 2011 3:40	24 May 2011 2:14	47
MRY040A	–23°36'53.40"	+119°45'35.40"	580	22 May 2011 4:30	24 May 2011 1:46	45
MRY041A	–23°31'18.66"	+119°45'48.48"	559	21 May 2011 4:50	23 May 2011 0:30	44
MRY042A	–23°25'58.68"	+119°48'05.76"	523	21 May 2011 6:40	23 May 2011 1:11	43

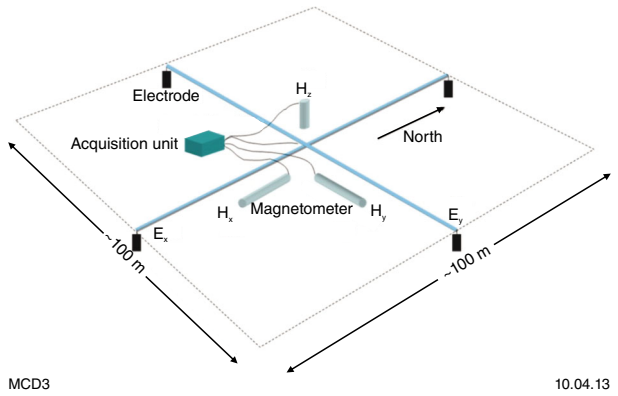

Figure 11. Schematic illustration of equipment set-up at each magnetotelluric (MT) station. *E*, electric field sensor; E_x, north–south component; E_y, east–west component; *H*, magnetic field sensor; H_x, H_y, horizontal magnetic field components; H_z, vertical *H* component

Electromagnetic soundings of the near surface at each station were made using a Monex Geoscope TerraTEM transmitter and receiver. A 100 m-sided square transmitter loop (transmission area = 10 000 m^2) was used with sides oriented north–south/east–west. The TRC-3 three-component receiver coil had an equivalent area of 1000 m^2. The TerraTEM 'intermediate' time series was used (135 channels between 0.0015 and 1900 ms). Four or more soundings were made at each site. Visual checks were made to ensure these data were self-consistent and not obviously noisy, with additional soundings made if necessary.

Data processing

Variations of the electric and magnetic field components are recorded as a function of time; thus, these data comprise time series and are in the 'time domain'. The MT data are subsequently converted to the 'frequency domain'. This conversion enables parameters of interest to be calculated as a function of frequency (or period) and subsequently used to model electrical property variations as a function of depth.

Examples of partial electric and magnetic field time series from two stations (Traverse 1, station 12 and Traverse 2, station 36) are shown in Figure 12. Station 12 is close to the centre of Traverse 1, and station 36 is north of the centre of Traverse 2. The time series were checked in the field to ensure that there had been adequate variation in the geomagnetic field for the data to be useful, and also to check that the equipment had been deployed correctly. Electric field measurements are designated *E*, and the north–south component is termed E_x and the east–west component, E_y. Magnetic field components are designated as *H*, with the same notation, plus H_z defining the vertical component.

Time-series data were processed using robust remote-reference algorithms supplied by Phoenix Ltd. Algorithms are based on the coherence-sorted cascade decimation method of Wight and Bostick (1981) and the heuristic robust approach of Jones and Jödicke (1984). Remote reference processing (Gamble et al., 1979) compares recordings from different locations to identify noise in the time series, while the coherence-based methods are based on statistical comparison of the various time series. A recording station simultaneously collecting data within the traverse was used as the remote reference.

Frequency–domain MT responses

Figure 13 shows a portion of the same datasets as shown in Figure 12 after being transformed into the frequency domain. Two parameters are shown: apparent (electrical) resistivity and phase as a function of period. Note that electrical resistivity (ρ; 'Rho' on Fig. 13) is the reciprocal of electrical conductivity.

In general, data quality from the east Capricorn Orogen survey is very good, as indicated by the small errors bars for station 12 up to periods of about 1000 s (Fig. 13). The data from station 36 are slightly variable as indicated by the scatter beyond about 300 s, although data are still of acceptable quality. A complete set of apparent resistivity and phase curves is shown in the Appendix.

The apparent resistivity values for each period were calculated in terms of the electric (*E*) and magnetic (*H*) fields:

$$\rho = \frac{1}{\omega\mu}\left|\frac{E}{H}\right|^2 \qquad \text{Equation 1}$$

where $\omega = 2\pi f$ is the angular frequency of the fields and μ is the magnetic permeability of the Earth. The ratio of the two fields is used to determine the impedance ($Z = E/H$), a measure of the opposition to the flow of alternating electric currents. As shown by Equation 1, apparent resistivity is related to the square of the impedance.

The MT impedance tensor contains four complex-valued transfer functions (Z_{xx} etc.) between the various orthogonal components of the horizontal electric and magnetic fields (Equation 2). Each MT impedance term can be used to estimate an apparent resistivity, which is a volumetrically averaged resistivity over the penetration depth of the signals.

$$\begin{bmatrix} Z_{xx} & Z_{xy} \\ Z_{yx} & Z_{yy} \end{bmatrix} \begin{bmatrix} H_x \\ H_y \end{bmatrix} = \begin{bmatrix} E_x \\ E_y \end{bmatrix} \qquad \text{Equation 2}$$

If the Earth's electrical structure is 1D (i.e. the Earth consists of a horizontally layered structure and hence only varies in one direction) or 2D (varies in two directions) with the *x*-direction parallel to strike and *y*-perpendicular, then $Z_{xx} = Z_{yy} = 0$. If the strike is known the data can be rotated accordingly, in which case the non-zero Z_{xy} and Z_{yx} impedance can be used to determine apparent resistivity as a function of frequency using Equation 1 where ρ_{xy} uses E_x and H_y and ρ_{yx} uses E_y and H_x (Equation 3). After rotation, *xy* data are called the transverse electric (TE)

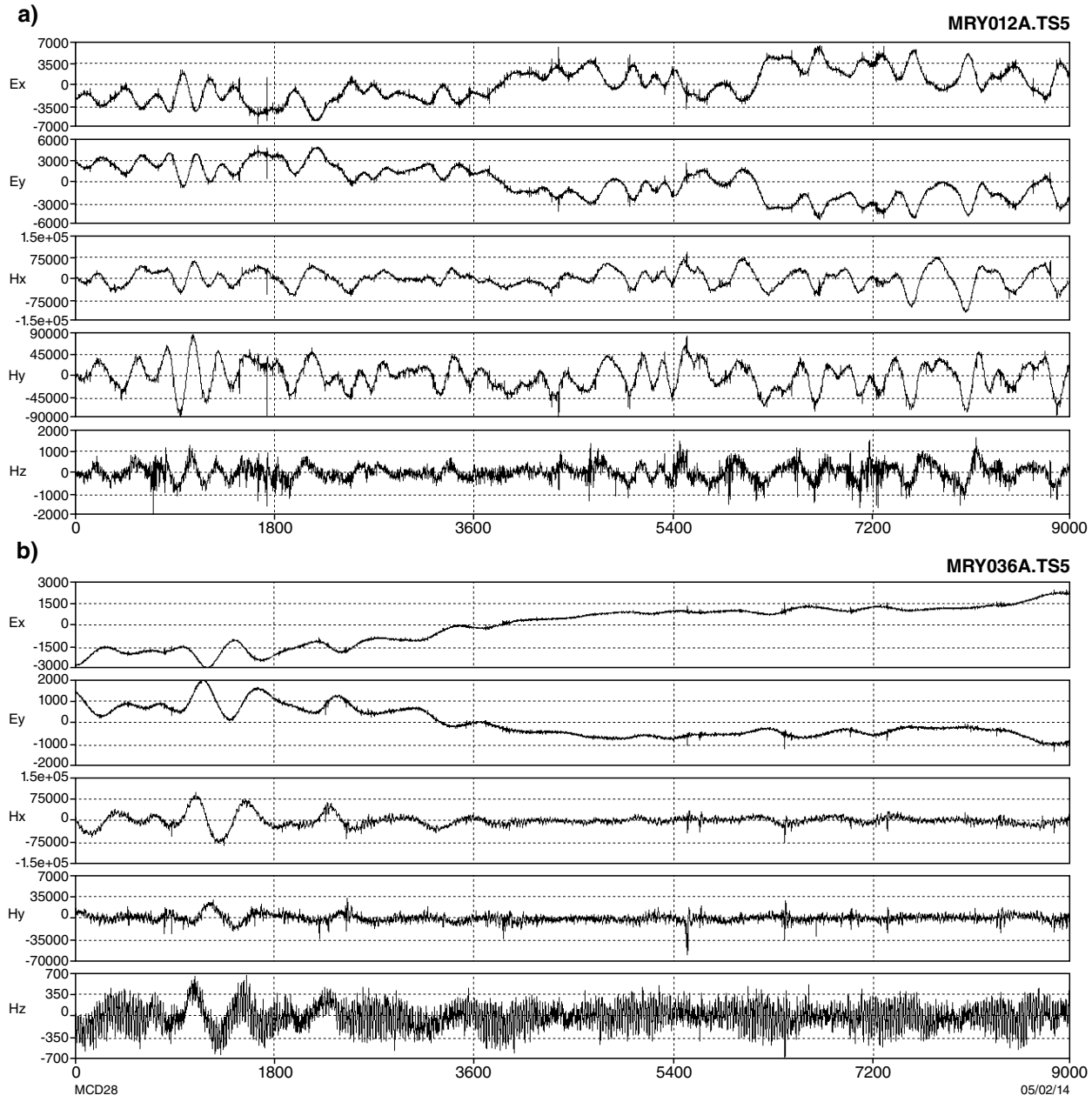

Figure 12. Examples of magnetotelluric (MT) time series from two stations for a 10-minute time segment of data; a) Traverse 1, station 12; b) Traverse 2, station 36. Units are micro Volts (μV) for electric (*E*) field data and nano Tesla (nT) for magnetic (*H*) field data.

mode, and *yx* is transverse magnetic (TM). In the TE mode the electric field is parallel to strike and the magnetic field is perpendicular. In the TM mode, the magnetic field is parallel to strike and the electric field is perpendicular.

$$\rho_{xy} = \frac{1}{\omega\mu}\left|\frac{E_x}{H_y}\right|^2 \qquad \rho_{yx} = \frac{1}{\omega\mu}\left|\frac{E_y}{H_x}\right|^2 \qquad \text{Equation 3}$$

Also important is the phase difference (ϕ) between the two fields: ϕ = arctan(E/H). The phase is defined as the lead of the electric field over the magnetic field.

Static corrections

MT data are prone to 'static shifts' caused by heterogeneous electrical properties in the near surface at a scale smaller than the resolving capability of the MT data (Dennis et al., 2011). The result is a frequency-independent shift, so that the entire curve is involved, of the apparent resistivity data parallel to the apparent resistivity axis. The amount of shift is called the static shift factor(s). Failure to account for this will lead to incorrect estimation of resistivities and the depths at which they occur during data modelling.

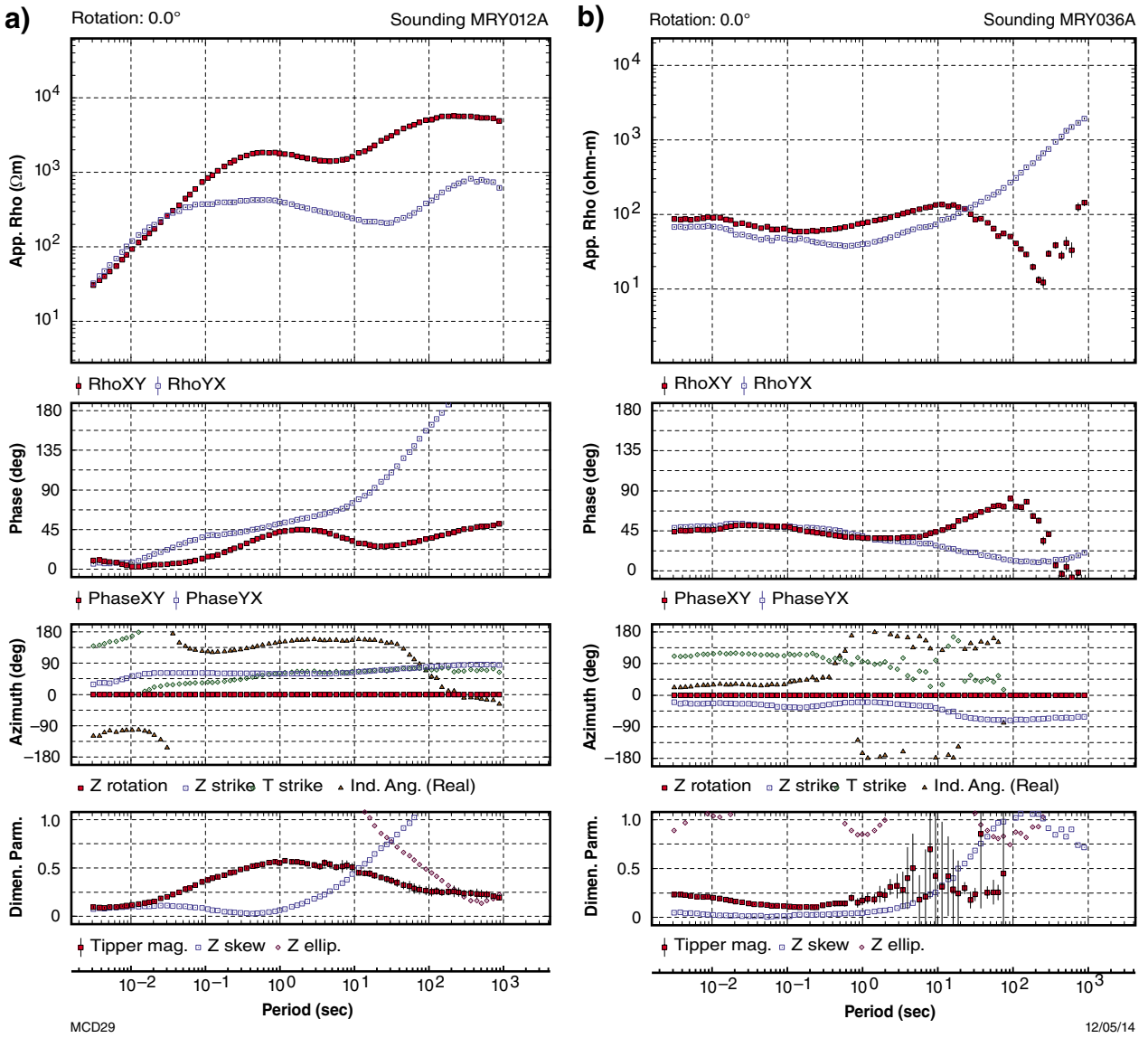

Figure 13. Examples of magnetotelluric (MT) soundings from the same two stations as Figure 12; a) Traverse 1, station 12; b) Traverse 2, station 36. Red symbols show the *xy* response and blue symbols show the *yx* response. Note the increased errors as the data approaches the longest periods (greatest depths).

There are various approaches to account for static shift. For example, the shift may be treated as an unknown variable in the data modelling. Alternatively, and as used here, static shifts were estimated using the time-domain (TD) electromagnetic soundings where available. These data were inverse-modelled to derive a two- or three-layered 1D Earth model that is consistent with the observed TD data. This model was then used to forward-model an MT response, which was compared with the observed MT data. The MT curves are translated so that they overlie the TD data. To achieve this comparison with accuracy, the time domain-derived and MT data curves must overlap. For the east Capricorn Orogen survey data, curves typically overlapped.

All the equivalent MT curves derived from the TD soundings are shown in the Appendix. The static shift factor dictates whether the apparent resistivity curves are moved up ($s > 1$) or down ($s < 1$). The mean *xy* static shift factor was 1.32, and for the *yx* data, 1.14.

Dimensionality and geoelectric strike

Most MT modelling algorithms assume the area of interest is geoelectrically 1D or 2D. In the 'normal' 2D modelling scenario, the direction of geoelectric strike is assumed consistent; that is, there must not be any localized, or off-profile, geoelectric property variations, and the strike direction must be known. The frequency-dependent variations in impedance are also used to determine electrical dimensionality and geoelectric strike direction of the subsurface.

The dimensionality of the MT data was assessed using the phase-tensor method of Caldwell et al. (2004). Unlike many other dimensionality estimation methods, this method evaluates only the phase variations because they are unaffected by galvanic distortions associated with near-surface changes in electrical conductivity. Also, the method does not rely on assumptions that the regional electrical structure is 1D or 2D.

The phase tensor is characterized by the maximum and minimum phase values, and the skew angle (β). The angle α is a measure of the tensor's orientation relative to the coordinate system and the ellipticity is a measure of the ratio of the maximum (Φ_{max}) and minimum (Φ_{min}) phase values. The phase tensor is commonly represented as an ellipse (Fig. 14), with the long and short axes of the ellipse representing the maximum and minimum phase values, respectively, and the orientation (α–β) of the major axis representing the direction of maximum current flow. A 1D subsurface will be represented by a circle. With the influence of two-dimensionality, the ellipticity increases. A 3D subsurface results in a skewed ellipse with the main axis deflected by an angle β from the symmetry axis (dashed line in Fig. 14).

Figure 15 shows phase tensor ellipses for each station in the east Capricorn Orogen survey for periods ranging from 0.01 to 1000 s (100 to 0.001 Hz). Shading is according to invariant minimum phase. The phase tensor ellipses show heterogeneous behaviour in both orientation and ellipticity as a measure of the ratio between the magnitudes of the maximum and minimum current flow for short periods less than one second. The minimum phase values are typically less than 45°, suggesting an increase in resistivity with depth (Caldwell et al., 2004). The subsurface as imaged by the short-period band between 0.01 s to less than 1 s can be described by a dominant 1D resistivity distribution, as shown by the mostly circular form of the ellipses (and hence no preferred current flow direction). An exception is the northern part of Traverse 2 (stations 38–42) and the central part of Traverse 1 (stations 8–15). Here, a strong resistivity contrast from electrically conductive to resistive is suggested by the very low minimum phase values.

Traverse 1 is characterized by a rapid change in minimum phase values for short periods (<1s) and shows a bimodal behaviour in the ellipse orientations around a central pivot point near station 10 for periods longer than 1 s. To the northwest, the phase tensors point north–south and rotate east–west to the east of the station 10.

The positive magnetic anomalies around station 25 (at the northern margin of the Marymia Inlier) on Traverse 2 are associated with a response in the impedance tensor at periods greater than 1 s. For periods longer than 10 s, the source of the magnetic anomaly has changed the orientation of the phase ellipses, and reduced the minimum phase in the northerly direction. Furthermore, the ellipses are strongly polarized along the northwest–southeast plane for all stations to the north for periods longer than 100 s (lower crustal depths).

Figure 16 shows phase tensors within a pseudosection presentation (a form of cross-sectional display where period is used as a pseudo-depth parameter). The colour of the individual ellipses is the skew value (β). Empirically, $-5° < \beta < 5°$ (yellow ellipses) indicates the data is predominantly 2D; however, red and blue ellipses indicate significant 3D characteristics. Both traverses have a strong 3D component of response. For Traverse 1, all data less than a period of 10 s are 3D, and a large fraction of the data at the northwest end are 3D to periods of 0.1 s. Traverse 2 is more consistent, as all recordings below 10 s are 3D.

The rose diagrams for the two traverses support the results of the phase tensor analysis (Fig. 17). At upper crustal levels (period <10 s), there is no preferred strike direction present due to the predominant 1D nature of the sediments and the heterogeneous nature of the upper crust. The strike angle as defined by Weaver et al. (2003) shows a preferred orientation of N60°E in the middle crust for periods around 1 s, rotating to N100°E in the lower crust and upper mantle (>100 s).

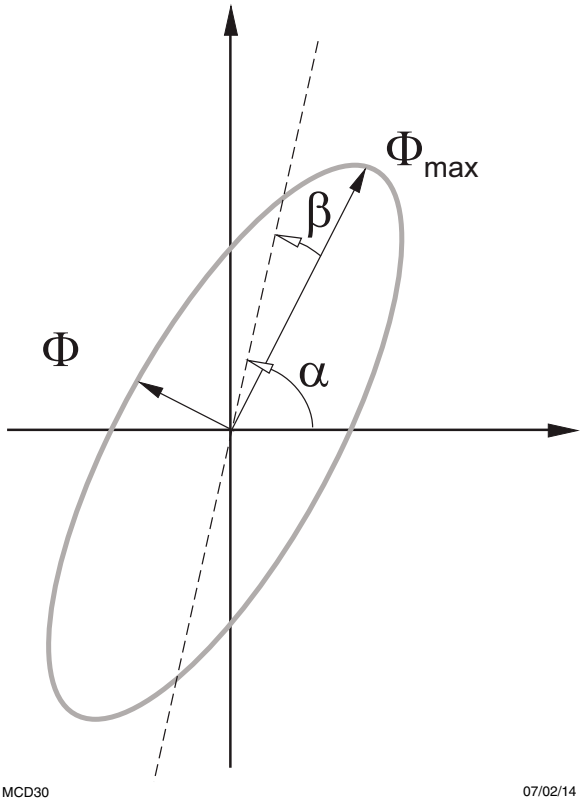

Figure 14. Graphical representation of the MT phase tensor illustrating parameters used to define the ellipse, from Caldwell et al. (2004). Angle α is a measure of the tensor's orientation relative to the coordinate system, β is the skew angle, dashed line is skew axis of a skewed ellipse, and the ellipticity is a measure of the ratio of the maximum (ϕ_{max}) and minimum (ϕ_{min}) phase values.

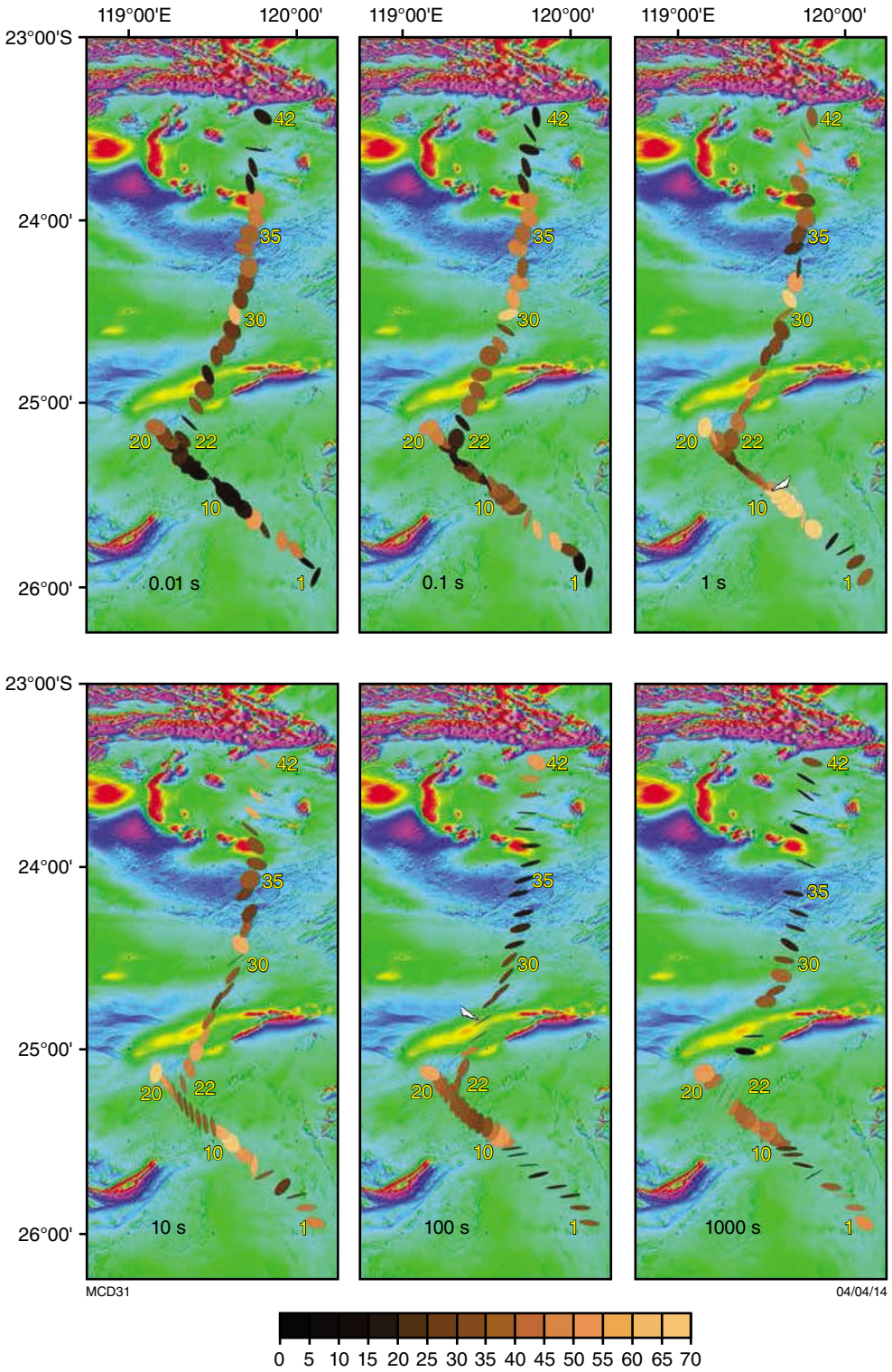

Figure 15. Phase ellipses for each MT station for six different periods. Ellipses are overlain on a total magnetic intensity (TMI) aeromagnetic image. Numbers show recording station positions.

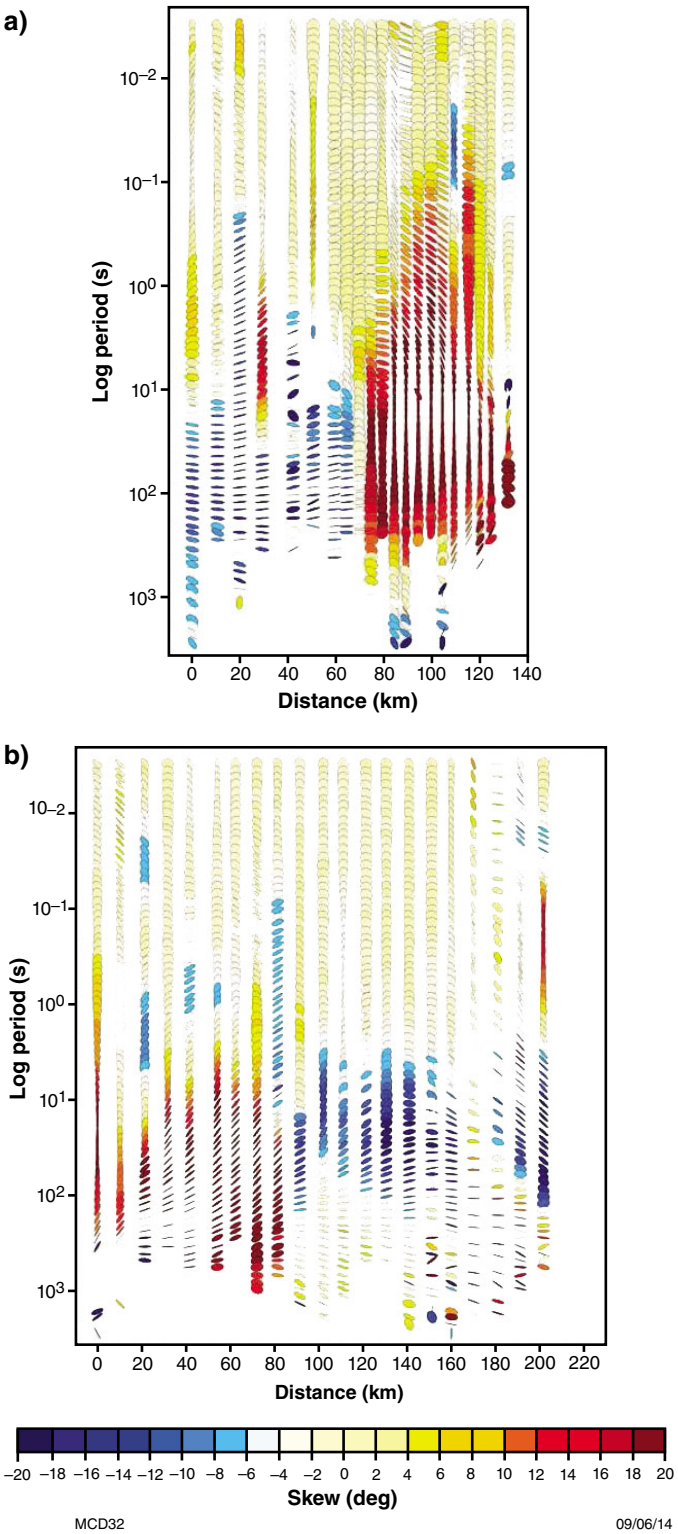

Figure 16. Pseudosection display of MT phase tensor data for distances along the traverse for: a) Traverse 1; and b) Traverse 2. The colour of the individual ellipses is the skew value (β); yellow ellipses indicate the data are predominantly 2D; red and blue ellipses indicate significant 3D characteristics

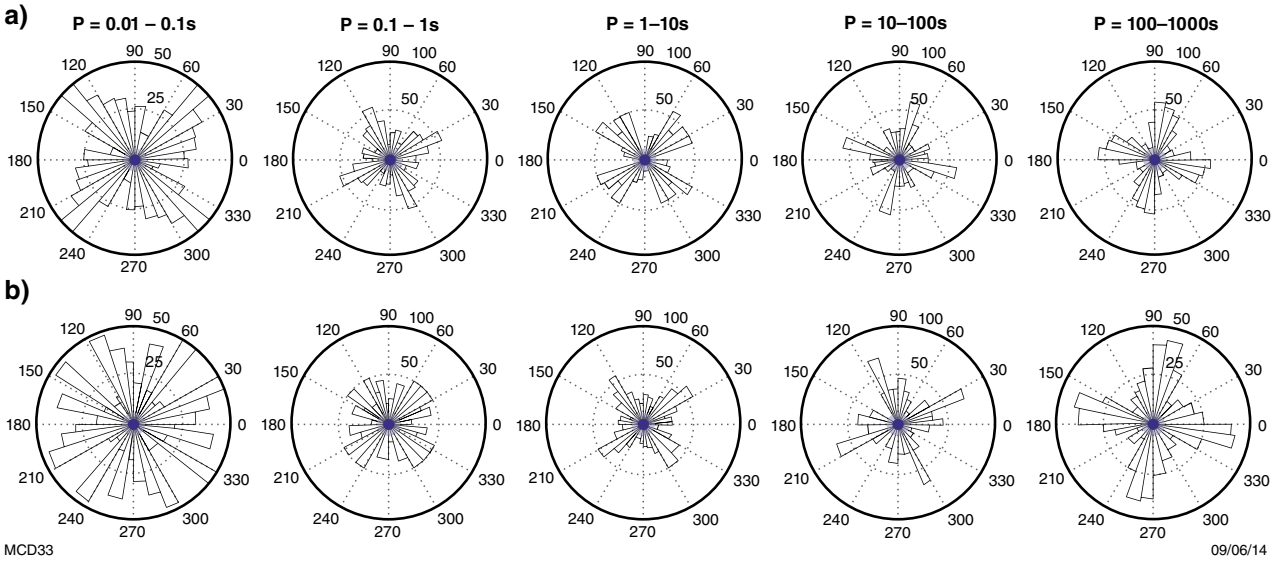

Figure 17. Rose diagrams showing the strike direction from phase tensor analysis for various periods (P): a) Traverse 1; b) Traverse 2. Strike directions are from *E* = 0. For Traverse 1 strike orientation is undefined for periods <0.1 s although it is west-southwest – east-northeast for crustal depths trending due east–west in the lower crust and upper mantle. For Traverse 2, strike direction is west-southwest – east-northeast for periods between 0.1 and 10 s and rotates to about east–west at lower crustal and upper mantle depths.

Data modelling

Figures 18 and 19 for Traverses 1 and 2, respectively, show TM and TE mode pseudosections of apparent resistivity and phase for all data points assessed as not overly noisy. Figures 20 and 21 show equivalent data for Traverses 1 and 2, respectively, after removal of data affected by 3D conductivity variations, with absolute skew less than 5°. The data are reasonably consistent in terms of station-to-station correlation, although the loss of data due to 3D responses is significant.

The apparent resistivity results allow an estimate of the depth to which the 2D data penetrate. The skin depth (δ) of electromagnetic fields is the distance over which the electromagnetic field's amplitude is reduced by 1/e of its surface value (i.e. 37%). This measured skin depth depends on the frequency of the fields and conductivity of the medium, as the amplitude of the electromagnetic field decreases exponentially. Skin depth is calculated where μ is the magnetic permeability of a homogenous medium (Henry/m), σ is conductivity in S/m, f is frequency in Hertz and the skin depth is in metres (Equation 4).

$$\delta = \frac{1}{\sqrt{\pi \mu \sigma f}} \qquad \text{Equation 4}$$

The magnetic permeability of most rocks is nearly the same as that in a vacuum ($\mu \times \mu_0 \times 4\pi \times 10^{-7}$ Henry/m), providing they are not highly magnetic (such as banded iron-formations) in the subsurface, allowing the expression to be written as Equation 5.

$$\delta = \frac{503.8}{\sqrt{\sigma f}} \qquad \text{Equation 5}$$

As noted previously, data from Traverse 1 are largely 3D at periods greater than 1 and 10 s (1–0.1 Hz; Figs 18 and 20), and those of Traverse 2 tend to 3D at periods greater than 10 s (0.1 Hz; Figs 19 and 21). Resistivities in the non-3D parts of the data are mostly in the range 20 to 500 Ωm. Table 2 lists the equivalent skin depths.

Skin depth and resistivity (Table 2) suggest that data from Traverse 1 are only useful to upper crustal depths at best. The data from Traverse 2 are useful at deeper levels, and only in the more resistive areas is the information relevant to depths below the mid-crust (given the seismically derived thickness of the crust in the area is around 40 km).

The 2D inversions of the data were created using the 2D non-linear conjugate gradient inversion algorithm of Rodi and Mackie (2001) as implemented in the WinGLink software (GEOSYSTEM SRL, 2008). Given the lack of responses from deeper conductivity variations, inversion was also undertaken using the entire TM mode dataset in an attempt to derive more depth information. The rationale for this approach is that TM data are typically less susceptible to 3D effects than TE mode data. In all cases the modelled conductivity variations showed poor compatibility with the known geology.

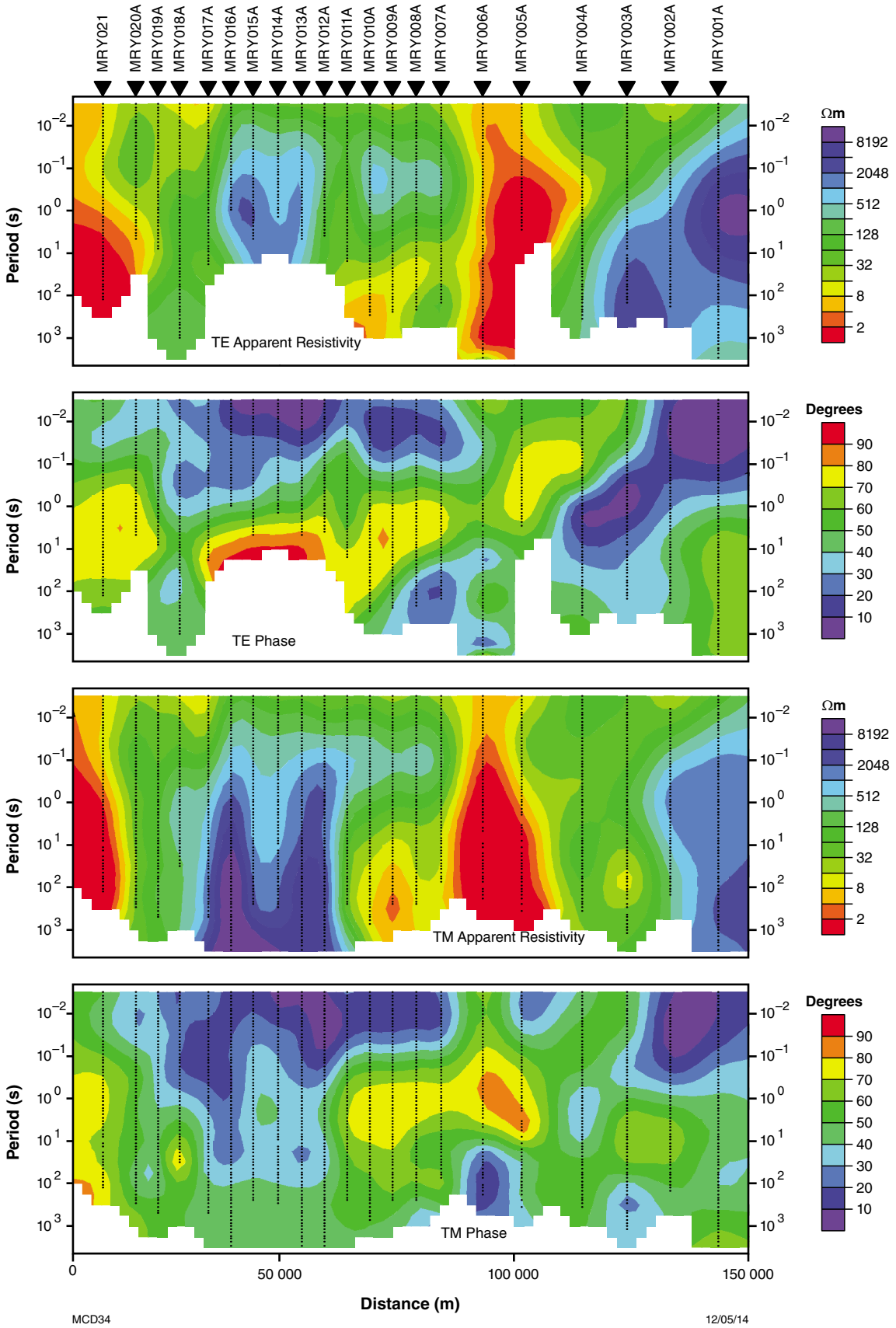

Figure 18. Pseudosections for Traverse 1 comprising data (both TE and TM modes) considered to have acceptable signal-to-noise ratios

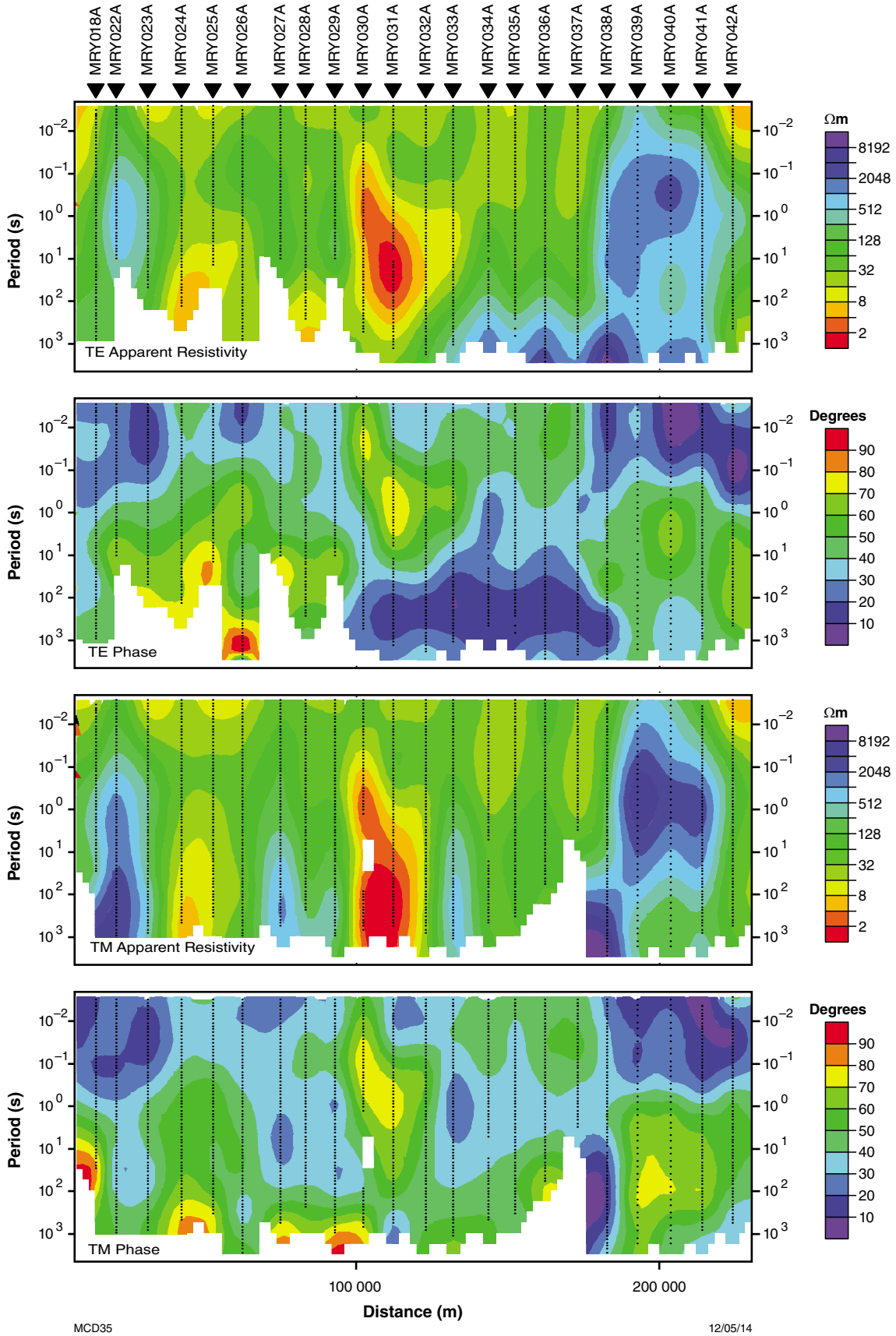

Figure 19. Pseudosections for Traverse 2 comprising data (both TE and TM modes) considered to have acceptable signal-to-noise ratios

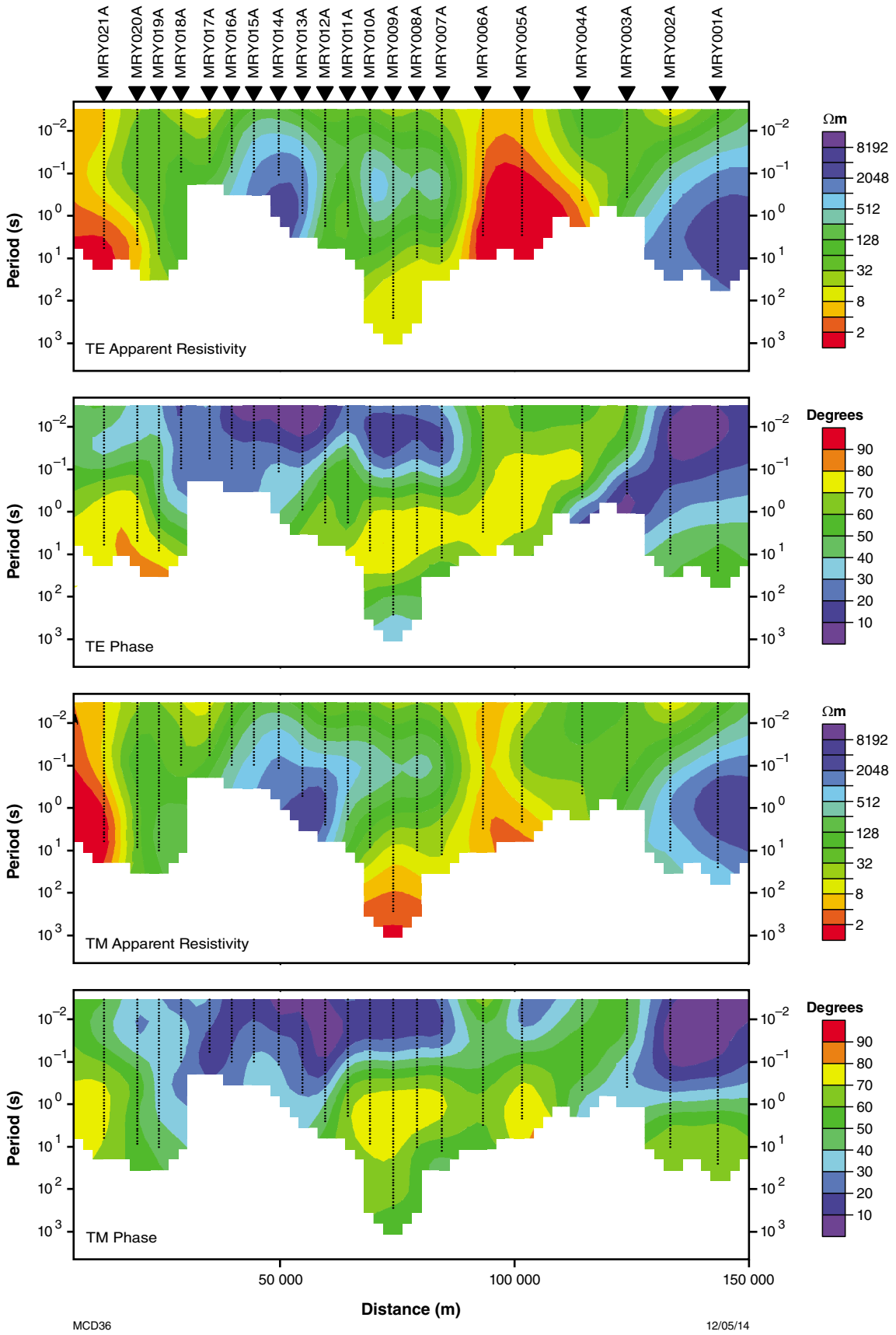

Figure 20. Pseudosections for Traverse 1 comprising data (both TE and TM modes) considered to have acceptable signal-to-noise ratios and no significant 3D influence as defined by the skew (β); –5° < β <5°

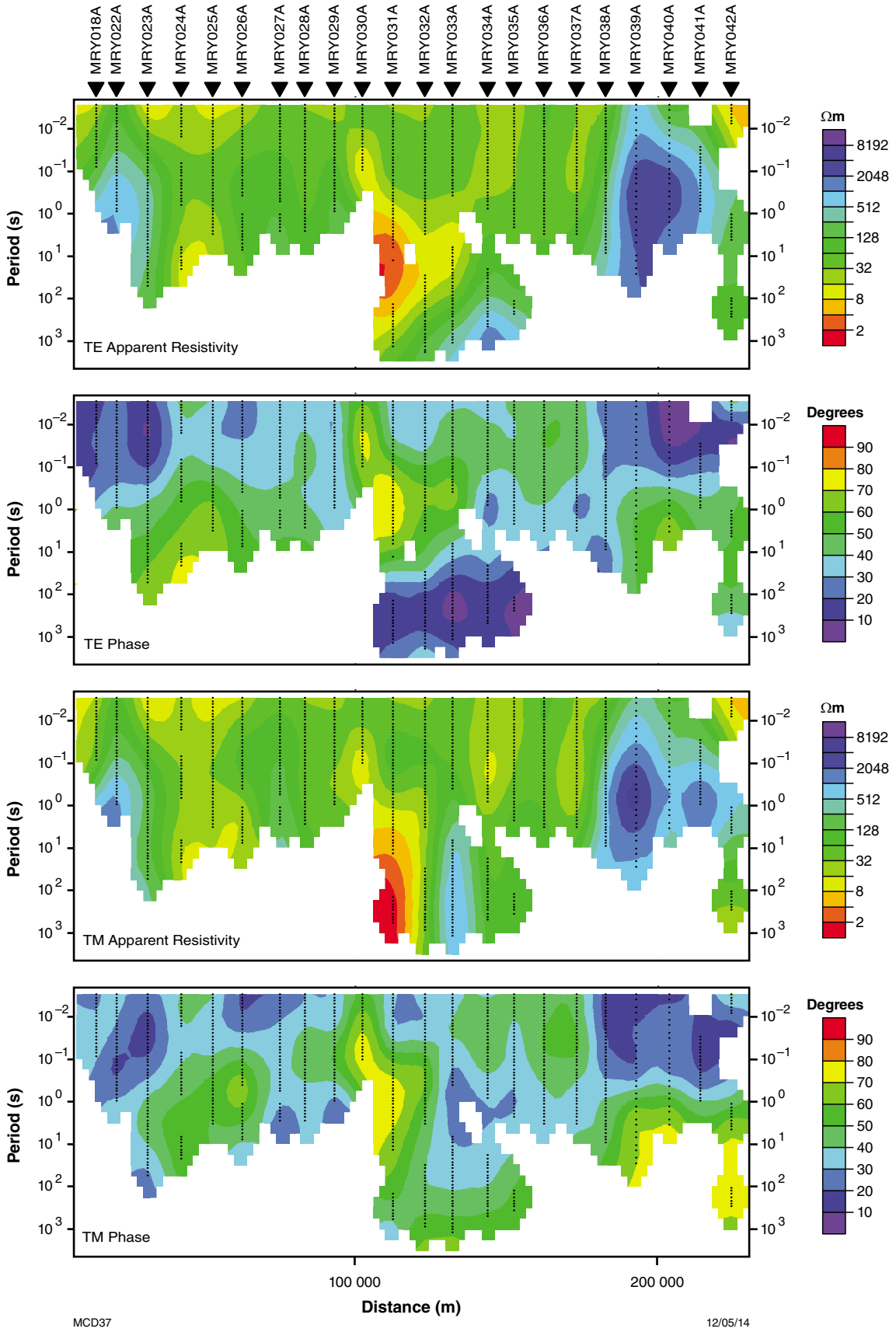

Figure 21. Pseudosections for Traverse 2 comprising data (both TE and TM modes) considered to have acceptable signal-to-noise ratios and no significant 3D influence as defined by the skew (β); –5° < β <5°

Table 2. Equivalent skin depth for selected frequencies and average resistivities

	Resistivity (Ωm)			
	20	*50*	*200*	*500*
Skin depth (m) at 1 s (1 Hz)	2 253	3 563	7 128	11 270
Skin depth (m) at 10 s (0.1 Hz)	7 127	11 270	22 540	35 638

3D modelling

The high contribution from 3D geoelectric variations to the data, and the general poor correspondence with known geology shown by the 2D modelling results, prompted trials using a 3D inversion algorithm. This 3D inversion is computationally intensive so repeated modelling of the data, for example for feature testing, is impractical. The data were processed at Leicester University using the algorithm described by Avdeeva and Avdeeva (2009). The data were modelled as a conductivity volume of 700 × 320 × 200 km (108 voxels × 44 voxels × 24 voxels), which fully encompasses the locations of the stations comprising the two traverses. Voxel dimensions were 3 km in the horizontal directions and varied from 500 m at the top of the volume to 25 m at its base. The starting model was one-half-space with a resistivity of 170 Ωm. The data were modelled at 12 periods: 0.43, 0.85, 1.7, 3.4, 6.85, 13.7, 27.03, 54.65, 108.7, 217.4, 436.7, and 877.2 s.

Initial results produced a poor fit to the data for periods greater than 100 s. Reweighting to try to improve the fit made little difference to the final result, although it reduced the overall root mean square (RMS) fit from about 3 to about 2.5. Figure 22 shows RMS values for different periods for each station.

Conductivity variations from 3D modelling

The results of the 3D modelling are shown in Figure 23. The results are vertical planar slices through the inverted conductivity volume that were selected so as to approximate the two traverses. The surface geology is shown above each section.

Traverse 1

The southeastern end of Traverse 1 lies on the Yilgarn Craton (Fig. 2), which appears as a region of high resistivity (labelled '1', white number, on Fig. 23). To the northwest, the Marymia Inlier also forms a resistive region (6; Fig. 23). Between the Yilgarn Craton and Marymia Inlier, the surface geology is dominated by Proterozoic sedimentary rocks of the Yerrida and Earaheedy Basins, which are shown in the survey as subhorizontal layers of variable resistivity (2, 3 and 5; Fig. 23). These flat-lying conductivity variations are displaced or truncated by steeply dipping structures.

Within the Marymia Inlier, a relatively narrow conductive layer that dips shallowly to the southeast may be a greenstone belt or a fault. The northwestern margin of the inlier appears to dip moderately towards the northwest beneath a flat-lying highly conductive layer (7) that coincides with sedimentary rocks of the Backdoor and Ilgarari Formations (Depositional Packages 5 and 6; Fig. 23) in the Collier Basin.

Conductivity also varies greatly in the mid to lower crust. The zone of high resistivity below the Yilgarn Craton (1) may be continuous with a resistive zone at depth (17) beneath the conductive Proterozoic basins. These two resistive zones are separated by a zone of moderate conductivity (9), which may be a fault. A zone of moderately northwest-dipping conductivity (8) separates resistive zones (17) and (6). Conductivity variations below zones of high conductivity, such as those of (3) and (5), are poorly constrained in MT surveys. However, deep conductive zones (i.e. 8) present where shallow conductors are absent, may be more reliable. Thus, the resistive zone (17) may be an artefact, whereas the conductive zone (8) may be reliable.

Traverse 2

The southern half of the traverse is almost entirely in sedimentary rocks of the Collier Basin, and for the five southernmost stations, runs close to the northern boundary of the Marymia Inlier (Fig. 2). At the southern end of the traverse, the Marymia Inlier is present as a resistive zone (10; Fig. 23) equivalent to that imaged in Traverse 1 (6). The northern margin of the inlier also appears to dip moderately northwards, beneath a prominent north-dipping zone of high conductivity (20).

The middle part of the traverse is defined by a series of shallow, moderate- to highly conductive zones (11, 15) which are most likely graphitic-rich sedimentary packages within the Edmund (15) and Collier Basins (11). The conductive feature (11) is underlain by a flat to shallow-dipping resistive layer, which may be the lower parts (Depositional Packages 1–3) of the Edmund Basin. The stratigraphy is dissected by numerous steeply dipping structures (Fig. 23).

The most prominent feature of Traverse 2 is the moderately north-dipping zone of high conductivity (20) that lies beneath station 25 (Fig. 23). The source of this feature does not appear exposed at the surface, which has been mapped as shallow-dipping sedimentary rocks of the Collier Basin (Fig. 2; Blay et al., 2014).

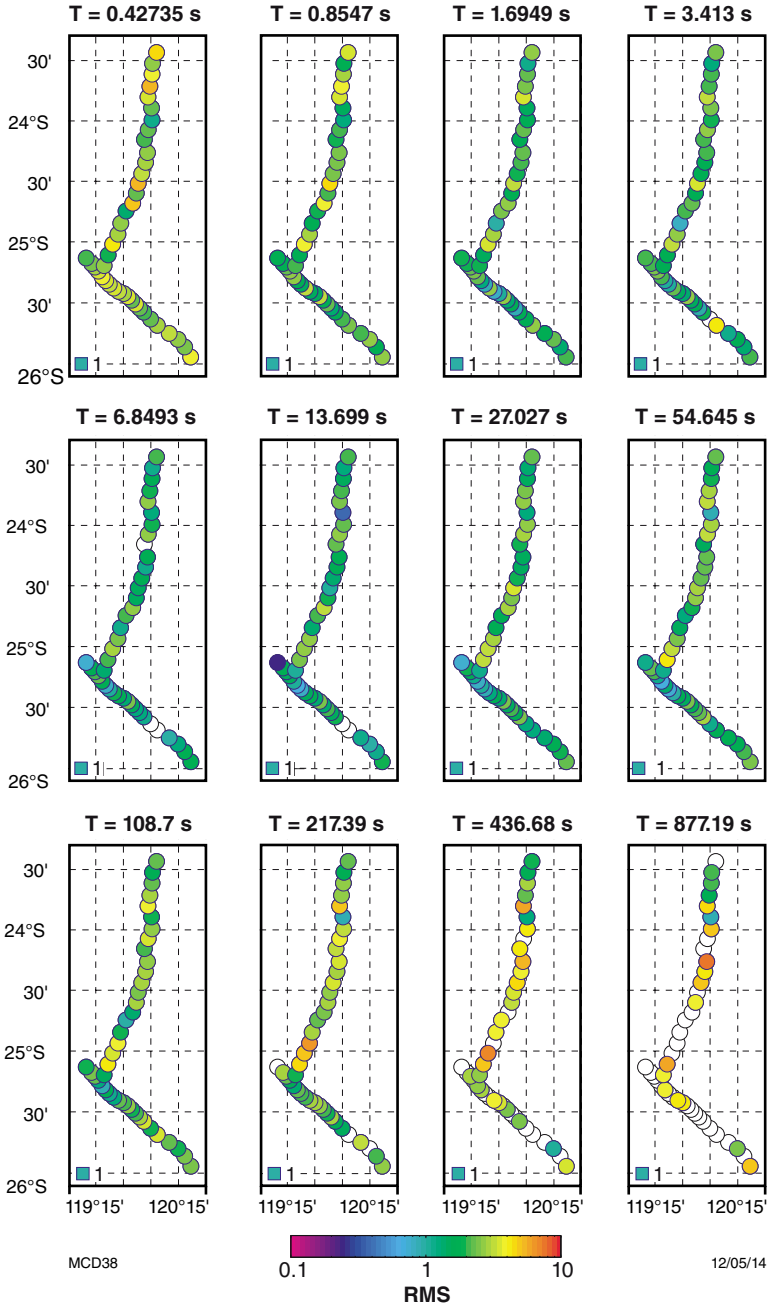

Figure 22. Root mean square (RMS) misfit values plotted as function of MT site number and period for the results of 3D inverse modelling after reweighting

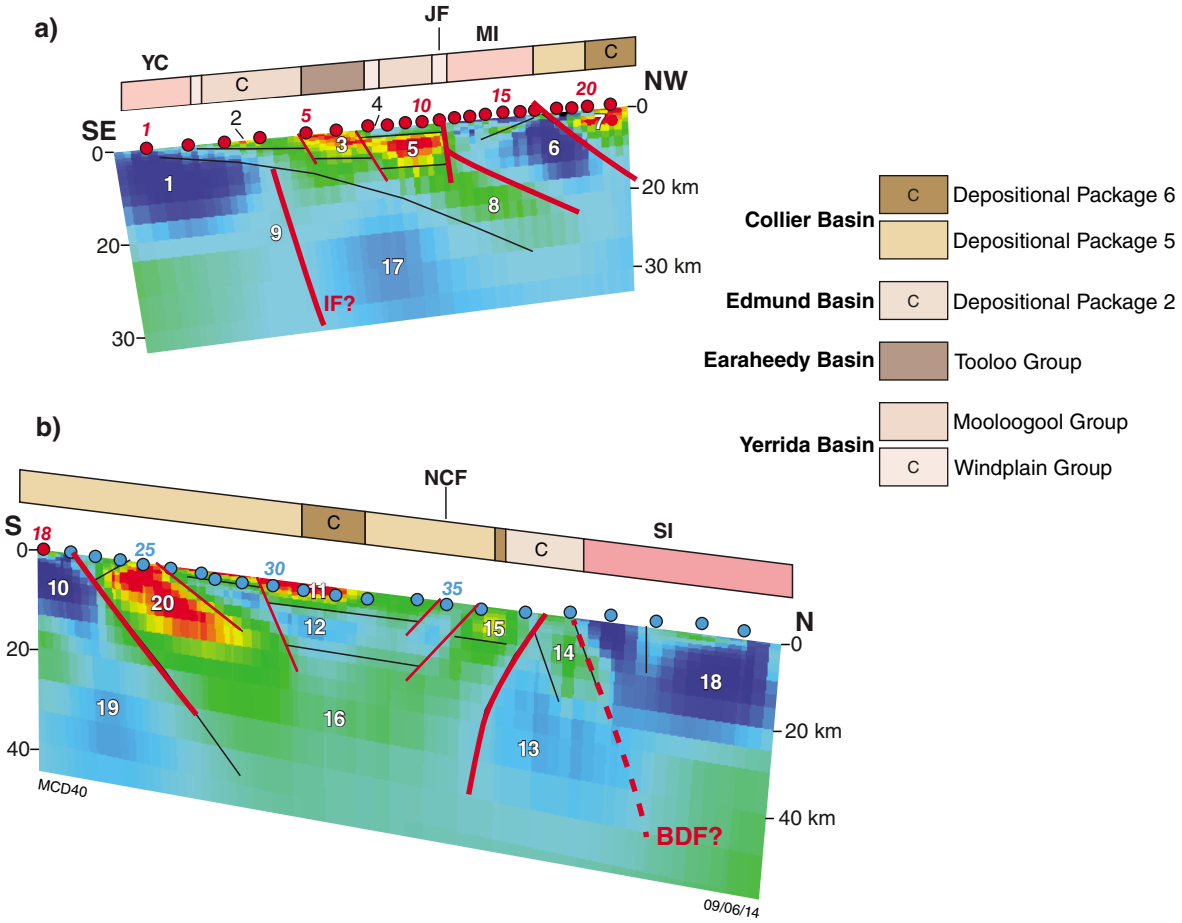

Figure 23. Preferred 3D electrical resistivity inversion results for: a) Traverse 1; and b) Traverse 2. White and black numbers refer to electrical features discussed in the text; numbers associated with red and blue circles across the tops of the traverses are measurement stations. BDF, Baring Downs Fault; IF, Ida Fault; JF, Jenkin Fault; MI, Marymia Inlier; NCF, Neds Creek Fault; SI, Sylvania Inlier; YC, Yilgarn Craton. Lithological units marked with 'C' indicate significant components or horizons of graphitic-rich material.

The northern part of Traverse 2 is defined by a prominent resistive zone (18), which is the Sylvania Inlier, that is, the Pilbara Craton (Fig. 23). The southern margin of this resistive zone is marked by a moderately north-dipping zone of high conductivity (14) that penetrates into the middle crust, where it is underlain by another region of high resistivity (13). The significance of the conductive layer (14) is unclear, as the rocks at the surface form part of a shallow-dipping succession of metasedimentary rocks from the lower part of the Edmund Group. It is possible that the conductive zone defines a moderately north-dipping fault or shear zone between the southern edge of the Pilbara Craton and another block to the south. Alternatively, resistive zones (18) and (13) may form a coherent part of the Pilbara Craton, suggesting that the conductive zone (14) is an intracratonic feature and not a major crustal structure.

The deep crustal conductivity structure of Traverse 2 can be divided into three main zones (Fig. 23). At the ends of Traverse 2, two resistive zones (13 and 19) are separated by a central region of high conductivity (16). Resistive zone (19) forms the northern extension of the Yilgarn Craton beneath the Marymia Inlier and is equivalent to resistive zone (17) in Traverse 1. The southern margin of the Pilbara Craton (13) has a steep south-dipping contact with the broad conductive zone (16) that underlies most of the central part of the traverse.

Feature testing

Three relatively conductive zones in the deep crust of Traverses 1 and 2 are considered significant to the tectonic interpretation (zones 8, 9, and 16 in Fig. 23). To test whether these zones were required by the model, the resistivities in these areas were increased, and the change to the RMS fit to the data increased substantially (Fig. 24). Changing the resistivity of zone 8 greatly affected the fit to the data at periods between 1 and 55 s, so this feature is considered reliable. The effect on zone 9 is less, although noticeable. Being deeper, the change to zone 16 affected the long-period data (50–100 s), increasing the RMS fit and so is also considered reliable.

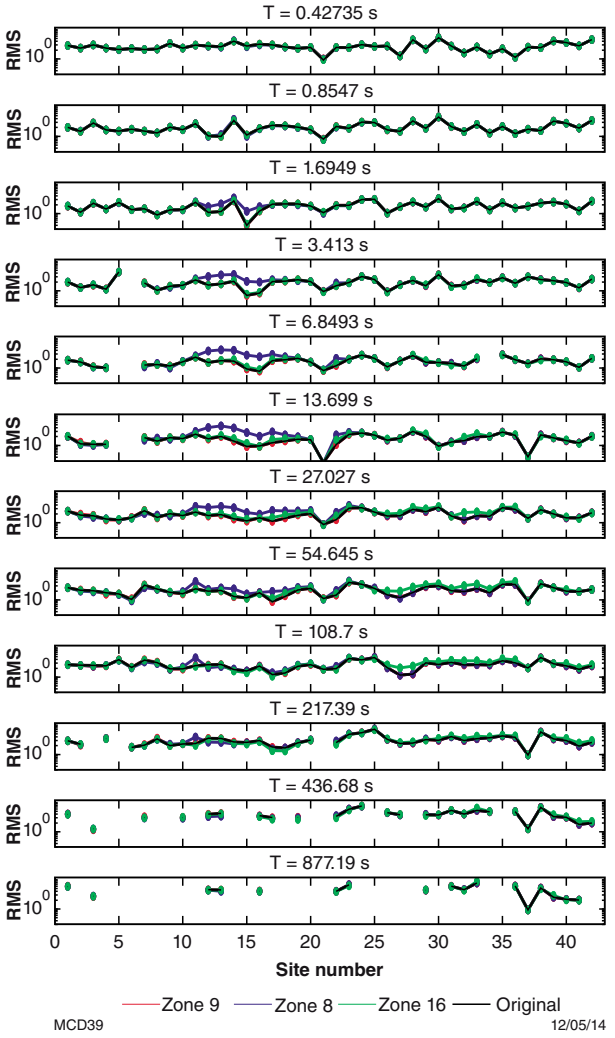

Figure 24. Feature testing of the results of the 3D inversion. Zones 8, 9, and 16 are conductive areas of the model (see Fig. 23).

Discussion

Confidence in the 3D MT model

The Capricorn Orogen is a challenging environment for MT surveying (Selway, 2007; Selway et al., 2009; Heinson et al., 2011). The data described here show substantial 3D electrical conductivity variations in the subsurface, and 2D modelling of these data produced results that are difficult to reconcile with the known geology. The situation is also complicated by high electrical conductivity of some units in the Proterozoic basins, due to their high graphite and sulfide contents. However, 3D modelling of the data has produced geologically plausible results and the broad-scale crustal architecture is well defined (Figs 23 and 25). The survey produced similar conductivity patterns (i.e. resistive to mildly conductive cratons and moderate to highly conductive orogenic belts) to those of Selway (2007) and Selway et al. (2009) farther west (Figs 1b and 10), and also with other MT surveys within Australia (Aitken et al., 2013a; Dentith et al., 2013; Milligan et al., 2013). However, the results of the MT survey conducted along the Capricorn Orogen seismic reflection line (Heinson et al., 2011) are significantly different (Figs 1b and 9); the reasons for this difference are currently unknown.

The results of wide-angle refraction seismic work (Drummond 1979, 1981; Drummond and Shelley, 1981) along a line almost coincident with this survey (line A–B–C in Fig. 1b) imply thicker, denser crust beneath the Marymia Inlier of the Yilgarn Craton, and shallower crust beneath the Pilbara Craton (Fig. 8a). These results are supported by a regional gravity profile across the orogen (Hackney 2004; Fig. 8b), and the calculated mean crustal

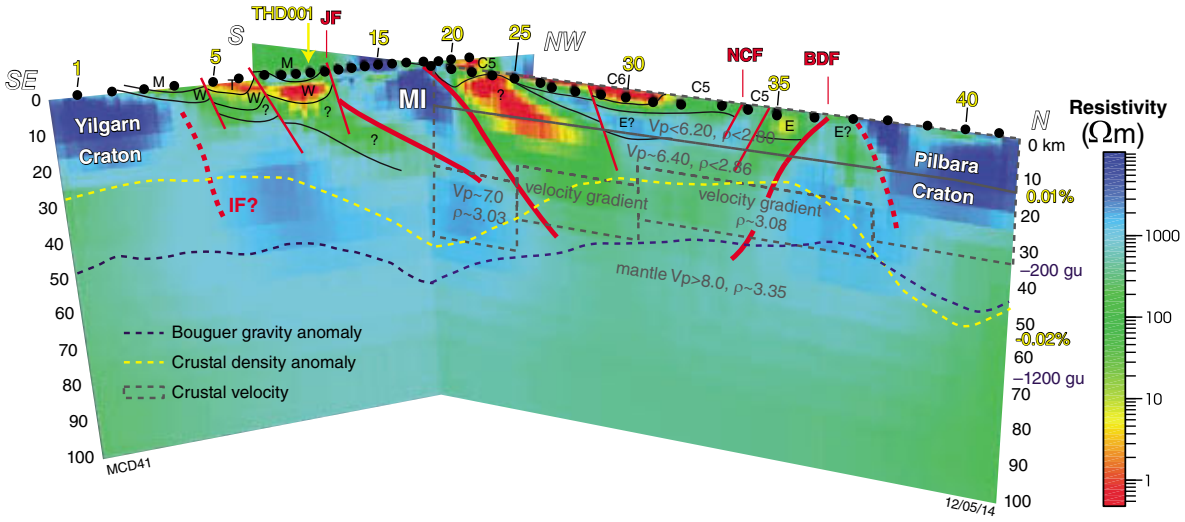

Figure 25. 3D resistivity model with Traverses 1 and 2 combined. Overlain are constraints derived from previous geophysical studies, including the crustal velocity of Drummond (1981) (dark grey solid and dashed boxes), mean crustal density (dashed yellow line, in %) and Bouguer gravity anomaly (dashed blue line, in units of gu) data of Aitken et al. (2013b). BDF, Baring Downs Fault; C5, Collier Group Depositional Package 5; C6, Collier Group Depositional Package 6; E, Edmund Group; IF, Ida Fault; JF, Jenkin Fault; M, Mooloogool Group; MI, Marymia Inlier; NCF, Neds Creek Fault; T, Tooloo Group; W, Windplain Group

density anomaly derived from the continent-scale crustal model of Aitken et al. (2013b) along the two MT transects (Fig. 25). The MT model shows relatively resistive crust to 25–30 km depth at both ends of the survey, coincident with the Yilgarn and Pilbara Cratons, and particularly thick and resistive crust, down to about 50 km beneath the Marymia Inlier. This deep resistive zone is coincident with a region of particularly dense crust that was modelled in the seismic refraction work (Drummond, 1979, 1981; Drummond and Shelley, 1981), and the gravity and crustal density anomaly models (Aitken et al., 2013b).

Beneath the cratonic regions the Moho appears well defined in the MT data (Fig. 25), imaged as a sharp interface between electrically resistive and conductive material. However, in the central part of the survey, such a transition is absent because the lower and mid-crust is of a similar conductivity to the underlying mantle, and so the Moho appears indistinct or 'fuzzy'. These relationships were also modelled in the seismic refraction work (Drummond 1979, 1981; Drummond and Shelley, 1981), which indicated a shallow, sharp Moho beneath the Pilbara and Yilgarn Cratons, and a region of lower crustal velocity gradients (a 'fuzzy' Moho) in the central part of the orogen (Figs 8a and 25).

The consistency of the MT model with the regional-scale geophysical datasets provides some confidence in the broad-scale architecture defined by the survey. However, the presence of several shallow, highly conductive sedimentary horizons prompts caution for over-interpreting the data, especially small-scale electrical features in the dataset.

Crustal architecture

The distinct variation in electrical conductivity across the eastern part of the Capricorn Orogen implies the presence of several discrete tectonic blocks, which are separated by major crustal-scale faults or shear zones (Fig. 25). The northern margin of the Yilgarn Craton seems composed of a collage of moderately north-dipping blocks (Fig. 25). The Yilgarn Craton itself is highly resistive, and appears to continue to the northwest beneath the conductive Proterozoic basins. The steeply dipping, moderately conductive feature at the southeastern end of Traverse 1 (Fig. 25) aligns with the northward projection of the Ida Fault beneath the Yerrida Basin (Fig. 2), providing some confidence that this feature is real, rather than an artefact beneath shallow-dipping, highly conductive, near-surface features.

The Marymia Inlier appears as a wedge-shaped feature of resistive crust bound on either side by more conductive material, the contacts of which may be major faults (Fig. 25). The southern margin of the inlier coincides with the Jenkin Fault (Fig. 2), which is imaged in the survey as a steeply north-dipping ?normal fault (Fig. 25) that appears to offset an earlier fault or shear zone contact between the inlier and underlying conductive crust. The northern margin of the inlier is covered by flat-lying metasedimentary rocks of the Collier Basin (Fig. 2). The nature of the contact between the inlier and pre-Collier Basin crust is not exposed. However, the conductivity contrast across this contact, and marked Bouguer gravity and crustal density anomalies (Fig. 26) across the inlier's northern margin, imply the presence of a major, previously unrecognized fault or shear zone, which is overlain by the shallow-dipping metasedimentary rocks of the Collier Basin. The wedged-shaped profile of the Marymia Inlier at depth is also reflected in its elongate, ribbon-like outcrop (Fig. 2), suggesting that the inlier may be a thin, fault-bounded sliver of para-autochthonous crust that rifted from the Eastern Goldfields Superterrane (Occhipinti et al., 1998c; Krapež and Martin, 1999; Pirajno et al., 2004).

Between the exposed northern part of the Yilgarn Craton and the Marymia Inlier, a highly conductive, shallow-dipping feature consistent with graphite- and sulfide-rich Proterozoic sedimentary rocks is dissected by steeply north-dipping faults, including the Jenkin Fault (Fig. 25). Surface mapping indicates that the conductive layer is not a single graphitic and sulfidic package, but comprises different conductive units within several different basins (Figs 2 and 25). The southernmost expression of this feature is within the Mooloogool Group of the Yerrida Basin. Between stations 5 and 7 (Figs 2 and 23), the conductive feature is a response to units within the Tooloo Group of the Earaheedy Basin and, directly on the southern side of the Marymia Inlier, the feature represents deeply buried conductors within the Windplain Group of the Yerrida Basin (Figs 23 and 25). This feature also implies that conductive features in these Proterozoic basins are not necessarily laterally continuous. The stratigraphy of the Windplain Group in the northernmost fault-bound section is particularly well known. A co-funded EIS diamond drillhole (THD001; Mueller, 2011), some 20 km to the northeast of Traverse 1 (Figs 2 and 25), intersected an anomalously thick (>1020 m) succession of graphitic shales, carbonaceous siltstones and sandstones, stromatolitic dolomites, and mafic rocks of the Windplain Group. The base of the succession was never reached. Combined with field mapping and the MT data, the Windplain Group appears to thicken substantially from the exposed Yilgarn Craton margin towards the Marymia Inlier to the northwest (Fig. 25). Although the steeply north-dipping faults that dissect these basins show evidence for reverse movements during folding and basin inversion, these structures may be reactivated growth-faults that formed during continental rifting and deposition of the Windplain Group in a continental sag-to-rift basin (Gee and Grey, 1994; Pirajno et al., 1998; Pirajno and Occhipinti, 2000). The identity of the underlying laterally continuous, moderately conductive crust is currently unknown, although it is possible that it is fluid-modified upper crust of the Yilgarn Craton that formed during extension and basin formation.

An MT survey across the western part of the Capricorn Orogen, some 250 km to the west (Fig. 1; Selway 2007; Selway et al., 2009), identified highly conductive crust between the Pilbara and Yilgarn Cratons that can be directly related to the well-exposed, variably metamorphosed granitic and metasedimentary rocks of the Glenburgh Terrane and Gascoyne Province (Fig. 10; Sheppard et al., 2010a). A similar region of conductive crust lies in the central part of this survey (most of

Traverse 2); however, because this region is covered almost entirely by sedimentary rocks of the Collier Basin, the nature of the underlying geology is particularly difficult to interpret. It is possible that this conductive region is crust of the Glenburgh Terrane and Gascoyne Province, or similarly exotic crust (ophiolitic, oceanic plateau or island arc crust) entrained between the cratons during ocean closure. The aeromagnetic total magnetic intensity (TMI) response to the highly conductive feature beneath station 25 is similar to that of granitic rocks of the Gascoyne Province, which underlie the Coobarra Dome about 75 km to the northwest (Figs 2 and 26a). However, similar conductive responses could be achieved by the structural, magmatic, or hydrothermal reworking of Archean crust or greenstone belts, thus not requiring the presence of exotic crust between the Pilbara and Yilgarn Cratons in this part of the orogen. Despite restricted data, the preservation of resistive crust in the exposed parts of the Yilgarn and Pilbara Cratons and Marymia Inlier, and the similar conductivity pattern in the MT survey to the west (Fig. 10; Selway 2007; Selway et al., 2009), tentatively suggest that the central part of this survey is underlain by rocks of the Glenburgh Terrane and Gascoyne Province (Fig. 27a). Steeply dipping normal faults in the upper crustal part of this conductive block affect the youngest rocks in the Collier Basin (Fig. 25), indicating movements during, or after, the 1030–955 Ma Edmundian Orogeny. These structures mirror the larger scale structure defined by the MT data, implying that the underlying pre-existing crustal architecture has influenced the style and orientation of subsequent deformation events (Johnson et al., 2013).

In the western part of the orogen, the Pilbara Craton is separated from the unexposed Bandee Seismic Province to the south by the moderate to steeply north-dipping Baring Downs Fault (Fig. 4; Johnson et al., 2011d, 2013). At the northern end of this MT survey, the change from resistive Pilbara Craton crust of the Sylvania Inlier to conductive material to the south is marked by a major moderate to steeply south-dipping fault or shear zone (solid red line marked BDF in Fig. 25). It is possible that this structure correlates with the Baring Downs Fault, and if so, its dip direction is opposite to that in the west. Electrically conductive material in the central part of the survey (Figs 23 and 25) may be the Bandee Seismic Province

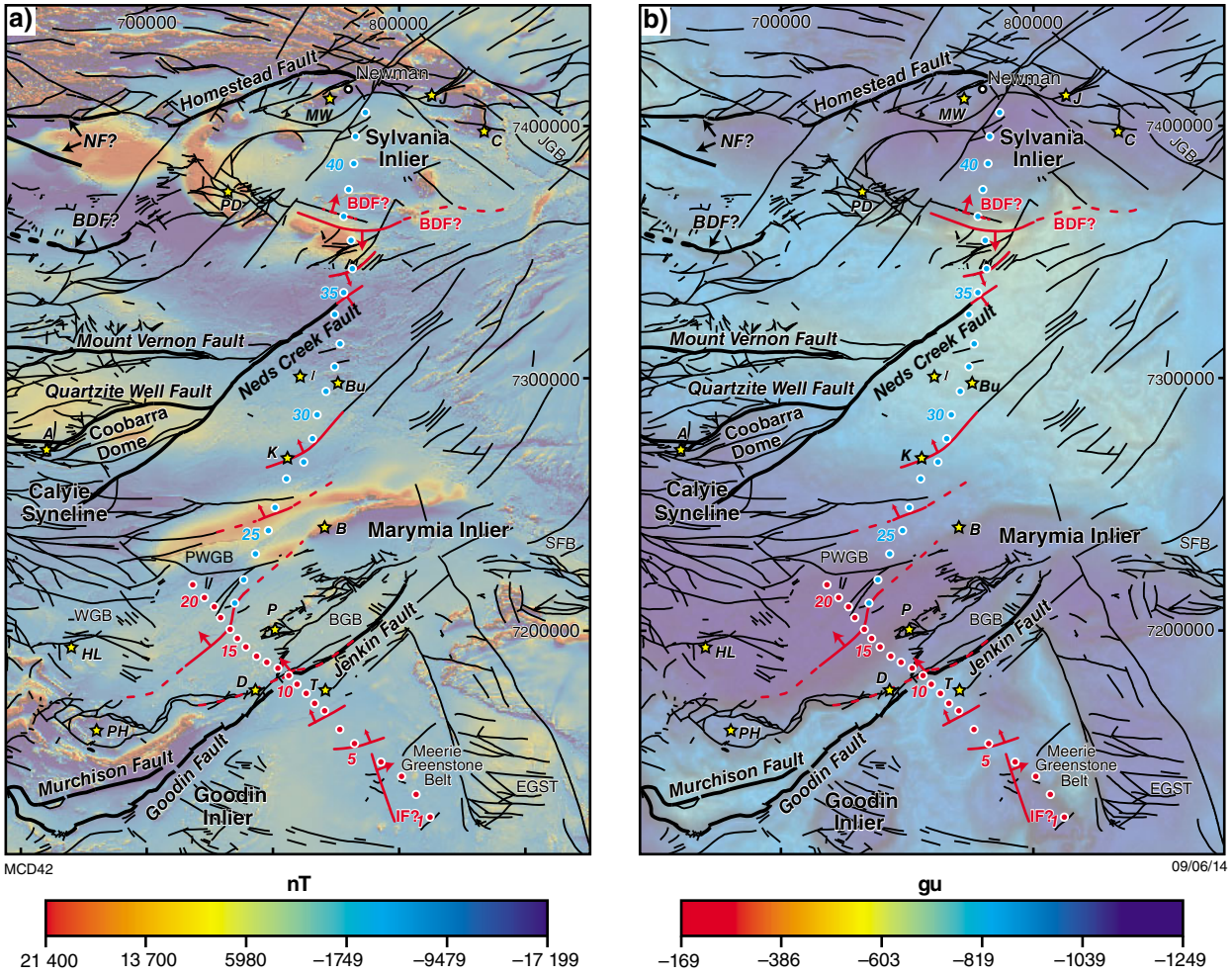

Figure 26. Surface location of major (thick red lines) and minor (thin red lines) faults identified from the MT data (arrows show dip direction). Other major (thick black lines) and minor (thin black lines) faults, derived from surface mapping, are overlain on: a) 300–500 m line spaced (TMI) aeromagnetic data; and b) 2.5 km spaced Bouguer anomaly gravity data. Abbreviations as for Figure 2; gu, gravity units

(Figs 4 and 27a). Alternatively, the contact between a steeply north-dipping conductive feature of unknown origin (shown by a dashed red line on Fig. 25) and the strongly resistive part of the Pilbara Craton at the northern end of the survey may be the Baring Downs Fault. Thus, the narrow wedge-shaped feature between the two steep, antithetic structures may be the variably conductive Bandee Seismic Province (Fig. 27a).

Correlation of crustal architecture across the orogen

The broad-scale architecture imaged by the MT survey shows several crustal-scale faults or shear zones that dip moderately towards the centre of the orogen (Figs 25 and 27a). This configuration is different from that in the western part of the orogen (Johnson et al., 2011d, 2013), which resembles moderately south-dipping structures (Fig. 4), implying there is a major change in crustal architecture across the orogen. This difference had previously been predicted from balanced crustal-scale cross-sections (Fig. 27b; purple dotted line in Fig. 1b) derived from the surface geology (Cawood and Tyler, 2004). The nature, origin, and identity of the structures identified in the MT survey, however, are difficult to determine due to the extensive cover of younger sedimentary rocks of the Collier Basin. Therefore, only general comparisons can be made with the more-detailed crustal architecture defined in the western part of the orogen (Johnson et al., 2011d; Johnson, 2013).

Depending on the interpretation of structures at the northern end of the survey, the crustal architecture may be relatively similar to that in the western part of the orogen (Fig. 4). Structural continuity can be achieved if the Baring Downs Fault (Fig. 4) correlates with the north-dipping structure (under station 37; Figs 23 and 25), implying the progressive narrowing of the Bandee Seismic Province from west to east. The major south-dipping structure that separates crust of contrasting electrical character (between stations 36 and 37) therefore could be the main suture between Pilbara Craton – Bandee Seismic Province crust and the Glenburgh Terrane. However, it is hard to justify this interpretation because the eastward projection of this suture from the west, the Lyons River – Quartzite

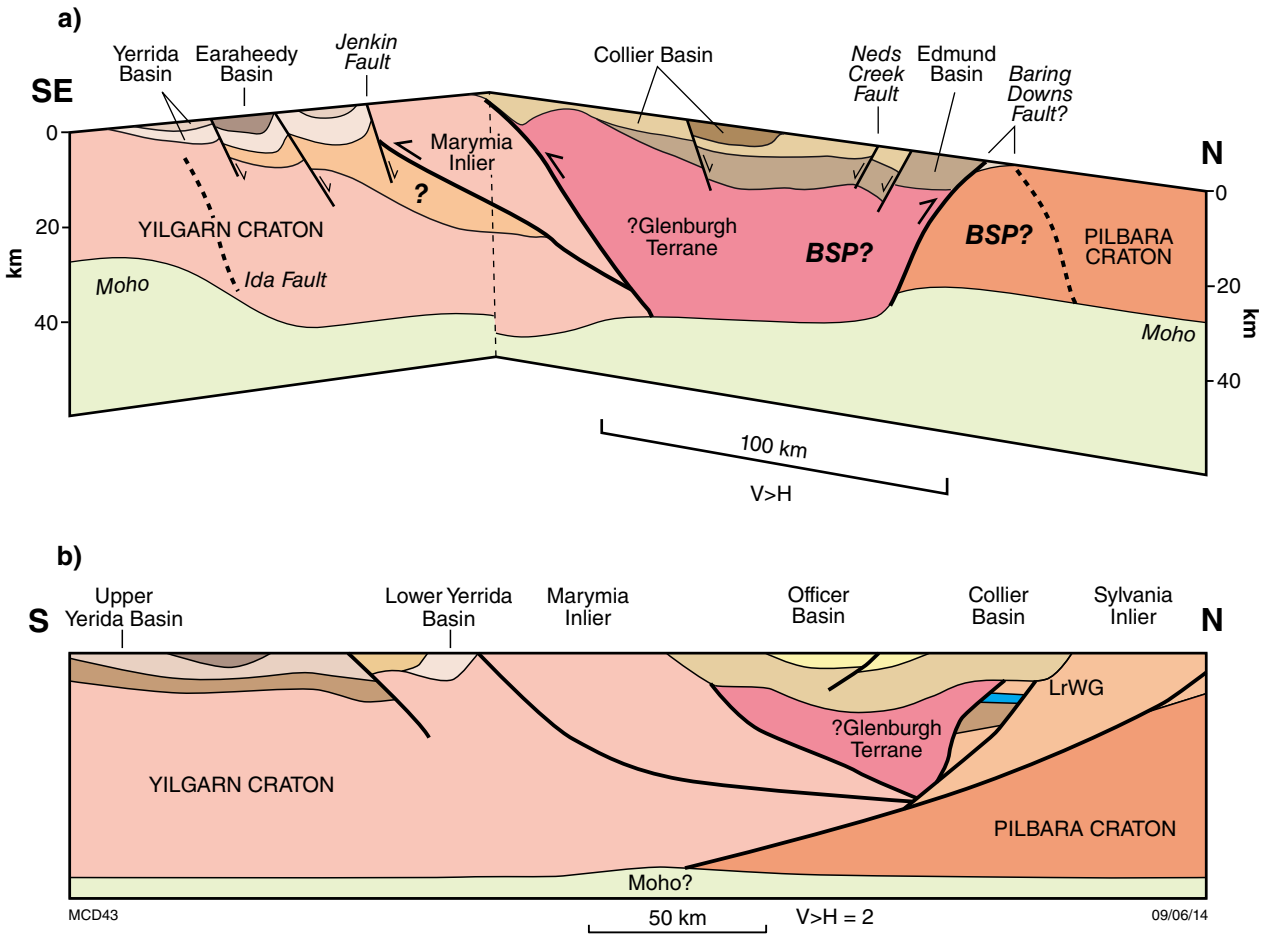

Figure 27. a) Geological 'cartoon' cross-section across the eastern part of the Capricorn Orogen interpreted from the MT results. BSP, Bandee Seismic Province; LrWG, Lower Windplain Group; b) balanced geological cross-section after Cawood and Tyler (2004), the location of which is shown by a dashed purple line in Figure 1b.

Well Faults (Johnson et al., 2011d, 2013), lies more than 100 km to the southwest where it appears to terminate on the Neds Creek Fault (Figs 1, 2 and 26). The simplest interpretation of the data suggests that the Baring Downs Fault dips moderately south and that the Bandee Seismic Province, if present this far east, must account for at least some of the highly conductive material in the central part of the survey (Fig. 25).

The north-dipping structural-grain, stacking of tectonic blocks and thickened continental root at the southern end of the survey (Fig. 27a) imply an architecture generated by thrusting and crustal thickening during collisional orogenesis. A similar pattern exists farther west, although the detailed architecture is complicated by backthrusting at the Errabiddy Shear Zone, and a reversal of the subduction polarity by the underthrusting of the Glenburgh Terrane beneath the Yilgarn Craton during the 2005–1950 Ma Glenburgh Orogeny (Fig. 4; Johnson et al., 2011d, 2013). The architecture of the western Capricorn Orogen appears to have been preserved relatively late in the orogenic cycle (Johnson et al., 2011d, 2013). The architecture defined here for the eastern Capricorn Orogen is much simpler, although it also appears to preserve a syn- to post-collisional arrangement (Fig. 27a). The major change in structural orientation and crustal architecture across the orogen may therefore relate to differences in the syn- to post-orogenic history of the collision zone, rather than any fundamental modifications to the pre-collisional architecture, for example, the location of island arcs or the subduction polarity.

Geotectonic history

Similar to the western Capricorn Orogen, the oldest event interpreted from the MT data appears to be the collision and accretion of the Bandee Seismic Province to the Pilbara Craton (Johnson et al., 2011d, 2013), sometime before the deposition of the c. 2775 Ma Fortescue Group.

The preservation of rift architecture along the northern part of the Yilgarn Craton suggests that separation of the Marymia Inlier from part of the Eastern Goldfields Superterrane of the Yilgarn Craton may have occurred during continental rifting and deposition of the Windplain Group of the Yerrida Basin. Although poorly dated, the deposition of the Windplain Group is tentatively constrained by a Pb–Pb date obtained on stromatolitic carbonates of the Bubble Well Member at c. 2170 Ma (Woodhead and Hergt, 1997). The main phase of gold mineralization (or upgrading) at Plutonic, at the southern end of the Plutonic Well greenstone belt (Fig. 2), is interpreted to have occurred at a similar time (c. 2200 Ma; Gazley, 2011).

During ocean closure, the polarity of subduction and arc magmatism may not have been greatly different from that in the western part of the Capricorn Orogen. Buried island arc or oceanic material may account for the highly conductive layer that lies structurally above the Marymia Inlier (Fig. 25). Collision of the Pilbara–Bandee–Glenburgh crustal block with the northern margin of the Yilgarn Craton during the 2005–1950 Ma Glenburgh Orogeny caused south-directed thrust stacking of the Marymia Inlier over the Yilgarn Craton margin and intense crustal thickening of the collisional margin (Fig. 27a). Subsequent reworking of these thrusts as normal faults during extension and deposition of the Minningarra Group of the Earaheedy Basin may have occurred during the 1820–1770 Ma Capricorn Orogeny, as highlighted by the age of various low-grade hydrothermal mineralizing events (Muhling et al., 2012).

The central and northern parts of the orogen show evidence for extensive post-Collier Basin (i.e. younger than c. 1070 Ma) extension. The normal faults parallel to the underlying crustal architecture indicate that, similar to the western part of the orogen, intracontinental reactivation and reworking is influenced by the pre-existing crustal architecture (Johnson et al., 2011d, 2013).

Conclusions

Although the Capricorn Orogen is a challenging environment for MT surveying, 3D modelling of the data has produced geologically plausible results. Similar to the western part of the Capricorn Orogen, the eastern part comprises numerous tectonic blocks that are separated by crustal-scale faults and shear zones. However, the broad-scale architecture of this part of the orogen is fundamentally different from that in the west of the orogen and resembles crustal structures that dip towards the centre of the orogen. The Yilgarn and Pilbara Cratons are resistive and separated by a large volume of conductive crust in the middle of the orogen. Although the nature and origin of this crust is not known, it is interpreted as Proterozoic crust analogous to the Glenburgh Terrane in the west. Therefore the Pilbara and Yilgarn Cratons do not appear in direct contact with each other in this part of the orogen.

The Marymia Inlier is most likely a para-autochthonous continental ribbon that was separated from the Eastern Goldfields Superterrane, possibly during rifting and deposition of the Windplain Group of the Yerrida Basin at c. 2170 Ma.

The present-day crustal architecture, as imaged in this survey, is a reflection of processes imparted late in the crustal thickening cycle. Therefore, any major structural differences across the orogen likely reflect complex collisional processes rather than any fundamental differences in the pre-collisional architecture, such as subduction polarity or the location and distribution of island arcs.

It is recommended that additional MT survey data be collected to link the existing eastern and western traverses and that both datasets be further modelled using 3D methods. This present work shows that MT methods, if acquired, processed and modelled correctly, can provide important information about the nature of the Capricorn Orogen at depth.

Acknowledgements

The eastern Capricorn Orogen MT survey was funded by the EIS of the Western Australian Government. Thanks to Ray Addenbrooke for invaluable assistance in the field. We are grateful to station owners at Neds Creek, Three Rivers, Kumarina, Bulloo Downs, and Sylvania for allowing access to their properties. Thanks to Ron Hackney for supplying a digital version of his crustal density model. Dr Anna Avdeeva undertook the 3D MT modelling.

References

Aitken, ARA, Dentith, MC, Evans, SF, Gallardo, LA, Joly, A, Thiel, S, Smithies, RH and Tyler, IM 2013a, Imaging crustal structure in the west Musgrave Province from Magnetotelluric and potential field data: Geological Survey of Western Australia, Report 114, 81p.

Aitken, ARA, Salmon, ML and Kennett, BLN 2013b, Australia's Moho: a test of the usefulness of gravity modelling for the determination of Moho depth: Tectonophysics, v. 609, p. 468–479.

Aitken, ARA, Joly, A, Dentith, MC, Johnson, SP, Thorne AM and Tyler, IM 2014, 3D architecture, structural evolution, and mineral prospectivity of the Gascoyne Province: Geological Survey of Western Australia, Report 123, 94p.

Avdeeva, DB and Avdeeva, DM 2009, 3D magnetotelluric inversion using a limited-memory quasi-Newton optimization: Geophysics, v. 74, no. 3, p. F45–F57.

Bagas, L 1999a, Early tectonic history of the Marymia Inlier and correlation with the Archean Yilgarn Craton, Western Australia: Australian Journal of Earth Sciences, v. 46, p. 115–125.

Bagas, L 1999b, The Archean Marymia Inlier — a review of its tectonic history and relationships to the Yilgarn Craton, *in* Geological Survey of Western Australia Annual Review 1997–98: Geological Survey of Western Australia, p. 85–90.

Begg, GC, Hronsky, JMA, Arndt, NT, Griffin, WL, O'Reilly, S and Hayward, N 2010, Lithospheric, cratonic, and geodynamic setting of Ni–Cu–PGE sulfide deposits: Economic Geology, v. 105, p. 1057–1070.

Blake, TS 1993, Late Archean crustal extension, sedimentary basin formation, flood basalt volcanism, and continental rifting. The Nullagine and Mount Jope Supersequences, Western Australia: Precambrian Research, v. 60, p. 185–241.

Blake, TS and Barley, ME 1992, Tectonic evolution of the Late Archean to Early Proterozoic Mount Bruce megasequence set, Western Australia: Tectonics, v. 11, p. 1415–1425.

Blay, OA, Cutten, HN and Thorne, AM 2014, Three Rivers Geological Series map (1:100 000 scale): Geological Survey of Western Australia.

Brakel, AT, Elias, M and Barnett, JC 1978, Explanatory notes on the Collier 1:250 000 Geological Sheet: Geological Survey of Western Australia, Record 1978/8, 38p.

Caldwell, TG, Bibby, HM and Brown, C 2004, The magnetotelluric phase tensor: Geophysical Journal International, v. 158, p. 457–469.

Cassidy, KF, Champion, DC, Krapež, B, Barley, ME, Brown, SJA, Blewett, RS, Groenewald, PB and Tyler, IM 2006, A revised geological framework for the Yilgarn Craton, Western Australia: Geological Survey of Western Australia, Record 2006/8, 8p.

Cawood, PA and Tyler, IM 2004, Assembling and reactivating the Proterozoic Capricorn Orogen: lithotectonic elements, orogenies, and significance: Precambrian Research, v. 128, p. 201–218.

Champion, DC and Cassidy, KF 2007, An overview of the Yilgarn and its crustal evolution, *in* Proceedings *edited by* FP Bierlein and CM Knox-Robinson: Geoscience Australia; Geoconferences (WA) Inc. Kalgoorlie '07, Kalgoorlie, Western Australia, 25 September 2007; Record 2007/14, p. 8–13.

Chave, AD and Jones, AG 2012, The magnetotelluric method: theory and practice: Cambridge University Press, Cambridge, 552p.

Compston, W and Pidgeon, RT 1986, Jack Hills, evidence of more very old detrital zircons in Western Australia: Nature, v. 321, p. 766–769.

Cutten, HN, Thorne, AM and Johnson, SP 2011, Geology of the Edmund and Collier Groups, *in* Capricorn Orogen seismic and magnetotelluric (MT) workshop 2011: extended abstracts *edited by* SP Johnson, AM Thorne and IM Tyler: Geological Survey of Western Australia, Record 2011/25, p. 41–48.

Dennis, ZR, Moore, DH and Cull, JP 2011, Magnetotelluric survey for undercover structural mapping: Central Victoria: Australian Journal of Earth Sciences, v. 58, p. 33–47.

Dentith, MC, Evans, S, Thiel, S, Gallardo, G, Joly, A and Romano, SS 2013, A magnetotelluric traverse across the southern Yilgarn Craton: Geological Survey of Western Australia, Report 121, 43p.

Drummond, BJ 1979, A crustal profile across the Archean Pilbara and sourthern Yilgarn cratons, northwest Australia: BMR Journal of Australian Geology and Geophysics, v. 4, p. 171–180.

Drummond, BJ 1981, Crustal structure of the Precambrian terrains of northwest Australia: BMR Journal of Australian Geology and Geophysics, v. 6, p. 123–135.

Drummond, BJ, Goleby, BR and Swager, CP 2000, Crustal signature of Late Archean tectonic episodes in the Yilgarn craton, Western Australia: evidence from deep seismic sounding: Tectonophysics, v. 329, p. 193–221.

Drummond, BJ and Shelley, HM 1981, Isostasy and structure of the lower crust and upper mantle in the Precambrian terrains of northwest Australia, from regional gravity studies: BMR Journal of Australian Geology and Geophysics, v. 6, p. 137–143.

Emergent Resources 2014, Beyondie Iron Project, viewed 1 April 2014, <http://www.emergentresources.com.au/index.php?option=com_content&view=article&id=9&Itemid=11>.

Froude, DO, Ireland, TR, Kinny, PD, Williams, IS, Compston, W, Williams, IR and Myers, JS 1983, Ion microprobe identification of 4100–4200 Myr-old terrestrial zircons: Nature, v. 304, p. 616–618.

Gamble, TD, Goubau, WM and Clarke, J 1979, Magnetotellurics with a remote reference: Geophysics, v. 44, p. 53–68.

Gazley, MF 2011, Metamorphism, geochronology and stratigraphy of an amphibolite-facies greenstone-hosted gold deposit: Plutonic Gold Mine, Marymia Inlier, Western Australia: Victoria University of Wellington, New Zealand, PhD thesis (unpublished).

Gazley MF, Vry, JK and Boorban, JC 2011, P–T evolution in greenstone-belt mafic amphibolites: an example from Plutonic Gold Mine, Marymia Inlier, Western Australia: Journal of Metamorphic Geology, v. 29, p. 685–697.

Gee, RD 1979, Structure and tectonic style of the Western Australian Shield: Tectonophysics, v. 58, p. 327–369.

Gee, RD 1990, Capricorn Orogen — Nabberu Basin, in Geology and mineral resources of Western Australia: Geological Survey of Western Australia, Memoir 3, p. 202–210.

Gee, RD and Grey, K 1994, Proterozoic rocks on the Glengarry 1:250 000 sheet — stratigraphy, structure and stromatolite biostratigraphy: Geological Survey of Western Australia, Report 41, 33p.

GEOSYSTEM SRL 2008, WinGLink user guide, release 2.20.02.01: GEOSYSTEM SRL, Milan, Italy, 473p.

Hackney, R 2004, Gravity anomlies, crustal structure and isostasy associated with the Proterozoic Capricorn Orogen, Western Australia: Precambrian Research, v. 128, p 219–236.

Halilovic, J, Cawood, PA, Jones, JA, Pirajno, F and Nemchin, AA 2004, Provenance of the Earaheedy Basin: implications for assembly of the Western Australian Craton: Precambrian Research, v. 128, no. 3–4, p. 343–366.

Heinson, G, Boren, G, Ross, J, Campanya, J, Thiel, S and Selway, K 2011, The Capricorn Orogen magnetotelluric (MT) transect, *in* Capricorn Orogen seismic and magnetotelluric (MT) workshop 2011: extended abstracts *edited by* SP Johnson, AM Thorne and IM Tyler: Geological Survey of Western Australia, Record 2011/25, p. 75–100.

Hickman, AH and Van Kranendonk, MJ 2008, Archean crustal evolution and mineralization of the northern Pilbara Craton — a field guide: Geological Survey of Western Australia, Record 2008/13, 79p.

Hronsky, JMA, Groves, DI, Loucks, RR and Begg, GC 2012, A unified model for gold mineralisation in accretionary orogens and implications for regional-scale exploration targeting methods: Mineralium Deposita, v. 47, p. 339–358.

Ivanic, TJ, Wingate, MTD, Kirkland, CL, Van Kranendonk, MJ and Wyche, S 2010, Age and significance of voluminous mafic–ultramafic magmatic events in the Murchison Domain, Yilgarn Craton: Australian Journal of Earth Sciences, v. 57, p. 597–614.

Johnson, SP, Sheppard, S, Rasmussen, B, Wingate, MTD, Kirkland, CL, Muhling, JR, Fletcher, IR and Belousova, E 2010, The Glenburgh Orogeny as a record of Paleoproterozoic continent–continent collision: Geological Survey of Western Australia, Record 2010/5, 54p.

Johnson, SP, Sheppard, S, Rasmussen, B, Wingate, MTD, Kirkland, CL, Muhling, JR, Fletcher, IR and Belousova, EA 2011a, Two collisions, two sutures: punctuated pre-1950 Ma assembly of the West Australian Craton during the Ophthalmian and Glenburgh Orogenies: Precambrian Research, v. 189, no. 3–4, p. 239–262, doi: 10.1016/j.precamres.2011.07.011.

Johnson, SP, Sheppard, S, Thorne, AM, Rasmussen, B, Fletcher, IR, Wingate, MTD and Cutten, HN 2011b, The role of the 1280–1250 Ma Mutherbukin Tectonic Event in shaping the crustal architecture and mineralization history of the Capricorn Orogen, *in* GSWA 2011 extended abstracts: promoting the prospectivity of Western Australia: Geological Survey of Western Australia, Record 2011/2, p. 1–3.

Johnson, SP, Sheppard, S, Wingate, MTD, Kirkland, CL and Belousova, EA 2011c, Temporal and hafnium isotopic evolution of the Glenburgh Terrane basement: an exotic crustal fragment in the Capricorn Orogen: Geological Survey of Western Australia, Report 110, 27p.

Johnson, SP, Thorne, AM and Tyler, IM (editors) 2011d, Capricorn Orogen seismic and magnetotelluric (MT) workshop 2011: extended abstracts: Geological Survey of Western Australia, Record 2011/25, 120p.

Johnson, SP, Thorne, AM, Tyler, IM, Korsch, RJ, Kennett, BLN, Cutten, HN, Goodwin, J, Blay, OA, Blewett, RS, Joly, A, Dentith, MC, Aitken, ARA, Holzschuh, J, Salmon, M, Reading, A, Heinson, G, Boren, G, Ross, J, Costelloe, RD and Fomin, T 2013, Crustal architecture of the Capricorn Orogen, Western Australia and associated metallogeny: Australian Journal of Earth Sciences, v. 60, no. 6–7, p. 681–705.

Jones, AG and Jödicke, H 1984, Magnetotelluric transfer function estimation improvement by a coherence based rejection technique (EM1.5), *in* 54th Society of Exploration Geophysics Annual General Meeting: Society of Exploration Geophysics; SEG AGM, Atlanta, Georgia, USA, 1984, Extended Abstracts v. 3, p. 51–55.

Krapež, B and Martin, DM 1999, Sequence stratigraphy of the Palaeoproterozoic Nabberu Province of Western Australia: Australian Journal of Earth Sciences, v. 46, no. 1, p. 89–103, doi:10.1046/j.1440-0952.1999.00692.

Martin, DM 1994, Sedimentology, sequence stratigraphy, and tectonic setting of a Palaeoproterozoic turbidite complex, Lower Padbury Group, Western Australia: The University of Western Australia, Perth, Western Australia, PhD thesis (unpublished).

Martin, DM 1998, Lithostratigraphy and structure of the Palaeoproterozoic lower Padbury Group, Milgun 1:100 000 sheet, Western Australia: Geological Survey of Western Australia, Report 62, 58p.

Martin, DM 2003, Peperite in the Backdoor Formation and its significance to the age and tectonic evolution of the Bangemall Supergroup, *in* Geological Survey of Western Australia Annual Review 2002–03: Geological Survey of Western Australia, p. 53–59.

Martin, DM, Li, ZX, Nemchin, AA and Powell, CM 1998, A pre-2.2 Ga age for giant hematite ores of the Hamersley Province, Australia: Economic Geology, v. 93, p. 1084–1090.

Martin, DM and Morris, PA 2010, Tectonic setting and regional implications of c. 2.2 Ga mafic magmatism in the southern Hamersley Province, Western Australia: Australian Journal of Earth Sciences, v. 57, no. 7, p. 911–931.

Martin, DM, Powell, CM and George, AD 2000, Stratigraphic architecture and evolution of the early Paleoproterozoic McGrath Trough, Western Australia: Precambrian Research, v. 99, p. 33–64.

Martin, DM, Sircombe, KN, Thorne, AM, Cawood, PA and Nemchin, AA 2008, Provenance history of the Bangemall Supergroup and implications for the Mesoproterozoic paleogeography of the West Australian Craton: Precambrian Research, v. 166, no. 1–4 (Assembling Australia: Proterozoic building of a continent), p. 93–110.

Martin, DM and Thorne, AM 2004, Tectonic setting and basin evolution of the Bangemall Supergroup in the northwestern Capricorn Orogen: Precambrian Research, v. 128, p. 385–409.

Milligan, PR, Duan, J, Fomin, T, Nakamura, A and Jones, T 2013, The Younami magnetotelluric (MT) transects, *in* Youanmi and southern Carnarvon seismic and magnetotelluric (MT) workshop (preliminary edition) *edited by* S Wyche, T Ivanic and I Zibra: Geological Survey of Western Australia, Record 2013/6, 171p.

Morris, RC and Horwitz, RC 1983, The origin of the iron formation-rich Hamersley Group of Western Australia — deposition on a platform: Precambrian Research, v. 21, p. 273–297.

Morris, PA and Pirajno, F 2005, Mesoproterozoic sill complexes in the Bangemall Supergroup, Western Australia: geology, geochemistry, and mineralization potential: Geological Survey of Western Australia, Report 99, 75p.

Muhling, PC and Brakel, AT 1985, Geology of the Bangemall Group: the evolution of a Proterozoic intra-cratonic sedimentary basin: Geological Survey of Western Australia, Bulletin 128, 266p.

Muhling, JR, Fletcher, IR and Rasmussen, B 2012, Dating fluid flow and Mississippi Valley type base-metal mineralization in the Paleoproterozoic Earaheedy Basin, Western Australia: Precambrian Research, v. 212–213, p. 75–90, doi: 10.1016/j.precamres.2012.04.016.

Mueller, DHA 2011, Thaduna Project (E52/1673, E52/1674, E52/1858, E52/2356, E52/2357 and E52/2405); Final report on drilling of THD001, a 1017.8 m vertical core hole on E52/1673 drilled pursuant to a funding agreement, Royalties for Regions, co-funded government–industry drilling program 2010/11; Sipa Exploration NL: Geological Survey of Western Australia, Report C144/2005 (open).

Müller, SG, Krapež, B, Barley, ME and Fletcher, IR 2005, Giant iron-ore deposits of the Hamersley province related to the breakup of Paleoproterozoic Australia: New insights from in situ SHRIMP dating of baddeleyite from mafic intrusions: Geology, v. 33, no. 7, p. 577–580.

Occhipinti, SA 2007, Neoproterozoic reworking in the Paleoproterozoic Capricorn Orogen: evidence from $^{40}Ar/^{39}Ar$ ages: Geological Survey of Western Australia, Record 2007/10, 41p.

Occhipinti, SA, Grey, K, Pirajno, F, Adamides, NG, Bagas, L, Dawes, P and Le Blanc Smith, G 1997, Stratigraphic revision of Palaeoproterozoic rocks of the Yerrida, Bryah and Padbury Basins (former Glengarry Basin): Geological Survey of Western Australia, Record 1997/3, 57p.

Occhipinti, SA, Myers, JS and Swager, CP 1998a, Geology of the Padbury 1:100 000 sheet: Geological Survey of Western Australia, 1:100 000 Geological Series Explanatory Notes, 29p.

Occhipinti, SA, Sheppard, S, Nelson, DR, Myers, JS and Tyler, IM 1998b, Syntectonic granite in the southern margin of the Palaeoproterozoic Capricorn Orogen, Western Australia: Australian Journal of Earth Sciences, v. 45, p. 509–512.

Occhipinti, SA, Sheppard, S, Passchier, C, Tyler, IM and Nelson, DR 2004, Palaeoproterozoic crustal accretion and collision in the southern Capricorn Orogen: the Glenburgh Orogeny: Precambrian Research, v. 128, p. 237–255.

Occhipinti, SA, Swager, CP and Pirajno, F 1998c, Structural-metamorphic evolution of the Palaeoproterozoic Bryah and Padbury Groups during the Capricorn Orogeny, Western Australia: Precambrian Research, v. 90, p. 141–158.

Pirajno, F, Bagas, L, Swager, CP, Occhipinti, SA and Adamides, NG 1997, A reappraisal of the stratigraphy of the Glengarry Basin, Western Australia, *in* Geological Survey of Western Australia Annual Review 1995–96: Geological Survey of Western Australia, p. 81–87.

Pirajno, F, Jones, JA, Hocking, RM and Halilovic, J 2004, Geology and tectonic evolution of Palaeoproterozoic basins of the eastern Capricorn Orogen, Western Australia: Precambrian Research, v. 128, no. 3–4, p. 315–342.

Pirajno, F, Hocking, RM, Reddy, SM and Jones, JA 2009, A review of the geology and geodynamic evolution of the Palaeoproterozoic Earaheedy Basin, Western Australia: Earth–Science Reviews, v. 94, p. 39–77.

Pirajno, F and Occhipinti, SA 1998, Geology of the Bryah 1:100 000 sheet: Geological Survey of Western Australia, 1:100 000 Geological Series Explanatory Notes, 41p.

Pirajno, F and Occhipinti, SA 2000, Three Palaeoproterozoic basins—Yerrida, Bryah and Padbury—Capricorn Orogen, Western Australia: Australian Journal of Earth Sciences, v. 47, p. 675–688.

Pirajno, F, Occhipinti, SA and Swager, CP 1998, Geology and tectonic evolution of the Paleoproterozoic Bryah, Padbury, and Yerrida Basins (formerly Glengarry Basin), Western Australia: implications for the history of the south-central Capricorn Orogen: Precambrian Research, v. 90, no. 3–4, p. 119–140.

Rasmussen, B and Fletcher, IR 2002, Indirect dating of mafic intrusions by SHRIMP U–Pb analysis of monazite in contact metamorphosed shale: an example from the Palaeoproterozoic Capricorn Orogen, Western Australia: Earth and Planetary Science Letters, v. 197, p. 287–299.

Rasmussen, B, Fletcher, IR, Bekker, A, Muhling, JR, Gregory, CJ and Thorne, AM 2012, Deposition of 1.88-billion-year-old iron formations as a consequence of rapid crustal growth: Nature, v. 484, p. 498–501.

Rasmussen, B, Fletcher, IR, Muhling, JR, Thorne, AM, Cutten, HN, Pirajno, F and Hell, A 2010a, In situ U–Pb monazite and xenotime geochronology of the Abra polymetallic deposit and associated sedimentary and volcanic rocks, Bangemall Supergroup, Western Australia: Geological Survey of Western Australia, Record 2010/12, 31p.

Rasmussen, B, Fletcher, IR, Muhling, JR and Wilde, SA 2010b, In situ U–Th–Pb geochronology of monazite and xenotime from the Jack Hills belt: implications for the age of deposition and metamorphism of Hadean zircons: Precambrian Research, v. 180, no. 1–2, p. 26–46.

Reading, AM and Kennett, BLN 2003, Lithospheric structure of the Pilbara Craton, Capricorn Orogen and northern Yilgarn Craton, Western Australia, from teleseismic receiver functions: Australian Journal of Earth Sciences, v. 50, p. 439–445.

Reading, AM, Tkalcic, H, Kennett, BLN, Johnson, SP and Sheppard, S 2012, Seismic structure of the crust and uppermost mantle of the Capricorn and Paterson Orogens and adjacent cratons, Western Australia, from passive seismic transects: Precambrian Research, v. 196–197, p. 295–308, doi: 10.1016/j.precamres.2011.07.001.

Rodi, W and Mackie, RL 2001, Nonlinear conjugate gradients algorithm for 2-D magnetotelluric inversion: Geophysics, v. 66, p. 174–187.

Selway, K 2007, Magnetotelluric investigation into the electrical structure of the Capricorn Orogen, Western Australia: Geological Survey of Western Australia, Record 2007/16, 39p.

Selway, K, Sheppard, S, Thorne, AM, Johnson, SP and Groenewald, PB 2009, Identifying the lithospheric structure of a Precambrian orogen using magnetotellurics: the Capricorn Orogen: Precambrian Research, v. 168, p 185–196.

Sheppard, S, Bodorkos, S, Johnson, SP, Wingate, MTD and Kirkland, CL 2010a, The Paleoproterozoic Capricorn Orogeny: intracontinental reworking not continent–continent collision: Geological Survey of Western Australia, Report 108, 33p.

Sheppard, S, Farrell, TR, Bodorkos, S, Hollingsworth, D, Tyler, IM and Pirajno, F 2006, Late Paleoproterozoic (1680–1620 Ma) sedimentation, magmatism, and tectonism in the Capricorn Orogen, *in* GSWA 2006 extended abstracts: promoting the prospectivity of Western Australia: Geological Survey of Western Australia, Record 2006/3, p. 11–12.

Sheppard, S, Johnson, SP, Wingate, MTD, Kirkland, CL and Pirajno, F 2010b, Explanatory Notes for the Gascoyne Province: Geological Survey of Western Australia, Perth, Western Australia, 336p.

Sheppard, S, Occhipinti, SA and Nelson, DR 2005, Intracontinental reworking in the Capricorn Orogen, Western Australia: the 1680–1620 Ma Mangaroon Orogeny: Australian Journal of Earth Sciences, v. 52, p. 443–460.

Sheppard, S, Occhipinti, SA and Tyler, IM 2004, A 2005–1970 Ma Andean-type batholith in the southern Gascoyne Complex, Western Australia: Precambrian Research, v. 128 (Assembling the Palaeoproterozoic Capricorn Orogen), p. 257–277.

Sheppard, S, Rasmussen, B, Muhling, JR, Farrell, TR and Fletcher, IR 2007, Grenvillian-aged orogenesis in the Palaeoproterozoic Gascoyne Complex, Western Australia: 1030–950 Ma reworking of the Proterozoic Capricorn Orogen: Journal of Metamorphic Geology, v. 25, p. 477–494.

Simpson, F and Bahr, K 2005, Practical magnetotellurics: Cambridge University Press, Cambridge, 270p.

Thorne, AM and Trendall, AF 2001, Geology of the Fortescue Group, Pilbara Craton, Western Australia: Geological Survey of Western Australia, Bulletin 144, 249p.

Thorne, AM, Tyler, IM, Korsch, RJ, Johnson, SP, Brett, JW, Cutten, HN, Blay, OA, Kennett, BLN, Blewett, RS, Joly, A, Dentith, MC, Aitken, ARA, Holzschuh, J, Goodwin, JA, Salmon, M, Reading, A and Boren, G 2011, Preliminary interpretation of deep seismic reflection line 10GA–CP1: crustal architecture of the northern Capricorn Orogen, *in* Capricorn Orogen seismic and magnetotelluric (MT) workshop 2011: extended abstracts *edited by* SP Johnson, AM Thorne and IM Tyler: Geological Survey of Western Australia, Record 2011/25, p. 19–26.

Trendall, AF, Compston, W, Nelson, DR, De Laeter, JR and Bennett, VC 2004, SHRIMP zircon ages constraining the depositional chronology of the Hamersley Group, Western Australia: Australian Journal of Earth Sciences, v. 51, no. 5, p. 621–644.

Tyler, IM 1991, The geology of the Sylvania Inlier and the southeast Hamersley Basin: Geological Survey of Western Australia, Bulletin 138, 108p.

Tyler, IM and Thorne, AM 1990, Capricorn Orogen — structural evolution of the northern margin, in Geology and mineral resources of Western Australia: Geological Survey of Western Australia, Memoir 3, p. 223–232.

Van Kranendonk, MJ, Ivanic, TJ, Wingate, MTD, Kirkland, CL and Wyche, S 2013, Long lived, autochthonous development of the Archean Murchison Domain, and implications for Yilgarn Craton tectonics: Precambrian Research, v. 229, p. 49–92.

Van Kranendonk, MJ, Smithies, RH, Hickman, AH and Champion, DC 2007, Review: secular tectonic evolution of Archean continental crust: interplay between horizontal and vertical processes in the formation of the Pilbara Craton, Australia: Terra Nova, v. 19, no. 1, p. 1–38.

Vickery, NM 2004, The Plutonic Gold deposit, Western Australia: Geology and Geochemistry of an Archaean orogenic gold system: The University of New England, Armidale, New South Wales, Australia, PhD thesis (unpublished).

Vielreicher, NM, Ridley, JR and Groves, DI 2002, Marymia: an Archean, amphibolite facies-hosted, orogenic lode-gold deposit overprinted by Palaeoproterozoic orogenesis and base metal mineralisation, Western Australia: Mineralium Deposita, v. 37, p. 737–764.

Wang, Q, Schiøtte, L and Campbell, IH 1998, Geochronology of supracrustal rocks from the Golden Grove area, Murchison Province, Yilgarn Craton, Western Australia: Australian Journal of Earth Sciences, v. 45, p. 571–577.

Weaver, J, Agarwal, A, Lilley, F, Macnae, J and Liu, G (editors) 2003, The relationship between the magnetotelluric tensor invariants and the phase tensor of Caldwell, Bibby and Brown, Three-dimensional Electromagnetics III: Australian Society of Exploration Geophysicists p. 1–8.

Wight, DE and Bostick, FX 1981, Cascade decimation — a technique for real time estimation of power spectra, *in* Proceedings: Institute of Electrical and Electronic Engineers: International Conference on Acoustics, Speech, and Signal Processing, Atlanta, Georgia, USA, 30 March 1981, p. 626–629.

Wilde, SA, Valley, JW, Peck, WH and Graham, CM 2001, Evidence from detrital zircons for the existence of continental crust and oceans on the Earth 4.4 Gyr ago: Nature, v. 409, p. 175–178.

Windh, J 1992, Tectonic evolution and metallogenesis of the Early Proterozoic Glengarry Basin: The University of Western Australia, Perth, Western Australia, PhD thesis (unpublished).

Wingate, MTD 2002, Age and palaeomagnetism of dolerite sills of the Bangemall Supergroup on the Edmund 1:250 000 sheet, Western Australia: Geological Survey of Western Australia, Record 2002/4, 48p.

Wingate, MTD, Kirkland, CL, Cutten, HN and Thorne, AM 2012, 143445: dolerite sill, Waldburg Homestead; Geochronology Record 1077: Geological Survey of Western Australia, 4p.

Wingate, MTD, Kirkland, CL and Thorne, AM 2010, 149019: felsic volcaniclastic rock, Tangadee Road; Geochronology Record 875: Geological Survey of Western Australia, 4p.

Woodhead, JD and Hergt, JM 1997, Application of the 'double spike' technique to Pb-isotope geochronology: Chemical Geology, v. 138, p. 311–321.

Wyche, S, Ivanic, T and Zibra, I (compilers) 2013, Youanmi and southern Carnarvon seismic and magnetotelluric (MT) workshop (preliminary edition): Geological Survey of Western Australia, Record 2013/6, 171p.

Appendix

Apparent resistivity and phase data for all recording stations

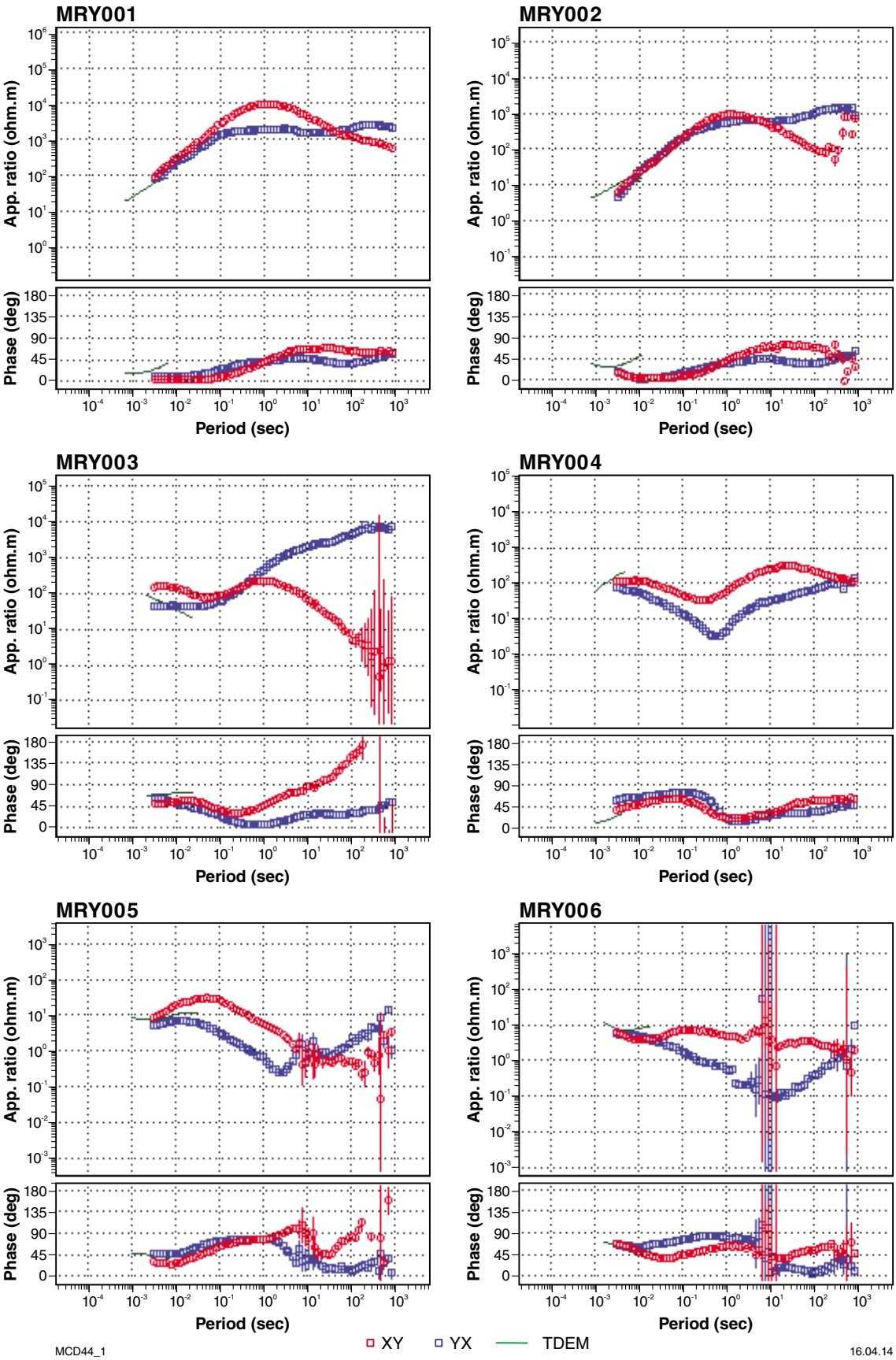

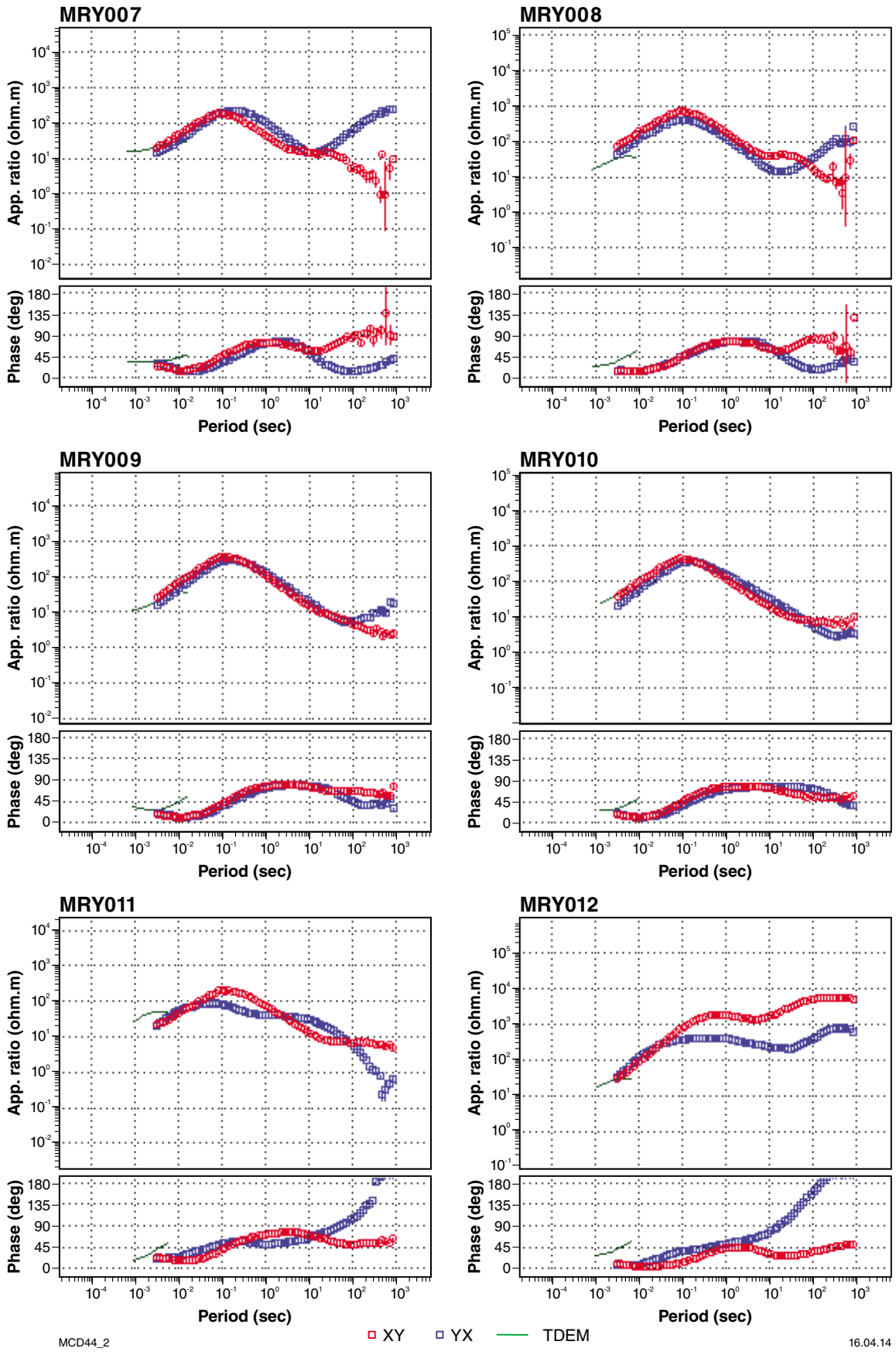
MRY007
MRY008
MRY009
MRY010
MRY011
MRY012
App. ratio (ohm.m)
Phase (deg)
Period (sec)
XY
YX
TDEM
MCD44_2
16.04.14

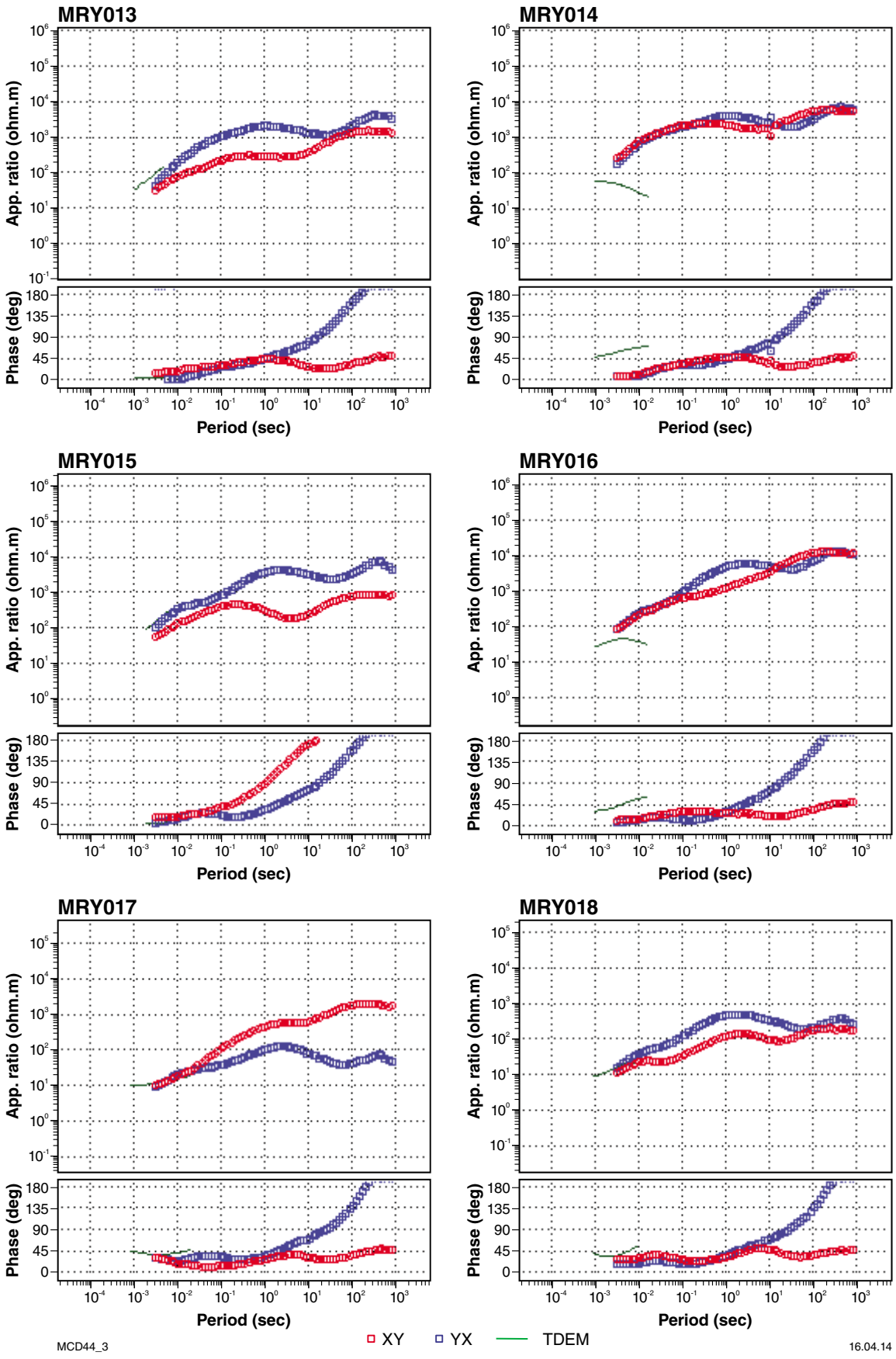
MRY013
MRY014
MRY015
MRY016
MRY017
MRY018
App. ratio (ohm.m)
Phase (deg)
Period (sec)
XY
YX
TDEM
MCD44_3
16.04.14

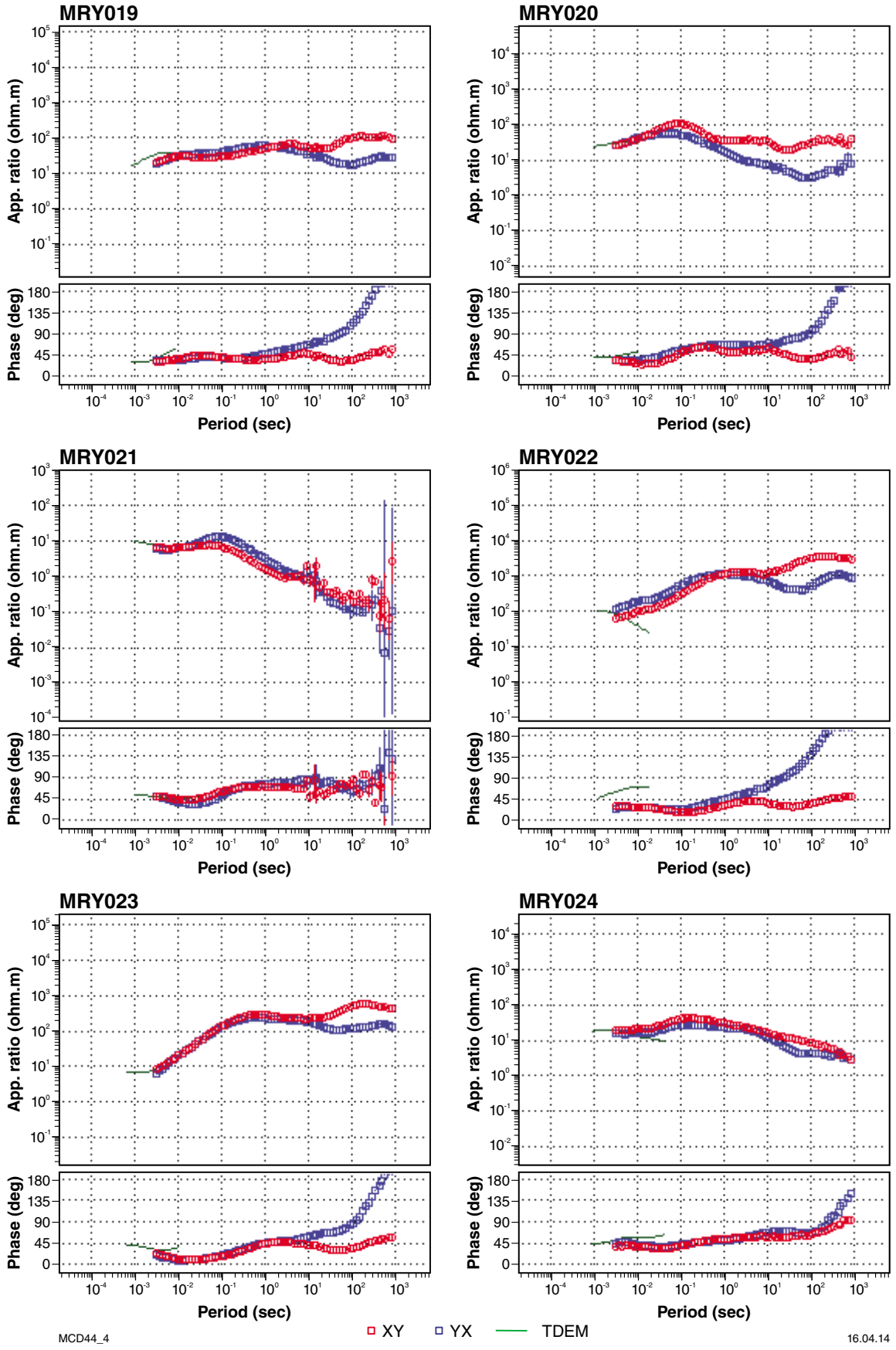
MRY019
MRY020
MRY021
MRY022
MRY023
MRY024
App. ratio (ohm.m)
Phase (deg)
Period (sec)
XY
YX
TDEM
MCD44_4
16.04.14

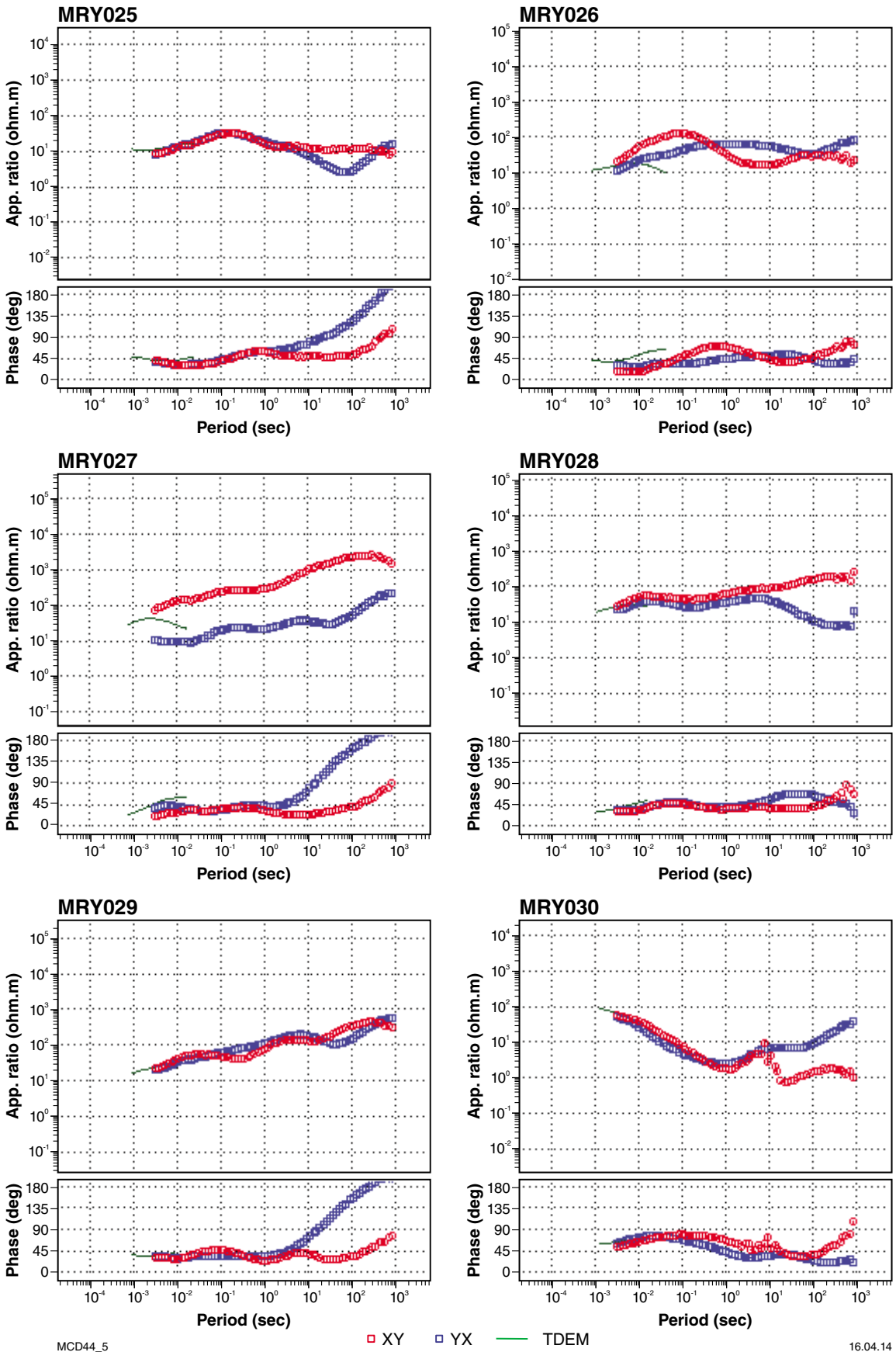
MRY025
MRY026
MRY027
MRY028
MRY029
MRY030
App. ratio (ohm.m)
Phase (deg)
Period (sec)
XY
YX
TDEM
MCD44_5
16.04.14

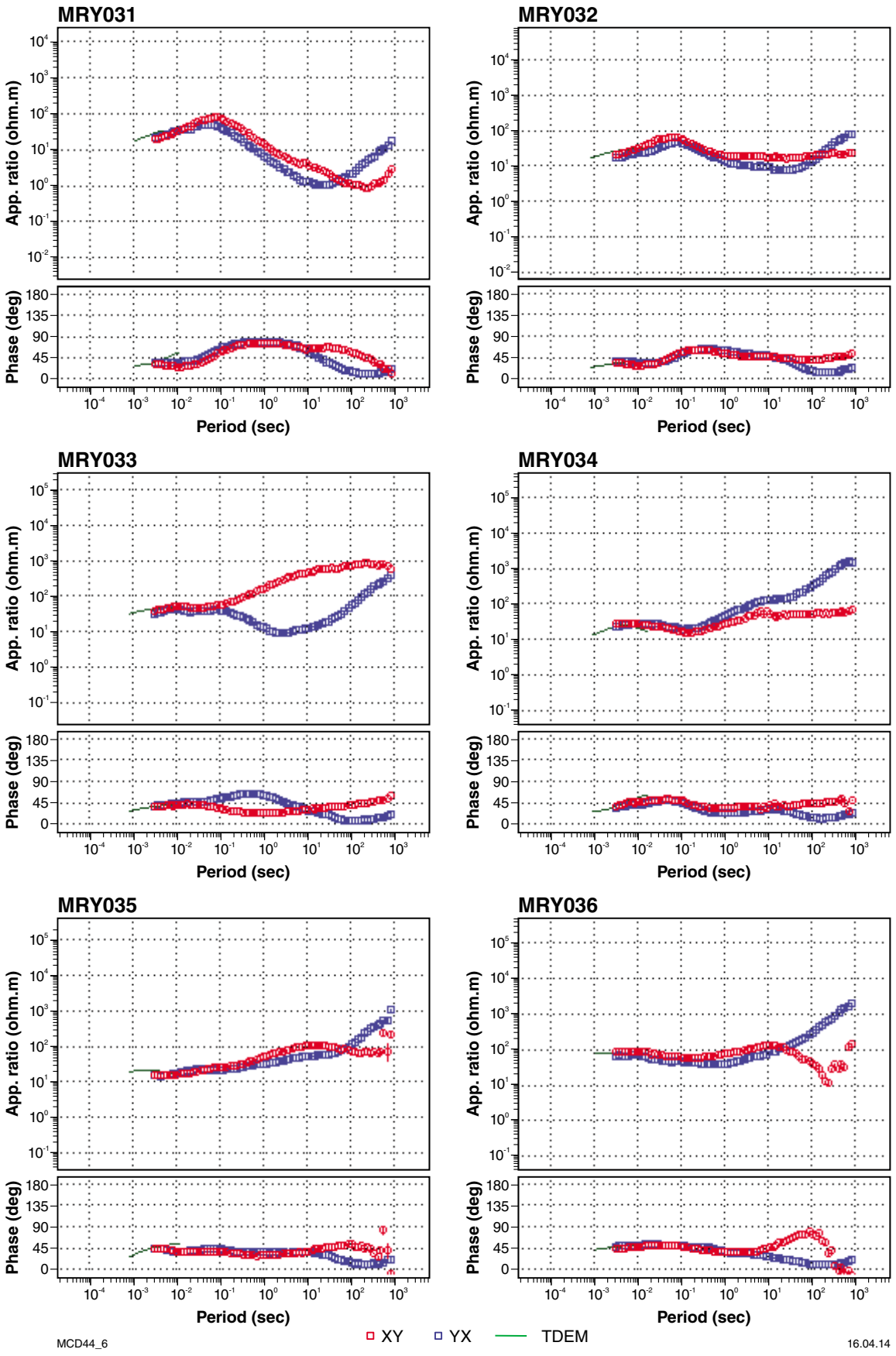
MRY031
MRY032
MRY033
MRY034
MRY035
MRY036
App. ratio (ohm.m)
Phase (deg)
Period (sec)
XY
YX
TDEM
MCD44_6
16.04.14

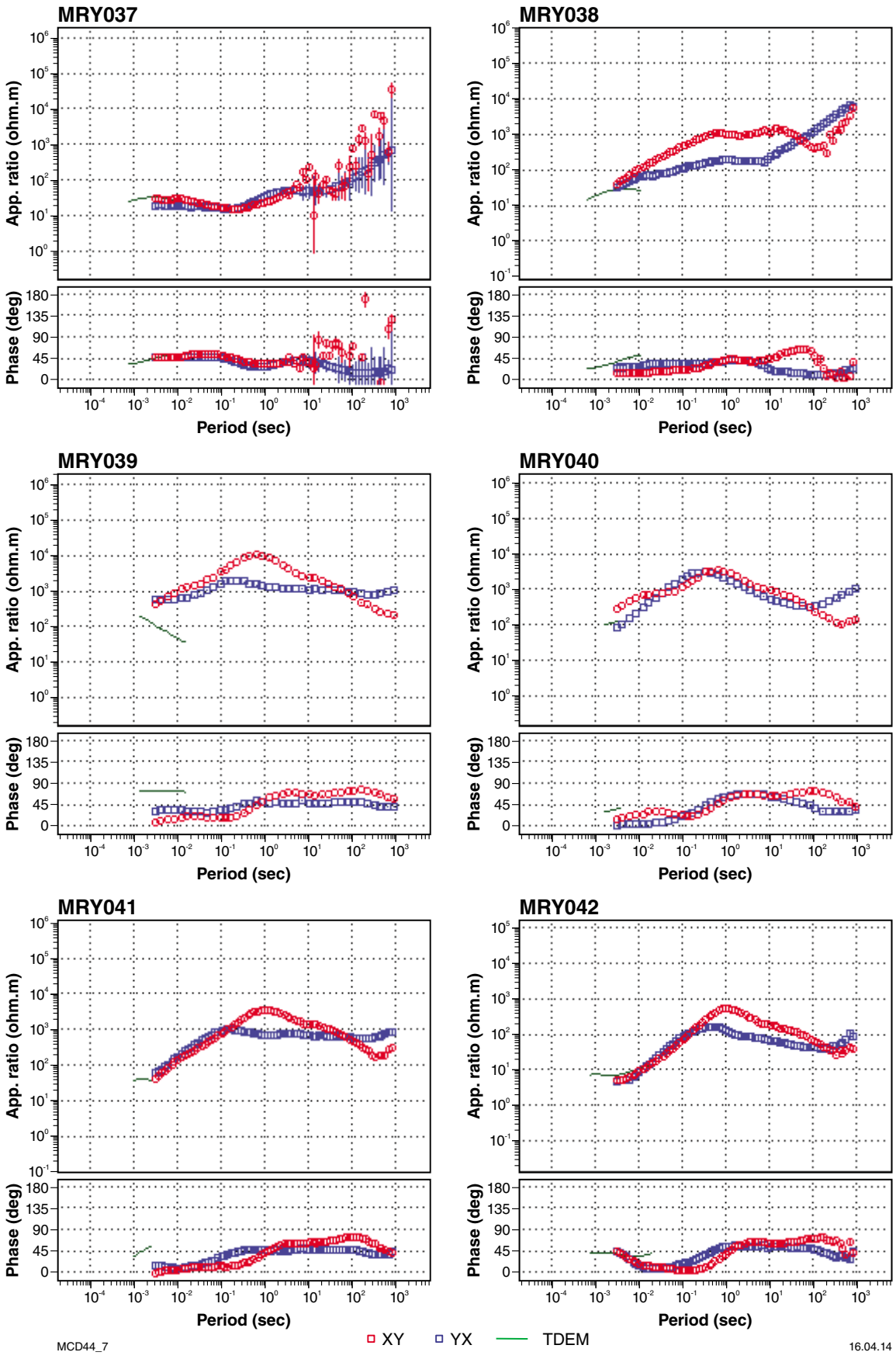
MRY037
MRY038
MRY039
MRY040
MRY041
MRY042
App. ratio (ohm.m)
Phase (deg)
Period (sec)
XY
YX
TDEM
MCD44_7
16.04.14

Two near-orthogonal magnetotelluric (MT) traverses were conducted across the eastern part of the Capricorn Orogen. The results show distinct variations in mantle and crustal electrical conductivity across the orogen, and are interpreted to represent a series of discrete tectonic blocks separated by crustal-scale faults or shear zones that dip towards the centre of the orogen. By contrast, in the western part of the orogen, the major structures consistently dip towards the south.

The Yilgarn and Pilbara Cratons are resistive and separated by a large volume of conductive crust in the middle of the orogen. Although the nature and origin of this crust is not known, it is interpreted as Proterozoic crust analogous to the Glenburgh Terrane in the western part of the orogen. Therefore, the Pilbara and Yilgarn Cratons do not appear in direct contact with each other in this part of the orogen.

The present-day crustal architecture, as imaged in this survey, is a reflection of processes imparted late in the crustal thickening cycle. Therefore, any major structural differences across the orogen likely reflect complex collisional processes rather than any fundamental differences in the pre-collisional architecture, such as subduction polarity or the location and distribution of island arcs.

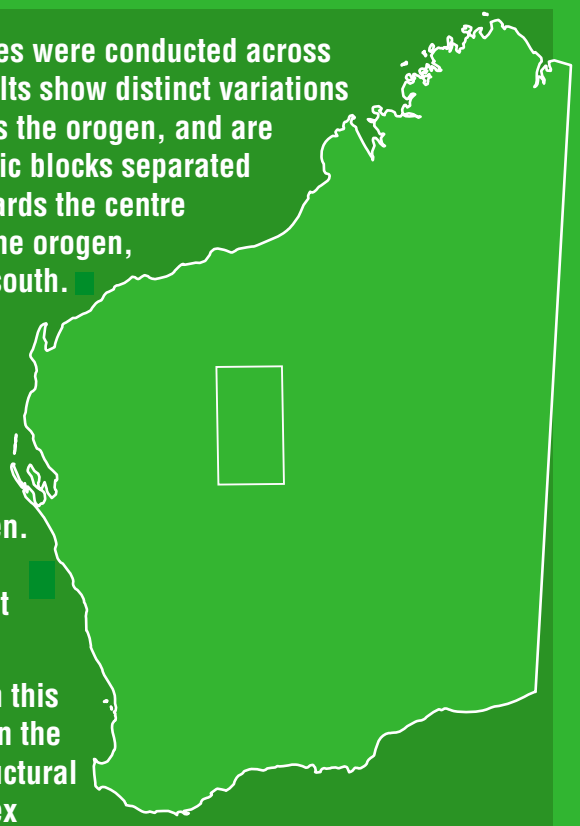

Further details of geological products and maps produced by the Geological Survey of Western Australia are available from:

Information Centre
Department of Mines and Petroleum
100 Plain Street
EAST PERTH WA 6004
Phone: (08) 9222 3459 Fax: (08) 9222 3444

www.dmp.wa.gov.au/GSWApublications

DENTITH et al.

A MAGNETOTELLURIC TRAVERSE ACROSS THE EASTERN PART OF THE CAPRICORN OROGEN

REPORT 135